THESIS FOR THE DEGREE OF DOCTOR OF PHILOSOPHY

Applications of chromophores and multiphoton techniques to study structure and interactions of bio-macromolecules in assembled state

Piotr Hanczyc

Department of Chemical and Biological Engineering
CHALMERS UNIVERSITY OF TECHNOLOGY
Göteborg, Sweden 2013

Applications of chromophores and multiphoton techniques to study structure and interactions of bio-macromolecules in assembled state

Piotr Hanczyc

ISBN: 978-91-7385-923-3

Doktorsavhandlingar vid Chalmers tekniska högskola
Serie Nr: 3604
ISSN: 0346-718X
Department of Chemical and Biological Engineering
Chalmers University of Technology
SE-412 96 Gothenburg
Sweden
Telephone +46 31 772 30 49

Department of Chemical and Biological Engineering
Chalmers University of Technology
Göteborg, Sweden 2013

Applications of chromophores and multiphoton techniques to study structure and interactions of bio-macromolecules in assembled state

Piotr Hanczyc

Department of Chemical and Biological Engineering
Chalmers University of Technology

Thesis abstract

The research presented in this thesis is concerned with the linear and nonlinear optical properties of biopolymers and the chromophores that bind to them. This thesis combines analyses of the interactions of biomolecules with technological improvements of already existing systems for bionanotechnology-related research. The importance of precise control of biosystems is essential in elucidating the fundamental properties of biomolecules, such as DNA and amyloid fibrils, or biomolecule-dye adducts. A starting point for such studies is to examine the structures of DNA oligonucleotides loaded either in a polymeric carrier or water-based buffers. The DNA secondary structure as a function of relative humidity reveals a strong dependence on polyvinyl alcohol (PVA) hydration level, which is of relevance for nanotechnological studies of DNA-based supramolecular systems. PVA gel systems provide possibilities to test models of nucleic acids interactions and distributions in cellular contexts, including the structural stability of the genetic material in the cell and PVA-based packaging for gene delivery. A method by which duplex oligonucleotides, which contain sequences designed to provide specific binding sites, become amenable to polarised-light spectroscopy opens up new possibilities for studying the structures of DNA complexes that contain small adduct molecules, as well as proteins. However, the polymer environment strongly destabilises the DNA-dye complex. A study of DNA-dye and PVA-dye interactions was carried out using a homologous set of dyes from the cyanine family while gradually increasing the charge and DNA affinity. The successful orientation in PVA of the ruthenium dimer $[\mu\text{-}(11,11'\text{-bidppz})(\text{phen})_4\text{Ru}_2]^{4+}$, which was bound by threading intercalation to DNA oligonucleotide duplex hairpins, reveals that binding modes depend both on the oligonucleotide sequence and the chirality of the probe. The enantioselective binding

properties of sterically rigid DNA probes, such as the studied ruthenium complex, can be used to increase the targeting specificities of short nucleic acids sequences, e.g., to inhibit transcription in a therapeutic context, such as the treatment of malaria or cancer. Moreover, ruthenium(II) complexes exhibit strong multiphoton absorption properties, discovered and quantified using a nonlinear spectroscopy Z-scan technique. In particular, the [(11,11′-bidppz)$(phen)_4Ru_2]^{4+}$ complex was found to exhibit very strong two- and three-photon absorption properties, which were enhanced by substitution at the *para* position in the dimer structure; these properties are not commonly observed in flexible dimer chromophores, such as the ethidium homodimer. Metal-organic complexes may represent a new generation of DNA- and amyloid fibril-staining agents that have the advantage of exhibiting strong nonlinear optical properties. Labelling with organic dyes is also a strategy for visualising aggregated states of proteins and there is a growing need for more specific and photostable binding chromophores. The binding of dimeric ruthenium complexes and a stilbene derivative to amyloid fibrils was examined in the context of applying multiphoton-based technologies for diagnostic purposes. Interestingly, the aggregated states of misfolded proteins exhibit remarkable multiphoton absorption properties, most probably due to cooperative mechanisms that involve aromatic amino acids that are densely packed in the β-sheet, rod-shaped structures of fibrils. These types of self-assembling bio-derived nanomaterials that exhibit specific nonlinear properties may be valuable in various applications, ranging from bio-imaging technology to photonics.

Keywords: One-photon spectroscopy; non-linear spectroscopy; linear dichroism; Z-scan; oxazole yellow dyes; PVA/DNA/dyes films; ruthenium complexes; two-photon absorption.

List of publications

I. Piotr Hanczyc*, Bjorn Åkerman, Bengt Norden

Short Oligonucleotides Aligned in Stretched Humid Matrix – Secondary DNA structure in Poly(Vinyl Alcohol) Environment,
Langmuir ***2012****, 28 (16), 6662-6669*

II. Piotr Hanczyc*, Bengt Norden, Bjorn Åkerman

DNA in a Polyvinyl Alcohol Matrix and Interactions with Three Intercalating Cyanine Dyes
The Journal of Physical Chemistry B ***2011****, 115 (42), 12192-12201*

III. Piotr Hanczyc, Per Lincoln, Bengt Norden*

Interactions of Binuclear Ruthenium (II) Complexes with Oligonucleotides in Hydrogel Matrix: Enantioselective Threading Intercalation into GC Context
The Journal of Physical Chemistry B ***2013****, 117 (10), 2947–2954*

IV. Piotr Hanczyc*, Bengt Norden, and Marek Samoc*

Two-Photon Absorption in Metal-Organic DNA Probes
Dalton Transactions ***2012****, 41(11), 3123-3125*

V. Joanna Olesiak-Banska*, Piotr Hanczyc, Katarzyna Matczyszyn, Bengt Norden, Marek Samoc

Nonlinear absorption spectra of ethidium bromide and ethidium bromide homodimer
Chemical Physics, ***2012****, 404, 33-35*

VI. Piotr Hanczyc, Marek Samoc, Bengt Norden*

Multi-photon absorption of Amyloid Protein Fibres.
Nature Photonics ***2013****, DOI: 10.1038/NPHOTON.2013.282*

Contribution report

Paper I-IV and VI	I planned the study, performed the experiments and analyzed the date. Main author of the paper.
Paper V	I contributed to preliminary studies, performed part of the experiments.

Publications not included in the thesis

I. P. Hanczyc*, K. Matczyszyn, K. Pawlik, J. Olesiak-Banska, H. Leh, M. Buckle

Spontaneous formation of liquid crystalline phases and phase transition in highly concentrated plasmid DNA
Liquid Crystals ***2011****, 8 (4), 461–468*

II. M. Samoc*, K. Matczyszyn, M. Nyk, J. Olesiak-Banska, D. Wawrzynczyk, P. Hanczyc, J. Szerementa, M. Wielgus, M. G. Humphey, M. P. Cifuentes,

Nonlinear absorption and nonlinear refraction: maximizing the merit factors
*Proc. SPIE 8258 82580V****2012***

Abbreviations

UV/Vis	Ultraviolet/Visible Light	OPA	One-photon absorption
LD	Linear Dichroism	2PA	Two-photon absorption
CD	Circular Dichroism	dsDNA	Double-strand DNA
NLO	Nonlinear Optics	ssDNA	Single-strand DNA
NLS	Nonlinear Spectroscopy		
OA	Open Aperture		
CA	Closed Aperture		
YO	Oxazole Yellow		
EB	Ethidium Bromide		

Table of Contents

1. Introduction

Biomacromolecules, such as nucleic acids (DNA or RNA) and proteins forming amyloid fibrils, have been intensively investigated over the past 60 years. Their importance lies in biological contexts of living organisms and the fact that mistakes in transcription, recombination or replication *in vivo* may cause serious diseases, such as various cancers (in the case of nucleic acids) or in the case of pathogenic protein aggregates, so-called amyloid fibrils, Alzheimer's and Parkinson's diseases. However, the biological and medical approaches represent only one aspect of biomolecules, since interdisciplinary studies of biomolecules often generate unexpected discoveries. The unique molecular properties of DNA, in particular the double helix structure, self-recognition, and chirality, as well as the β-sheets of amyloid fibrils have attracted attention in laboratories that are focused on nanotechnology, materials science, electronics, and photonics.

The scientific story of DNA began in 1869 when Johann F. Miescher identified a weakly acidic substance of unknown function in the nuclei of human white blood cells, and this was subsequently termed 'nucleic acid' by P.A. Levene[1]. However, research on the chemical structure of DNA had to wait until new analytical techniques became available. X-ray diffraction images taken by Rosalind Franklin and the results of bacterial transformation experiments partly revealed the nature of DNA. Bearing in mind these discoveries, in 1953, James Watson and Francis Crick [2] proposed a double helix model for the three-dimensional structure of DNA. In addition, they correctly deduced that the genetic information was encoded in the form of the sequence of nucleotides in the structure and that the complementary base-pairing provided a copying mechanism. In parallel with discoveries in the area of nucleic acids, new methods for the isolation of genetic material were developed, as were protocols for the synthesis *in vitro* of short DNA sequences. Paper I describes a study of the structural and molecular properties of DNA oligodeoxynucleotides in polyvinyl alcohol (PVA), which is known to act as a carrier for gene expression-modifying drugs and is generally considered to be a good vector system for a wide range of biomolecules and organic ligands. PVA has been also used in linear dichroism studies in which the investigated samples had to be oriented macroscopically. It was shown that the secondary structures of oligonucleotides in PVA are strongly related to the dielectric constant, hydrophobic interactions, and hydration level of PVA.

At the molecular level, DNA participates in two major processes: transcription and replication, which are of fundamental importance for cellular functions in living organisms. DNA is transcribed or replicated only when a signal appears from, for example, a regulatory protein that binds to a specific region of the DNA sequence. Thus, if the binding specificity and strength of this regulatory protein can be mimicked by a small synthetic molecule, the function of the DNA can be inhibited or activated. Thus, synthetic molecules can act as 'DNA drugs' in gene therapy by inhibiting protein synthesis or replication to induce a cellular response, e.g., apoptosis in cancer cells. These DNA drugs can bind to DNA in two different non-covalent modes, which involve electrostatic attraction and hydrophobic effects, termed 'groove binding' and 'intercalation'. Briefly, groove-binding drugs are usually long, crescent-shaped molecules that fit in the minor groove of the double helix and facilitate binding by promoting van der Waals interactions. In addition, these drugs can form hydrogen bonds with DNA bases, typically to the N-3 of adenine and the O-2 of thymine. Most minor groove-binding drugs bind to A/T-rich sequences. Intercalators contain planar heterocyclic groups that stack in the helix structure between adjacent DNA base pairs. The complex, together with other factors, is thought to be stabilised by π-π stacking interactions between the drug and DNA bases. Intercalators cause strong structural perturbations of the DNA helix and as a consequence, inhibit the replication and transcription of DNA. Non-covalent binding is reversible and can be controlled externally by the concentration of the intercalating agent and ionic strength. Understanding the forces that are involved in the binding of small molecules to DNA is challenging and represents an important area of research. In Paper II, it is shown how DNA-binding dyes respond to changes in the polymer environment, such as those affecting the hydration level, dielectric constant, and ionic strength. This is of fundamental importance for unravelling the mystery of molecular recognition in general and DNA binding in particular in less-hydrophilic media, such as PVA, which is often used as a delivery platform for gene expression-modifying drugs. In Paper III, the advantage of the PVA system whereby short oligonucleotides of defined sequences can be aligned was exploited, and DNA interactions with enantioselective metal-organic drugs based on ruthenium were explored. Polarised light spectroscopy and luminescence kinetics experiments revealed two distinct binding modes and the enantioselectivity of the $[(11,11'\text{-bidppz})(\text{phen})_4\text{Ru}_2]^{4+}$complex with respect to guanosine-cytosine (GC) stretches/motifs. The same dimeric ruthenium (II) complex was compared with the monomeric equivalent, and new dimeric derivatives were investigated with respect to their

nonlinear absorption properties (in Paper IV). All of the components were found to exhibit strong two- and three-photon absorption properties, while the rigid dimer complex in particular showed strong enhancement for substitutions in the *ortho*- and *para*- positions, which together with the DNA sequence specificity and enantioselectivity suggests a new class of biomolecules markers with potential applications in biology and medicine, including the use of advanced multiphoton-based techniques. Paper V includes a comparison of the nonlinear properties of classical DNA staining agents, ethidium bromide and ethidium homodimer, showing that with respect to fluorescence quantum yield and binding sites, dimeric molecules are not necessarily the ideal choice for labelling applications.

Metal-organic compounds also find application in the labelling of amyloid fibrils, as described in results section of this thesis. The term amyloid was first introduced by Rudolph Virchow in 1854 to denote a macroscopic tissue abnormality that he discovered using a positive iodine staining reaction. Nearly 60 years later, at the time of the discovery of the double helix of DNA, similar experimental methods were used in studies of amyloid aggregates. Thus, electron microscopy (EM) and X-ray diffraction were helpful in elucidating the structures of these protein aggregates. EM imaging of the ultrathin sections of amyloidotic tissues revealed that amyloids have a regular fibril structure of around 80–100 Å in width. X-ray diffraction analyses confirmed the EM results and further showed that the fibrillar structure was chiral, being composed of β-pleated sheets ordered in a long repeated sequence, with the polypeptide backbone being oriented perpendicularly to the fibril axis (crossed β-structures). Currently, it is assumed that almost all proteins that are in the process of misfolding are eventually able to form irreversibly insoluble amyloid fibril aggregates, the presence of which may lead to serious diseases, such as Alzheimer's, Creutzfeldt–Jakob and Parkinson's diseases. One approach has been to stain and visualise malfunctional regions for subsequent therapeutic purposes. In results section, it is shown that metal-organic complexes can be used for the effective staining of amyloid fibrils. The main advantage that these compounds have over the classical staining agents is that owing to metal-to-ligand charge transfer (MLCT) transitions, it is possible to shift the excitation wavelength to near-infrared (NIR) using two-photon absorption (2PA). If the wavelength is in the transparent range, cells and tissues are not damaged by the light irradiation with light, which means that this technique could be used for diagnostic and therapeutic applications in patients. Given their relatively moderate toxicity, at least when used at low concentrations, ruthenium(II)

complexes can be considered as an interesting set of dyes for the visualisation of aggregated states *in vivo*. Furthermore, stilbene 420, which has a structure that is similar to that of Congo Red, can be considered as a prototype for designing specific binding molecules with good nonlinear optical properties for targeting amyloids[3]. However, there remains a demand for less-invasive methods and technologies, aimed at eliminating labelling with organic markers. In Paper VI, we report a breakthrough discovery in demonstrating that amyloids with a high content of aromatic amino acids can exhibit a nonlinear response through a cooperative mechanism to absorb light. An important aspect with respect to applications is that the aggregated state of a protein (but not the monomeric native protein) absorbs light in a multiphoton process. This opens up various opportunities to detect the regions of the proteins that are associated with aberrant biological function while other components, such as nucleic acids, proteins, and cellular factors, remain virtually "invisible".

Before summarising the results in a more comprehensive manner, this thesis will brief the reader regarding the theoretical backgrounds of DNA, amyloid fibrils, and binding chromophores, together with a brief review of the fundamental concepts. The presented results were obtained using polarised light spectroscopy in combination with fluorescence, representing a powerful combination of tools for studying biomolecules and the interactions with organic chromophores[4]. Among the advantages of linear spectroscopy methods are enhanced sensitivity and allowing dynamic studies of molecular interactions and applications to different systems (e.g., stretched polymer films). However, some processes can be investigated only using nonlinear spectroscopy, which is another topic of this thesis. Using femtosecond laser techniques, amyloid-dye adducts were investigated with respect to multiphoton excitation. In the case of aggregated proteins and some biomolecules that bind to dyes, the Z-scan technique was used for determining the nonlinear absorption cross section coefficients, providing insight into the impact of structure on the nonlinear properties of the materials.

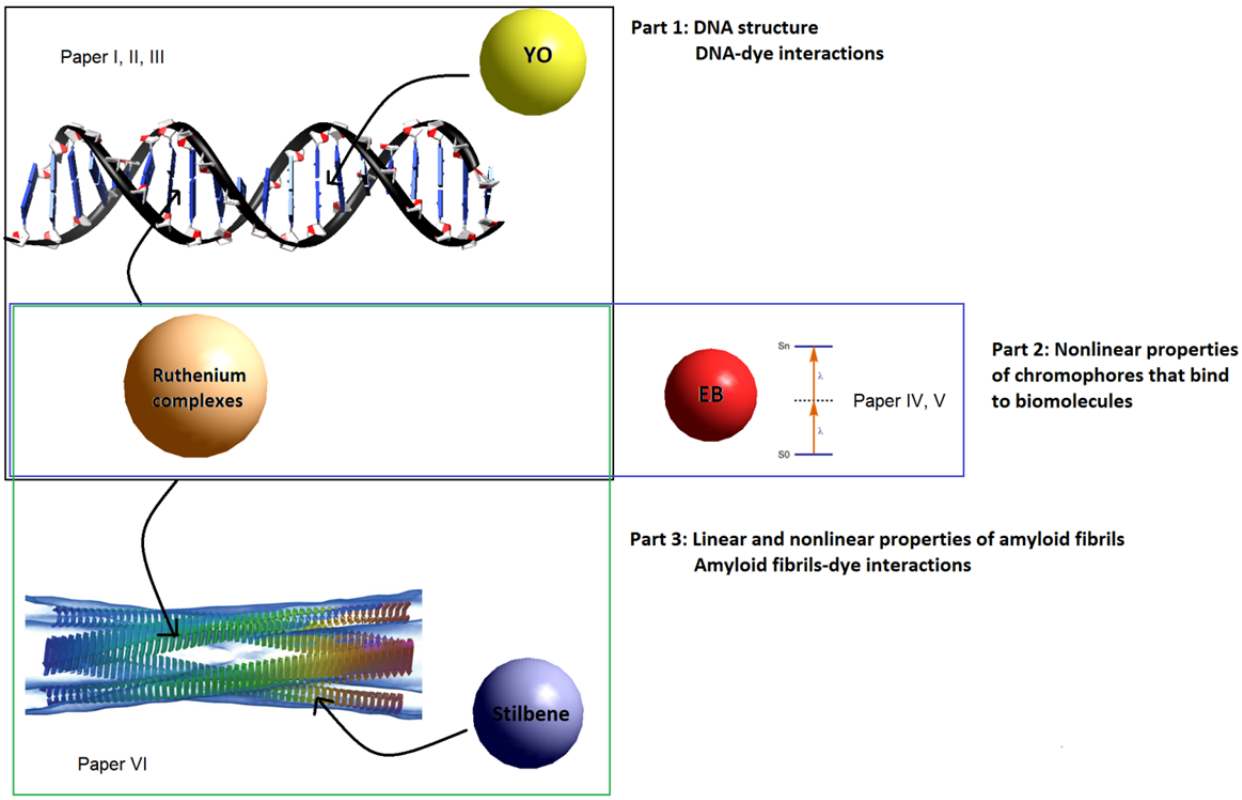

Fig. 1 Schematic overview of the topics covered in Papers I–VI of the thesis. Papers I–III relate to DNA and DNA-dye/drug studies, Papers IV and V report on nonlinear optical effects of biomolecules binding to dyes/drugs, and the remaining part is concerned with the multiphoton absorption phenomena of amyloid fibrils in the presence or absence of interactions with binding molecules (Paper VI).

2. Chemical Background

2.1 Polyvinyl alcohol (PVA) in studies of biomolecules

PVA has a relatively simple chemical structure, with a linear alkane chain and a pendant hydroxyl group (Fig. 2) The monomer vinyl alcohol unit is unstable, which means that it spontaneously rearranges to form a tautomer- acetaldehyde. Therefore, PVA is produced by the polymerisation of vinyl acetate to polyvinyl acetate (PVAc), followed by the efficient hydrolysis (>98.5%) of PVAc to PVA. The degree of hydrolysis is the most important step in determining the chemical properties, solubility, and the crystallinity of PVA. As a result of polymerisation and hydrolysis, the molecular mass of PVA varies widely, so the appropriate choice of PVA form for research purposes is essential, since polymer properties, such as adhesion, mechanical strength, and diffusivity, are dependent uponthe average molecular mass.

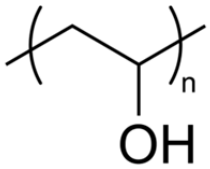

Fig. 2 The PVA monomer.

PVA is a water-soluble, nontoxic, noncarcinogenic polymer that is widely used in the pharmaceutical industry. However, before it can be used for biological or medical applications, it has to be crosslinked. Several methods are available for efficient crosslinking, including chemical methods that employ difunctional crosslinking agents, such as monoaldehydes, and techniques based on electron beam- or γ-irradiation. Finally, it is possible to sequentially freeze and thaw PVA hydrogels so as to induce cross-linking[5]. Such gels exhibit a high degree of swelling in water and rubbery elastic properties. PVA is thought to be capable of simulating natural tissues and is readily accepted into the body[6]. It has been used incontact lenses[7], for the lining for artificial organs[8], and for drug delivery applications[9]. Besides its uncontested importance in pharmaceutical and bioengineering fields, PVA has attracted much attention from researchers of genetics in recent years. As examples, PVA can be used as a host for polar molecules and biomolecules, such as DNA, and it can be used as a

drug carrier, through the formation of nanoparticles that contain both PVA and DNA[10]. However, these composites are scarcely described or understood. Given its properties, PVA is a valuable polymer host for studying the physical and chemical properties of biomolecules and biomolecule-drug interactions. The biggest advantage of PVA as a host material is that the hydration level is easily controlled during experimental processes, which is important for understanding the influence of external forces (e.g., hydrophobic interactions) on nucleic acid structures. In the case of DNA, it is possible to switch between different conformations in a controlled and reversible manner. Humidifed hydrogels contain approximately 50% water and the DNA in PVA-DNA composites is in the classical B-conformation. If the film becomes dehydrated, a change in the DNA secondary structure to produce the A-conformation is possible.

Incorporating into the PVA matrix either free oligonucleotides or oligonucleotides with bound dye creates several research opportunities. Stretched humid PVA allows the study of macroscopically anisotropic systems using versatile spectroscopic techniques, including linear dichroism, the use of which has been traditionally confined to long fragments of DNA (>500 base pairs [bp]) that can be aligned by shear flow. Such long DNA sequences have not generally been amenable to analyses of systematic variations in the binding sites of the nucleic acids. With the PVA matrix system, short DNA duplexes of defined sequence and as short as 20 bp[11] can be easily aligned in the stretched polymer matrix. However, a serious disadvantage of the PVA system is the low dielectric constant of the medium that surrounds the DNA, as this competes with the hydrophobic interactions occurring in the interior of the DNA and thus with the binding of added hydrophobic probe molecules. Thus, the interactions of traditional intercalators (ethidium bromide) and minor-groove binders (DAPI or Hoechst reagent) cannot be studied, as these dyes have a stronger preference for the PVA environment, in which they become aligned in parallel with the polymer chains. In contrast, tetravalent DNA chromophores, which bind more strongly and dissociate slowly, may be studied in PVA, as they remain bound to the DNA despite the lower dielectric constant of the surrounding medium. Exploiting the advantage of strong binding to DNA by multivalent ligands, the PVA system has been developed and used to study the molecular recognition properties of nucleic acids (Papers II and III).

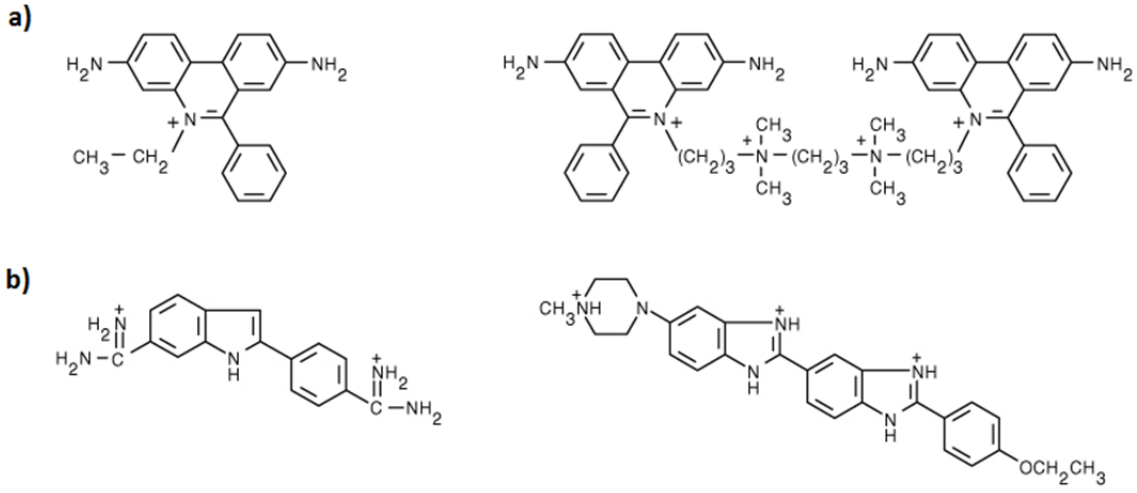

Fig. 2.1 Examples of standard DNA-binding chromophores. Shown are the structures of classical intercalators, a) ethidium (top left) and its homodimer derivative (top right), and of groove-binders, b) DAPI (bottom right) and its derivative Hoechst 33342.

2.2 Structures and possible conformations of DNA

A DNA double helix is built of two long polynucleotide chains of two types of nucleotides: purines (adenine [A], guanine [G]) and pyrimidines (thymine [T)], cytosine [C]), whereby A pairs with T and G pairs with C [Fig. 2.2]. In addition to the nitrogen-containing bases, each DNA nucleotide contains a 5-carbon deoxyribose sugar and a phosphate group. The chains are formed by the phosphate group of one nucleotide being attached to the sugar of the following nucleotide by a phosphodiester bond between the C-3 end of one molecule and the C-5 end of the other. The phosphate-sugar backbone is on the outside, while the attached bases are on the inside of the double helix, attached to the C-1 atom of the pentose sugar. Upon formation of the helix, two grooves can be distinguished, a shallow major groove, and a narrow and deeper minor groove, which are formed between the intertwining strands. DNA consists of antiparallel strands of alternating sugar and phosphate groups, and the alternating chains are held together by multiple hydrogen bonds between complementary nucleobases, so-called base pairing. The overall helical structure is determined also by the π-π stacking interactions between the neighbouring bases in the stack formed in each single strand. The stacking interactions become stronger as the length of the DNA sequence increases.

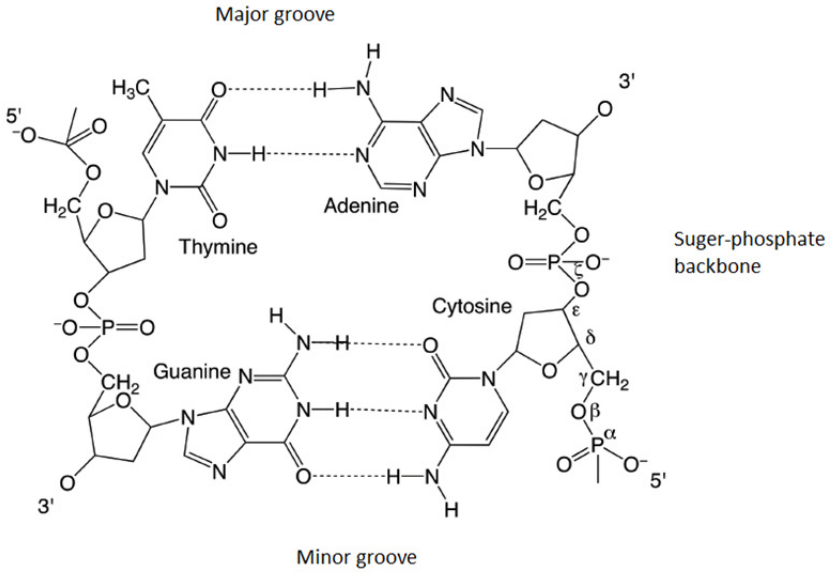

Fig. 2.2 Model of base pairing and nucleotide structures in DNA.

As a consequence of double-helix formation, the interior environment between the DNA aromatic bases becomes hydrophobic due to base-base stacking, while the external parts of the helix are negatively charged due to the phosphate groups in the backbone, which attract water and counter-ions, such as Na^+. The duplex structure is "polymorphic" and can adapt to different environmental conditions, such as changes in hydration, dielectric constant, and ionic strength. In these adaptive responses, the DNA conformation may be changed. The most common DNA conformation is a B-canonical conformation [Fig. 2.3], in which one turn of the helix is approximately 3.4 nm (34 Å) in length and 2 nm (20 Å) in width, consisting of 10bp (where one base is 3.4 Å in length). The structure is a right-handed helix with bases positioned almost perpendicularly to the helix axis and considered to have an average twist of 36°, making 10 bp per turn of 360°. To generate the stable B-conformation of DNA, two hydration shells are needed around the helix: a primary shell that contains approximately 35 water molecules that are strongly interacting with DNA phosphate groups; and a secondary layer that contains an additional 10 weakly interacting water molecules per bp. If the environment becomes dehydrated, DNA adopts the A-conformation [Fig. 2.3], which is more compact in that it has 11 bp per turn of the helix, with each base increasing the length by 2.4 Å. In the A-conformation, all the bases are positioned farther from the helix axis, making the

interior part hollow. On the outside, the major groove becomes deep and narrow and the minor groove becomes shallower. The A-conformation is also found in double-stranded RNA and DNA-RNA hybrids. GC sequences are more prone to adopt the A-conformation[12]. In the presence of a large excess of salt, the Z-conformation can be induced [Fig. 2.3],which unlike the right-handed A- and B-forms is a left-handed helix, winding in a zig-zag pattern, with one turn containing 12 bp and having a total length of 4.5 nm (45 Å). In addition to the above-mentioned conformations of the DNA duplex, there are also some natural distortions that arise due to local folding structures[13], such as hairpins and internal loops or mismatching base pairs, as will be briefly described in the following chapter.

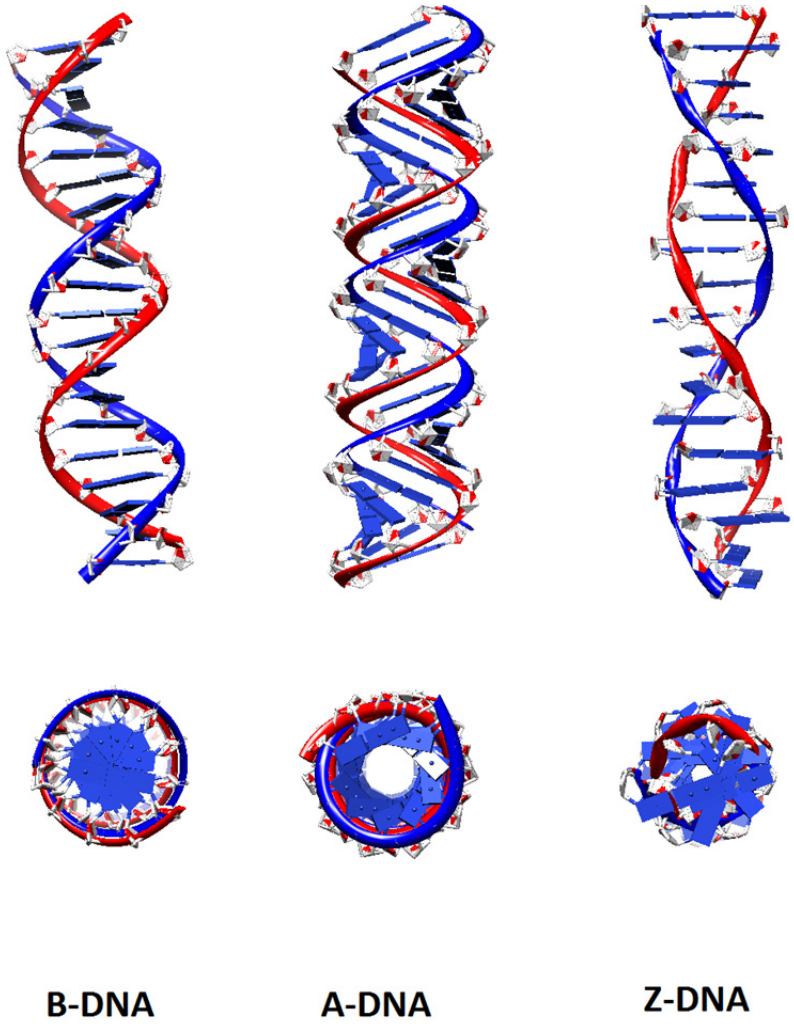

Fig. 2.3 Three different conformations of the DNA double helix in side-view and top-view.

2.3 Short synthetic DNA: secondary structures, properties and applications

Since solid-phase synthesis offers possibilities for preparing short DNA stretches with defined sequences, studies of specific nucleic acid properties can be performed. Oligonucleotides can be designed and modified to mimic naturally occurring regions of DNA that contain errors. For example, non-duplex structures, such as bulges, base mismatches, hairpin loops or higher tertiary structures [Fig. 2.4], represent structural alterations that may cause errors in replication or recombination and lead to serious defects in the functioning of the molecular machinery in the cell. However, some of these structures form spontaneously in RNA, and their activities are not fully understood. These structures may be associated with specific catalytic and regulatory functions in the cell, e.g., tRNA of about 80 nucleotides can transfer a specific amino acid to a growing polypeptide chain at the ribosomal site of protein synthesis during translation.

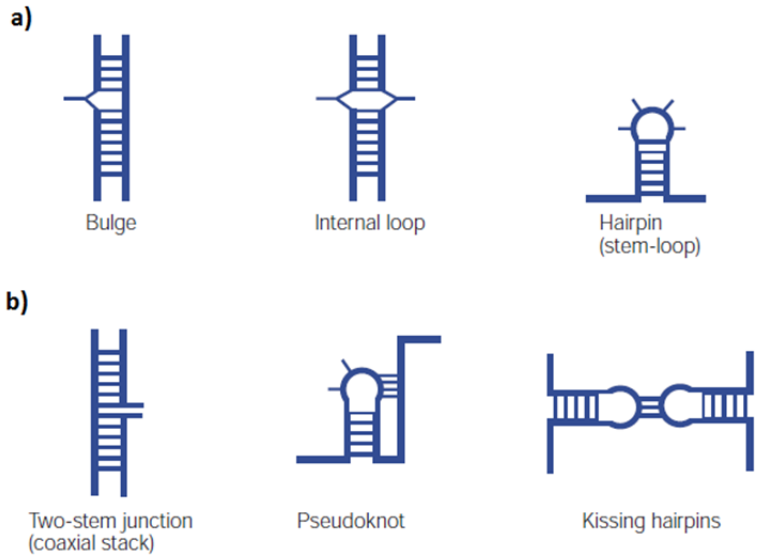

Fig. 2.4 Examples of non-duplex structures: a) various secondary structural elements; and b) tertiary structural elements. In general, bulges have one or more unpaired bases in one strand that can stack either on the inner side or the outer side of the backbone. A similar pattern of behaviour for the bases can be observed in internal loops, albeit on both strands where unpaired nucleotides often engage non-Watson–Crick base pairing, which leads to further tertiary complex structures. Free bases in hairpin loop structures are at the apex of the double-stranded helix.

As mentioned above, the formation of non-duplex structures has a different starting point in DNA than in RNA, and in DNA the change may be mutagenic. Changes in nucleic acid sequences due to mutations can lead to serious degenerative diseases or even be lethal. While many of these mutations are silent, they may be activated in subsequent generations. A severe mutation results in aberrant or impaired activity or loss of function of a particular gene. Further accumulation of mutations may induce degenerative human diseases and cancer. Molecular recognition of degenerated DNA regions is therefore an important area of research, and it may suggest solutions to existing problems at the gene level. In this context, investigations regarding the development of specific DNA drugs and improving the efficiency of drug delivery are valuable. The approach proposed in this thesis involves the formation of a composite, whereby DNA is incorporated into a matrix of PVA, which is a water-soluble synthetic polymer that acts as an excellent host matrix for hydrophilic molecules, such as DNA, by virtue of having a high content of water[14]. The dense gel environment, which can be considered as an artificial system that mimics molecular crowding in the cell nucleus, is an excellent model for investigating how the structural properties of oligonucleotides are affected by subtle changes in the environment, i.e., water activity and confinement within a polymer. The obtained information is of high relevance for delivering a drug through the hydrophobic environment of a membrane, as in the transfection of short DNA pieces into the cell, and further into the nucleus. The ease with which the hydration level of PVA can be controlled facilitates the manipulation of the factors that can affect DNA structure and conformation. With respect to the environment inside the membrane, the influence that hydrophobicity exerts on the secondary structures of short DNA fragments is of special interest. Comparing hydrogel, in which the maximum water content is around 50% (when the film is humidified at100% relative humidity [r.h.]), with a pure aqueous solution, it is clear that the conditions around the DNA are completely different. Therefore, PVA is an ideal system for investigating how different conditions (e.g., hydrophobic interactions, lower dielectric constant) influence the overall DNA structure. For synthetic oligonucleotides, the length and sequence composition can be designed and thus, the rate of internal DNA interactions (hydrogen bonding, stacking, and base pairing) can be controlled, so as to allow studies of how the hydrophobic forces in the polymer environment influence the secondary structures of short DNA sequences. By varying the level of PVA hydration, which is controlled *via* the r.h.

(Table 1), it is possible to change the water activity (and consequently, the equilibrium) of the entire studied system.

Table 1 Salt buffers used for the hydration of PVA gel films

Saturated aqueous buffer solution at bottom of chamber	Relative humidity (r.h.) in closed chamber containing the film sample (%)
NaCl	75
KBr	80
Na_2CO_3	90
Na_2SO_4	93
H_2O	100

This study of the PVA system is also relevant to research focused on polymer hydrogels as delivery platforms for gene therapy, since short DNA sequences and duplex RNA (siRNA) are extensively exploited in genetics as tools for targeting DNA, as in the antigene strategy[15] or RNA-antisense strategy[16]. For the latter application, the nucleic acids are usually presented in mixtures with nontoxic polymers, such as polyethyleneimine (PEI)[17], polyethylene glycol (PEG)[18] or PVA[14c,19], which may constitute protective shells for the delivery process. Even though these polymers are widely used in the pharmaceutical industry, little is known about their influences on the properties and conformations of nucleic acids[20].

In this thesis, it will be shown that the PVA matrix is useful for studies of oligonucleotide-dye interactions and DNA-based nanoconstructs on a macroscopic scale. Short synthetic DNA is being used widely in modern nanobiotechnology, whereby oligomers are used as building blocks in two- and three-dimensional nanostructures[21]. DNA is an attractive material, since single strands of DNA can be easily hybridised, branched structures are stable, and it is easy to synthesise desired sequences. Relying on basic knowledge, a first attempt to use oligonucleotides as a structural material was made by Seeman in the early 1980s. The underlying idea was inspired by structures that form spontaneously in nature: Holliday junctions, in which the basic structure comprises a four-way junction that is formed during gene recombination, for example in fungi[22]. Seeman suggested that this motif could serve for

the construction of more complicated 2D structures using artificial short sequences of DNA, which should remain stable and enable the possibility to modify them into different shapes. One of the simplest examples is the DX molecule [Fig. 2.5], which is sufficiently rigid and can generate a periodic unit structure in two dimensions, measuring up to a few micrometers in either dimension.

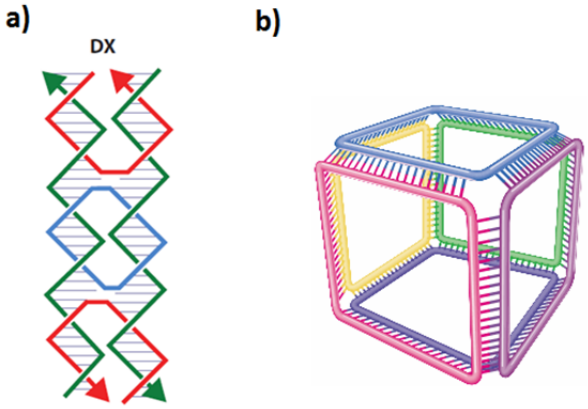

Fig. 2.5 Two simplest DNA nanostructures: a) 2D DX; b) 3D cube.

Control of the structure of a material would be incomplete without the ability to produce 3D constructs of high quality. The simplest possible case, a cube, was demonstrated in 1991. Each edge of the cubic structure was as long as 7 nm, which was equivalent to 20 bp of DNA[23]. The technology was developed further, with the primary goal of precisely positioning small objects, such as nanoparticles or proteins conjugated with biotin/streptavidin, with nanotechnological precision. Another focus has been on nanoscale cages, in which DNA-comprising constructs are proposed as capsules, for example for drug delivery. In this context, DNA origami can be used to create an addressable surface area of roughly 100-nm squares[24] in all three dimensions. DNA origami has been widely used since its introduction owing to the ease with which the architecture of the design, as well as dynamics of the nanoconstructs, can be controlled. In the field of therapeutics, a striking example of how it is possible to lock and unlock a 3D box was shown by Andersen[21c], whereby certain organic drugs, nanoparticles or proteins can be placed in the box and released upon delivery by, for example, an enzymatic reaction.

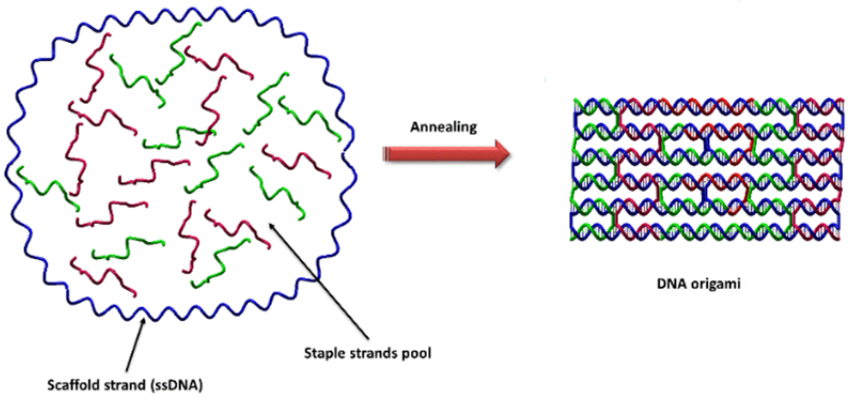

Fig. 2.6 Mechanism through which DNA nanostructures are formed using the DNA origami technique. A long, scaffold, single-strand DNA (blue) and short, single-stranded oligonucleotides (acting as staples) are mixed together and allowed to hybridise, so as to form a nanostructure of the desired architecture and shape.

Another rapidly developing field in which oligonucleotides are extensively used involves conjugation to nanoparticles that vary in diameter from a few nanometers up to micrometers. Usually, noble metal particles (Au or Ag) are used, since their binding strategies are already well-established. Briefly, the DNA and surface of the metal undergo electrostatic interactions. However, since these interactions are nonspecific, control of the binding position is not possible. An alternative strategy relies on modifying one of the ends of the DNA strands with a thiol group or using streptavidin/biotin binding. Attaching a thiol is commonly used, since strong binding opens up research and application opportunities. For instance, metal nanoparticles, such as gold, can be covered with a dense shell of synthetic oligonucleotides that exhibit co-operative properties thanks to their polyvalent surfaces. These properties have found applications in programmable crystallisation[25], enzyme-free biodiagnostic assays[26], and even in electronics[27]. Thiolated DNA connected to a metal also exhibits interesting cell-uptake properties, which may be used for antisense gene regulation[28]. It has been shown that the ability of such a DNA composite to bind a complementary nucleic acid is several orders of magnitude greater than that observed for normal hybridisation in bulk solution; this has been linked to the dense packing and high local concentration of the DNA on the metal surface[26]. In addition, counterions that interact with the phosphate backbone are screening also the adjacent oligonucleotides, and the strong electrostatic attraction increases the local ionic strength above that seen in a solution. The increase in local ionic strength increases the local

stability of the duplex, as well as the effective binding constant, which is directly associated with DNA-nanoparticle interactions. Another interesting application is the building of advanced nanostructures in a controllable fashion. In this context, short duplex DNA is a powerful tool to drive the assembly and tune the optical properties of metals, which are related to plasmon resonance in the visible-light range and strongly depend on the distance between the metal nanoparticles. This leads to another batch of applications, including DNA-binding dyes that exhibit enhanced fluorescence due to surface plasmon interactions[29] or molecular rulers with long-range FRET[30]. For all these applications, the most important factor is the precise control of the designed nanostructure on a molecular level. An important issue then is how to maintain control over the multiple steps involved in the building of more complex nanoconstructs that are based on DNA. Of particular interest is the ability to define the number of oligonucleotides bound to each particle. Alivisatos and colleagues have demonstrated a method for the binding of synthetic single-stranded DNA (ssDNA) so as to produce a significant effect on DNA-gold nanoparticle mobility in gel electrophoresis. Depending on the number of ssDNA moieties bound to each Au particle, a few dark red bands were clearly distinguishable in the electrophoresis gel due to the plasmon resonance of gold[31]. Even though the method is rather limited, since an increase in particle size or a decrease in oligonucleotide length will severely reduce the separation efficiency, it allows the formation with reasonable precision of a nanostructure on a relatively large scale, as well as control over each step in the preparation process. Using either gel electrophoresis or HPLC, it is possible to derive versatile DNA-Au nanostructures [Fig. 2.7] of the desired size and shape. Indeed, the generation of well-characterised nanostructures in reasonable amounts opens up possibilities to study the constructs by polarised light spectroscopy methods, which are very useful but require consumption of the material. Unlike single molecule experiments or microscopic characterisation, polarised light spectroscopy provides information about the structures and interactions of nanoconstructs on a macroscale, as it reflects the average values for the entire sample studied.

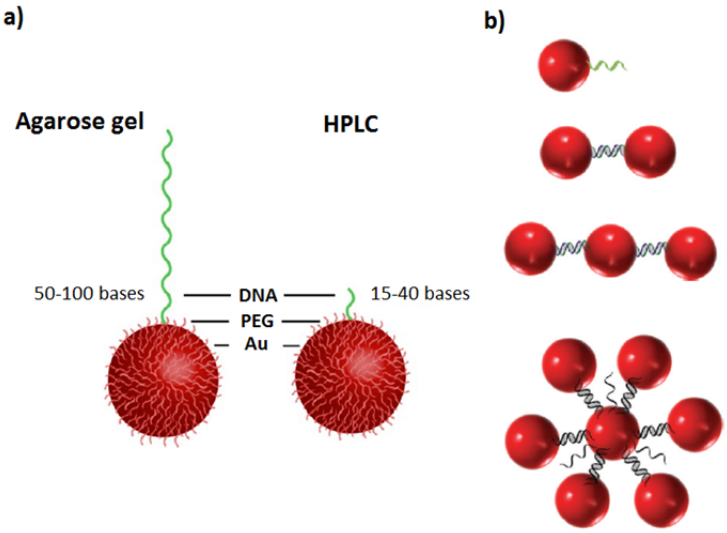

Fig. 2.7 Functionalisation of gold nanoparticles with DNA. a) Two methods for the separation of conjugates with a defined number of bound single-stranded DNA: agarose gel and HPLC. b) Possible nanostructures built from gold spherical nanoparticles and DNA, including dimers, trimers, and hexagons[32].

In addition to the uncontested advantage of DNA nanotechnology in positioning different nano-objects with nanometer precision, such constructs of well-established design can also be useful for the intrinsic properties of DNA. For example, dimer systems in which one Au particle is attached to ssDNA and a second Au is attached to a complementary strand are easily constructed. Such systems in which only one double-stranded DNA is connecting two Au particles can be used to mimic single-molecule overstretching experiments whereby DNA is stretched by pulling DNA-bound polystyrene beads using optical tweezers[33]. In this case, the nanoparticles can act as anchors when incorporated into, for example, a highly viscous polymeric environment, and the restriction of their mobility should allow for the induction of helical extension of all the oligonucleotides (on average) on a macroscopic scale upon stretching of the polymer. The system can be assessed by absorption spectroscopy, including linear dichroism.

Even though some of the experiments mentioned here may be difficult to conduct in practice, they are elegant examples of a technology providing tools for the exploration of complex molecular machinery in biological systems and they demonstrate that biology is an excellent source of inspiration and sometimes building blocks (e.g., DNA) for developing artificial technologies. On the one hand, 2D and 3D nanostructures or the coupling of DNA to

nanoparticles and quantum dots[25,32a,34] provide interesting implementations of nanotechnology in bio-related fields. On the other hand, there is still a general lack of knowledge as to how such nano-objects are affected by changes in the external conditions, such as water content variations or the presence of hydrophobic forces. These factors have important implications for technological applications and implementation in biology where drugs (for example) need to pass through different media and where external forces have crucial influences on successful delivery. More specifically, understanding how water activity influences basic building blocks in DNA-based nanotechnology is of fundamental importance and remains an open question for researchers. In terms of the application of nanobiotechnology where individual DNA strands act as structural elements, it is essential to understand the molecular interactions at the gene level in the nucleus and in spores that have a low content of water.

2.4 DNA-dye interactions

DNA as a carrier of genetic information is crucial for the cellular machinery. Any errors in the DNA sequence may lead to the expansion of mutations and carcinogenesis. Also, the host DNA is a target for viruses, whereby the injection of viral sequences leads to infections that vary from the common cold to HIV, which is caused by retroviruses. A direct therapeutic method is to inhibit replication of the invading DNA, for example by using synthetic molecules. Depending on the type of interactions between the DNA and synthetic molecules, covalently or non-covalently binding drug molecules are used. Non-covalent interactions occur naturally in biological systems, e.g., in the binding of DNA by proteins or small ligands, and are reversible, depending on system equilibrium. It remains unclear as to how this interplay affects all the weaker forces, such as hydrogen bonding, van der Waals attractions, stacking or hydrophobic interactions, which play crucial roles in the proper functioning of the cellular processes.

Three major binding modes for the DNA helix can be distinguished: external binding, groove binding, and intercalation.

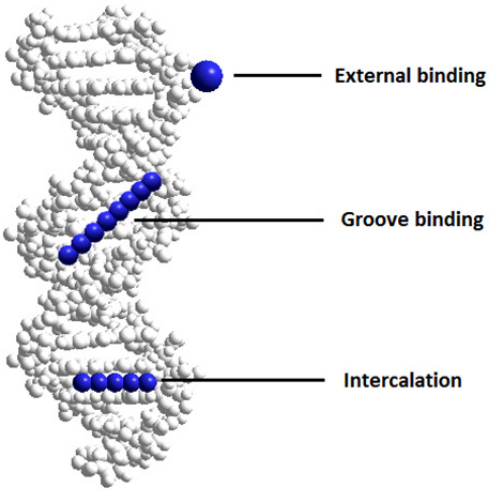

Fig. 2.8 Schematic of possible DNA binding modes.

The greatest impact on the overall DNA structure and its properties involves intercalation, whereby chromophores, which are usually composed of heterocyclic aromatic rings, are inserted between adjacent base pairs in a virtually randomly distributed fashion. This was first reported already in 1961 by Lerman, who used acridines in his experiments[35]. This discovery opened new opportunities for probing the structure of DNA, as well as for investigating in detail DNA-dye interactions. In general, intercalation leads to unwinding of the DNA helix and a length increase of approximately 30% at saturation with nearest neighbour exclusion. The base pairs surrounding the intercalation pocket are commonly separated by a distance of 3.4 Å, which is equivalent to one additional base in a strand[13]. Intercalation inhibits the replication of DNA. However, due to their weak sequence specificities and relatively high toxicities, simple organic molecules are difficult to control and have a limited range of applications. Nevertheless, the simple structures and well-established properties of organic chromophores make them the candidates of choice for studying molecular recognition of nucleic acids in different media, as compared to in solution. In general, little is known about the influences of weaker forces on system equilibrium when a drug is bound to the double helix.

A large group of DNA binding dyes is the cyanine chromophores, which can be divided into two different groups based on structure: symmetrical and unsymmetrical. The first group consists of two benzazole groups, while the second one is composed of one benzazole and one quinoline or pyridine group. The common feature of the two groups is that the nitrogen centres are connected by a system of conjugated carbon atoms. In the simplest structure, the

dye molecule has one positive charge, which is distributed between the two nitrogen atoms. It is possible and relatively easy to tune the optical properties of these dyes by changing the size of the conjugated system. Thus, by employing minor modifications, cyanine dyes have been constructed that cover all parts of the visible spectrum for absorption. One representative of the family of cyanine dyes is unsymmetrical oxazole yellow (YO) and its two derivatives: YO-PRO and dimeric YOYO.

The YO-based dyes are examples of DNA-binding molecules [Fig. 2.9] that intercalate the base pairs and have absorbance maxima that are well-separated from that of the DNA band[36]. An interesting feature of these chromophores is that small changes in the structure increase binding affinity for the DNA helix. The addition to the end of the nitrogen atom in the aliphatic chain of a protonated nitrogen converts a monovalent YO to a divalent molecule Thus, divalent YO-PRO has higher DNA binding affinity than monovalent YO owing to its stronger electrostatic interaction with the double helix. Further extension of the aliphatic chain leads to the formation of a YOYO dimer that can bind even more strongly than YO-PRO, most likely because the two YO monomers are connected by a *bis*-cationic linker[37], which is similar to the linker that was originally used to enhance the DNA affinity of ethidium bromide by forming its homodimer[38] [Fig. 2.1a]. The binding constants of the YO-type of dyes to DNA are listed in Table 2. The set of cyanine dyes is useful for probing DNA molecular recognition when the duplex is exposed to different environments and forces.

Table 2Binding affinities to DNA of oxazole yellow dyes.

	Charge	K_a^b (M^{-1})*
YO	+1	$1.0 \cdot 10^6$
YO-PRO	+2	$1.6 \cdot 10^7$
YOYO	+4	$\sim 1 \cdot 10^{10}$

* K_a^b (M^{-1}) – binding constant

Since intercalation is force-controlled and is driven by the equilibrium of the system, it can be a reversible process. As expected for the cationic YO-based dyes, the DNA affinity decreases[39] when the ionic strength is increased; consequently, the rate of dissociation is also increased[40]. An interesting feature of the YO-type dyes is strong fluorescence upon binding to the DNA duplex (enhancement by up to 3200-fold[37] as compared with a dye without DNA).

In contrast, no emission enhancement is observed in the presence of ssDNA. Strong fluorescence emission upon interaction with DNA is related to intramolecular rotation between the quinoline and the benzo-oxazole moieties, and this is suppressed when the YO chromophores slide between the DNA bases into the intercalation pocket[41]. Another interesting feature of cyanine dyes is their sensitivity to environmental changes, as evidenced by the red shift they exhibit when binding to DNA[36,41].

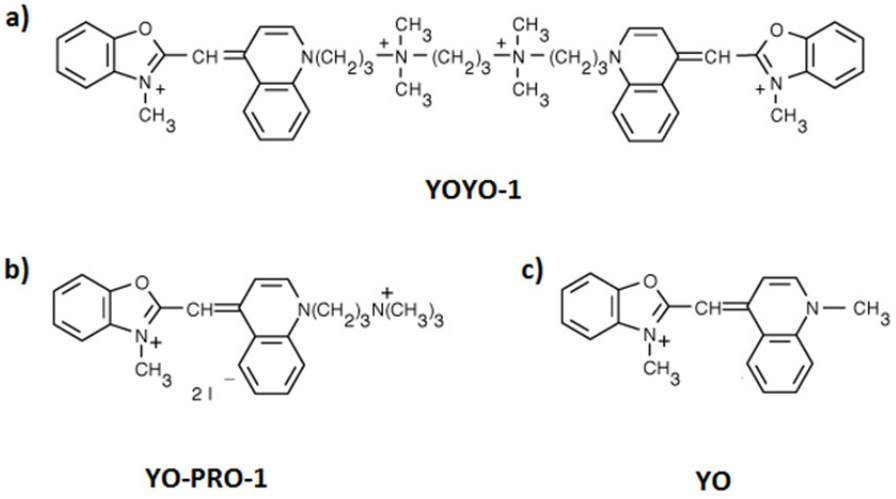

Fig. 2.9 Chemical structures of oxazole yellows from the cyanine dye family. (a) YOYO-1; (b) YO-PRO-1; (c) YO.

YOYO is a particularly useful probe in this respect because the shape of its absorption spectrum is sensitive to the polarity and viscosity of the environment[41]. Given the enhanced fluorescence it demonstrates when the mobility of the dye is restricted and its high affinity for duplex DNA,YOYO has been successfully applied in pre-staining electrophoresis experiments[42], as well as in microscopy[43] and single-molecule studies[44]. In electrophoresis, the strong binding to duplex DNA allows for reductions in dye concentration and avoids the need to soak the entire gel. In microscopy studies, these chromophores possess desirable properties in that the observation time can be extended owing to the high binding constant of the interacting dye molecule. These chromophores have also proven to be extremely useful in single-molecule experiments in which optical tweezers are used to overstretch the DNA duplex. Combining this technique with fluorescence microscopy provides new possibilities

for probing DNA secondary structures. The oxazole yellow dimer YOYO and other intercalating dimers, such as POPO, have been used for this purpose[45], since they bind exclusively to double-stranded regions, whereas rapid dissociation occurs when the DNA strands become separated as a consequence of stretching. This feature of cyanine dyes that allows for visualisation of the kinetic response to a pulling force was applied and revealed that some parts of a long mixed sequence of DNA become single-stranded, whereas in other regions a transition to another conformation occurs, since the intercalators remain bound and emit fluorescence[44]. Even though these powerful techniques did not give a clear answer as to whether long DNA sequences eventually change their conformation to so-called S-DNA or become melted[33], the results of fluorescence microscopy and staining suggest that both processes operate in parallel in different regions of the DNA [Fig. 2.10 a].

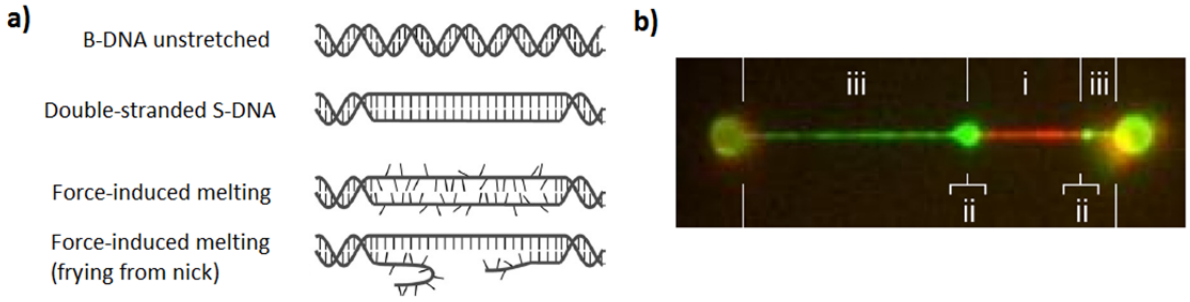

Fig. 2.10 Single-molecule overstretching of DNA. A) Possible transitions of B-DNA double helix resulting in either an S-DNA conformation change or partial melting of some duplex regions upon application of force (in pN). B) Overstretching DNA stained with different dyes: i) intercalation of POPO into a double-stranded region; ii) relaxed single-stranded DNA bubbles labeled with GFP; iii) stretched single-stranded regions connected to the beads[45].

It is necessary to have control over the DNA sequence, and this can be achieved using synthetically designed oligonucletide sequences. It has been shown that stretched short DNA sequences composed mostly of AT start to melt at around 60 pN and eventually denature, whereas GC-rich sequences, under a similar pulling force, undergo a reversibile transition to the S-conformation while mainitaining the duplex form[33]. The questions remain as to whether an overstretched conformation can occur *in vivo* under certain conditions and whether the stretched form can be obtained on a macroscopic scale, at least in the case of GC oligonucletides, so that X-ray scattering or spectroscopic methods could be applied. Alternatively, using intercalation-based experimetns, it maybe possible to probe the nature of

the stretched state. The PVA polymer system can be considered as themethod of choice for this type of study, as will be described and discussed in the *Results* section.

2.5 Ruthenium complexes and threading intercalation

The development of ruthenium complexes was primarily a response of the scientific community to the energy crisis in the 1970s. Ruthenium(II) ion in complex with organic bipyridine ligands was believed to catalyse the reaction of water splitting into hydrogen and oxygen. However, the theoretical predictions were not supported by practical experiments and these projects were mostly unsuccessful. Nonetheless, ruthenium complexes have found applications in many different fields, from solar cells to biomolecular recognition[46].

Short oligonucleotides of defined sequence are nowadays often used in studies of DNA-drug prototype interactions, since the structure can be tuned and more-specific drugs can be designed[47]. Highly specific and enantioselective DNA-binding transition metal complexes constitute an interesting class of markers that exhibit versatile properties, which due to their rigid coordination framework and the possibilities to vary the 3D structure, can be tailored to specific tasks with respect to DNA structure and sequence composition[48]. Ruthenium(II) complexes, in particular those comprising the dipyrido[3,2-*a*:2′,3′-*c*]phenazine (dppz) ligand and derivatives thereof, have been studied intensively due to their sensitive environmental luminescence, which makes them useful as spectroscopic probes for DNA[49]. For example, upon intercalation into DNA, the $[Ru(bpy)_2dppz]^{2+}$complex shows a large increase in luminescence intensity[50], whereas when it is dissolved in polar solvents, such as water, it is completely quenched ("light-switch effect"). The prototype for the newly developed DNA-binding ruthenium(II) complexes was $[Ru(phen)_2dppz]^{2+}$ [Fig. 2.11], which was introduced by Barton and co-workers almost three decades ago[51]. Subsequently, various derivatives have been developed, including dimeric structures in which two monomeric $[Ru(phen)_2dppz]^{2+}$ moieties are connected by a single bond between the dppz moieties, so that the resulting dimeric complex is both bulky and relatively rigid; a substantial thermal opening in the DNA double helix is necessary for entrance to the dppz moiety intercalation site[52]. When the bridging ligand of the binuclear complex is intercalating DNA the two ruthenium centres are positioned in opposite grooves of the DNA helix. This mechanism for docking the ruthenium(II) complex in between the DNA base pairs yields a remarkably high binding affinity for the DNA, with a K_a value of$\approx 10^{12} M^{-1}$ in low salt concentrations (10mM NaCl).

The diazadppz ring system between the base pairs in DNA is also associated with an increase in luminescence (~7000-fold enhancement)[53],as is the case for the monomeric parental compound. This unusual threading intercalation mode of binding reveals an unprecedented sensitivity of the association and dissociation kinetics to the DNA sequence, and such binuclear complexes appear to be promising candidates for developing therapeutics for cancer treatment[54] based on selective generation of cytotoxic singlet O_2. Moreover, the dimeric structures have the unique property of selective sequence recognition for long stretches of AT (>10 bp), a feature that may be valuable for combating certain parasites, such as *Plasmodium* in malaria. These complexes represent a set of promising next-generation DNA markers. *In vivo* studies have revealed that the complexes have low levels of toxicity for cells in the dark, while they mediate photo-activated cleavage of genetic material upon light irradiation, which leads to immediate apoptosis of the cells. All these features make ruthenium(II) complexes useful in biotechnological contexts, both as DNA and RNA probes. Since binuclear complexes have the advantage of strong binding to DNA, it is possible to study the specificity of the complexes for various modifications created in synthetic oligonucleotides, so as to gain a better understanding of the molecular recognition properties of specific hairpins or mismatches in the DNA sequences.

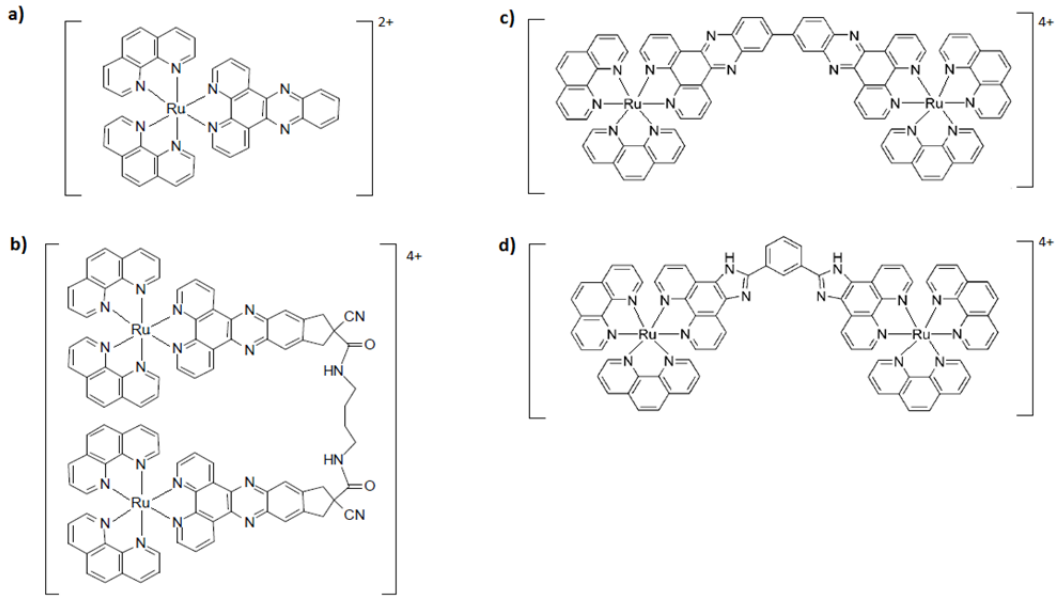

Fig. 2.11 Structures of ruthenium complexes. a) $[Ru(phen)_2dppz]^{2+}$; b) $[\mu\text{-}C4(cpdppz)(phen)_4Ru_2]^{4+}$;c) $[(11,11'\text{-}bidppz)(phen)_4Ru_2]^{4+}$; d) $[11,11'\text{-}bipb(phen)_4Ru_2]^{4+}$.

Coordination of organic ligands, most commonly phenantrolines or bipyridines, to divalent ruthenium ions results in the creation of two distinct enantiomeric forms, the right-handed Δ and the left-handed Λ forms. Both forms of monomeric complexes are known to intercalate DNA, albeit with large differences in binding geometry with respect to the double helix axis. The level of complexity increases when one considers binuclear complexes that are known to thread-intercalate AT, while the interactions with GC remain unclear. Since short oligonucleotides with different modifications are amenable to study using the entire set of spectroscopic tools, including linear dichroism, detailed characterisations of the two enantiomers (ΔΔ and ΛΛ) of the binuclear complex $[(11,11'\text{-bidppz})(phen)_4Ru_2]^{4+}$[Fig. 2.11c] and their interactions with DNA will be presented in the *Results* section of this thesis. Strong electrostatic interactions suppress dissociation of the complex once it is threaded between DNA bases, which facilitates monitoring of the kinetics of the DNA-ruthenium(II) complex interactions. The tetravalent charge is a prerequisite when DNA-drug interactions are studied in PVA, as the binding equilibrium is affected by the polymeric environment and the DNA-drug complexes are generally destabilised due to the low dielectric constant of the surroundings, which decreases the contribution of hydrophobicity to the binding energy[20].

2.6 Nonlinear properties of chromophores that bind to biomolecules

Since Nicolaas Bloembergen carried out his pioneering research in nonlinear optics in the 1960s[55], this field has increasingly attracted attention from the scientific community. Over time, nonlinear optical effects have found many interesting applications. Nonlinear optical properties of certain inorganic crystals like e.g. borates, niobates, vanadates are widely exploited for generation of new laser wavelengths by frequency mixing phenomena, while nonlinear absorption properties of many organic molecules are also finding application in nano-photonics and bio-photonics, Multiphoton absorption (often leading to efficient excitation of upconverted emission) effects in biomolecule-labelling dyes are extensively exploited in various fields, including bio-photonics[56] and nanotechnology[57], as well as in diagnostic and therapeutic applications[58]. The simultaneous absorption of two or more photons that are present in the high-intensity region of a focused laser beam, resulting in high spatial resolution and significant penetration depth (due to the use of low-energy photons outside the absorption edges),allows performing of non-invasive studies *in vivo* without causing damage to biological or other materials[59]. Those features have led to a wide range of

new applications, including photochemical control of drug delivery[60], photodynamic therapy (PDT)[61], and non-bleaching microscopic imaging[62]. Together with nonlinear characterisation of molecules and chromophores, various techniques have been developed. In the late 1980s, W. Webb and co-workers introduced and explained the principles of two-photon excited fluorescence microscopy (TPFM), which produced impressive improvements in fluorescence imaging[63]. The key to this new technique was to increase the contrast obtained by the removal of out-of-focus fluorescent light. Currently, TPFM is used in studies of biomolecules where high resolution and quality are important aspects of the research[64]. A set of standard dyes used in molecular biology and bio-related research was characterised in the context of 2PA cross-sections and two-photon fluorescence excitation[56,65]. To ensure efficient excitation of the dyes, information about the spectral dependence of the 2PA cross-section, $\sigma_2(\omega)$, is required. The value of σ_2 is a measure of the probability of simultaneous absorption of two photons by a molecule, usually expressed in Göppert Mayer (GM) units, whereby $1GM=10^{-50}cm^4s\ photon^{-1}$. In the case of biomolecule chromophores, σ_2 can be determined either from the two-photon excited fluorescence[65] or directly by transmission measurements made using the Z-scan technique[66], which will be described in detail in the *Methods* section, as this is the technique of choice for determining the nonlinear properties of the materials presented in this thesis.

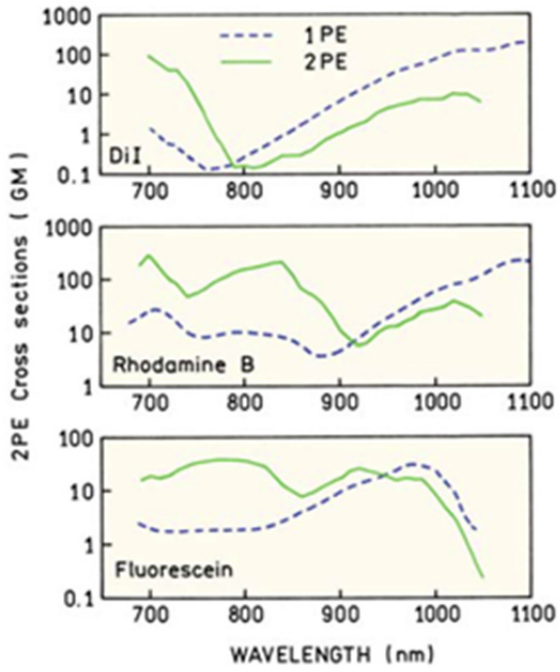

Fig. 2.12 Examples of two-photon absorption spectra (green solid line) of standard dyes used for labelling biomolecules, DNA, and proteins. The one-photon absorption spectra (blue dashed line) are replotted at twice the absorption wavelength for comparison[56,65].

In general, for fluorescent molecules (including chromophores) such as those presented in Figure 2.12, the nonlinear absorption cross-section can be determined by examining the intensity of fluorescence due to two-photon excitation. However, this approach can sometimes be misleading, since both the absorptive and emissive properties of the chromophores are changed upon binding to biomolecules, such as DNA or amyloid fibrils. Therefore, the measured efficiency of two-photon excited fluorescence is actually that of the biomolecule-dye adduct rather than that of the chromophore itself. In addition, often the two-photon spectra do not follow the same trend as the one-photon spectra replotted for the purpose of comparison [Fig. 2.12], which indicates that for multiphoton excitation not only there may be a different origin of the light-matter interactions than in the one-photon process (this is especially important in the case of centrosymmetric structures where the mutual exclusion principle holds, i.e. the excited states that are available in one-photon absorption are two-photon inactive and vice-versa), but also the biomolecule-chromophore interaction must be considered. Thus, it seems more reasonable to first determine the nonlinear absorption coefficients and then measure the two-photon fluorescence in the presence of the biomolecule.

This can be performed with the Z-scan technique. A good example of when an open aperture Z-scan is superior to measurements by two-photon excitation of fluorescence is the analysis of ethidium bromide (EB) and its homodimer [Fig. 2.1]. Both compounds exhibit relatively strong fluorescence when stacked between DNA bases[67]. Regarding the DNA-dye interaction, the dimer has higher affinity (see Table 2),which makes is more convenient to use in molecular recognition studies, although for multiphoton applications it has some disadvantages, and measuring the 2PA by two-photon excitation can give misleading results. Clearly, the 2PA will be higher due to extension of the chromophore by the aliphatic linker, although dimeric dyes are self-quenching owing to the short distance between the monomeric units and it can be problematic to obtain valid results using the two-photon fluorescence approach (the stronger the fluorescence, the stronger will be the quenching).This also explains why results obtained by different techniques may vary with respect to their absolute GM values. Thus intensive research has been conducted on the synthesis of chromophores with high two-photon absorption cross-section (2PA), efficient fluorescence (or luminescence), good photochemical stability[65,68], and the ability to bind specifically to biomolecules. This is the reason why coordination complexes are attracting so much attention. Specificity and enantioselectivity towards some regions of DNA combined with large 2PA cross-sections and the "light-switch" effect makes these complexes promising candidates for various multiphoton-based applications. In addition, the high-level stability of these substitution-inert, luminescent, metal coordination compounds makes them convenient candidates for the development of a new class of nonlinear chromophores.

While standard absorption and luminescence spectroscopic techniques have been widely applied to the ruthenium complexes, 2PA phenomena have not been adequately explored. Girardot *et al.* reported on nonlinear absorption in the region of the metal-to-ligand charge transfer (MLCT) transitions of 1,10-phenanthroline complexes substituted with fluorenes and other derivatives[69],albeit at a single wavelength[70],which limits the conclusions that can be drawn. Another strategy was to study octameric bipyridyl complexes with various metals, and in this case it was concluded that compounds with ruthenium(II) metal have the highest 2PA cross-sections in the intra-ligand charge transfer (ILCT)[71] region, although once again the experiments were performed only at a single wavelength[72]. Ruthenium(II) complexes are also interesting in the context of *in vivo* research because they can act as a source of cytotoxic O_2 species, which is the principle of photodynamic therapy (PDT) whereby energy transfer

between the triplet fundamental O_2 and the excited triplet state generates cytotoxic singlet oxygen. The goal of PDT is to use the phototoxicity of the singlet excited dioxygen to induce apoptosis in cancer cells. In principle, photosensitisers should: (1) be non-phototoxic;(2) possess an amphiphilic character, so as to be able to pass through the membranes; and (3) absorb light in the infrared region (700–1000 nm), within which cells and tissues are not damaged by light irradiation. In this sense, ruthenium(II) complexes, acting as good multiphoton absorbers and emitters when bound to nucleic acids, may serve as precursors for developing next-generation drugs for therapies such as PDT[73]

2.7 Amyloid fibrils

Proteins represent a large and very diverse class of complex organic chemical compounds that are essential for living organisms and for the proper cellular functioning at the molecular level. Proteins, which are composed of one or more long chains of amino acids connected by peptide bonds, have distinct and varied three-dimensional structures, usually containing α-helices and β-sheets, as well as looping and folded chains. They perform a vast array of functions, including the catalysis of metabolic reactions, replication of DNA, and the transportation of molecules from one location to another in the cell. Many of the important molecular components of the body, such as enzymes, antibodies, and haemoglobin, are in fact proteins. The level of complexity associated with protein activities sometimes leads to malfunctioning of the cellular machinery. In some instances, peptides or polypeptides undergo a self-fibrillisation process that leads to the formation of amyloid structures[74]. This process is enhanced by certain mutations that affect protein folding, so as to generate erratic structures and loss of the original biological function(s), and eventually to self-assembled isolable aggregates, which are implicated in various diseases, including Alzheimer's disease, Parkinson's disease, and (contagious) Creutzfeldt–Jakob disease[75]. Amyloid fibrils are generally composed of antiparallel β-sheets that are oriented perpendicularly to the long axis of the fibril, which can be as long as several micrometres but have a diameter of only 8–10 nm[76]. This natural biopolymer aggregate exhibits unusual material properties: a pull strength comparable to that of steel; mechanical shear stiffness similar to that of silk; and high rigidity[77]. Amyloid fibrils have attracted considerable interest in the past few years owing to their proven medical relevance in initialising serious diseases. Therefore, new diagnostic tools are in demand. However, protein fibrils may also be considered as a new class of self-

assembling nanoscale biopolymer material with properties that could be useful in various applications.

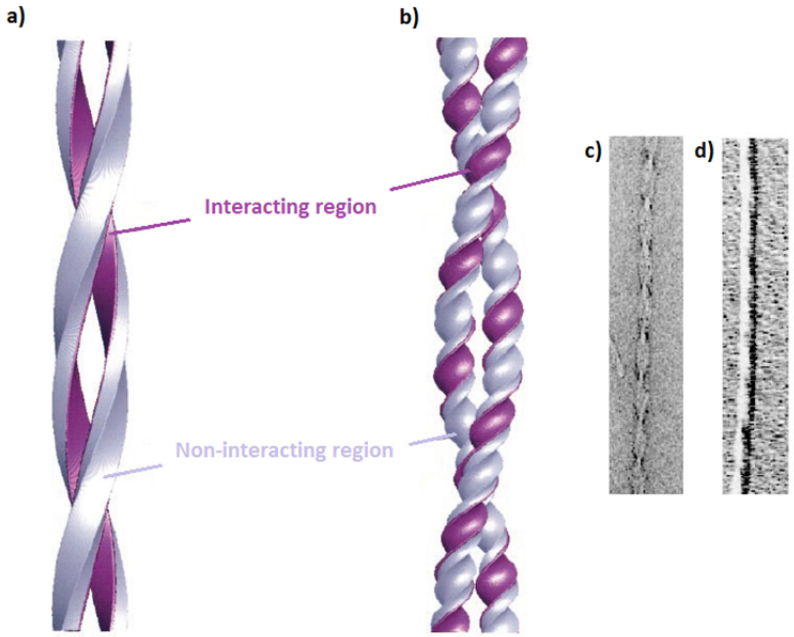

Fig. 2.13 Models and electron micrographs of amyloid fibril structures. a) Simplified two protofilament fibril model showing the interacting regions (purple) and non-interacting regions (grey). b) Supercoiled pair of protofilaments in which the regions involved in packing interactions rotate around each protofilament. The interacting regions are fixed relative to the cross-β-structure and other regions accommodate large loops or folded domains that are not involved in protofilament construction, c) TEM images of amyloid fibrils, which can be visualised either by negative staining with heavy metals or (d) by metal shadowing[76a].

There are only a few methods to test whether proteins are converted into amyloid fibrils. Unfortunately, most of these methods are indirect, such as staining with fluorescent dyes, stain polarimetry, X-ray analysis. It is possible to directly determine the conformation of the proteins using circular dichroism to detect changes in the chirality of the protein upon fibrillisation. Small-angle X-ray scattering is increasingly used to study fibril formation in solution. This is a relatively simple test to determine if a structure contains cross-β-sheets in the fibrils by placing the sample in an X-ray diffraction beam. Valuable information regarding fibril size and shape can be obtained using this method. Proposed model pathways for

fibrillisation suggest that concentration and time are the factors that determine the final quaternary structure of the amyloid[78].

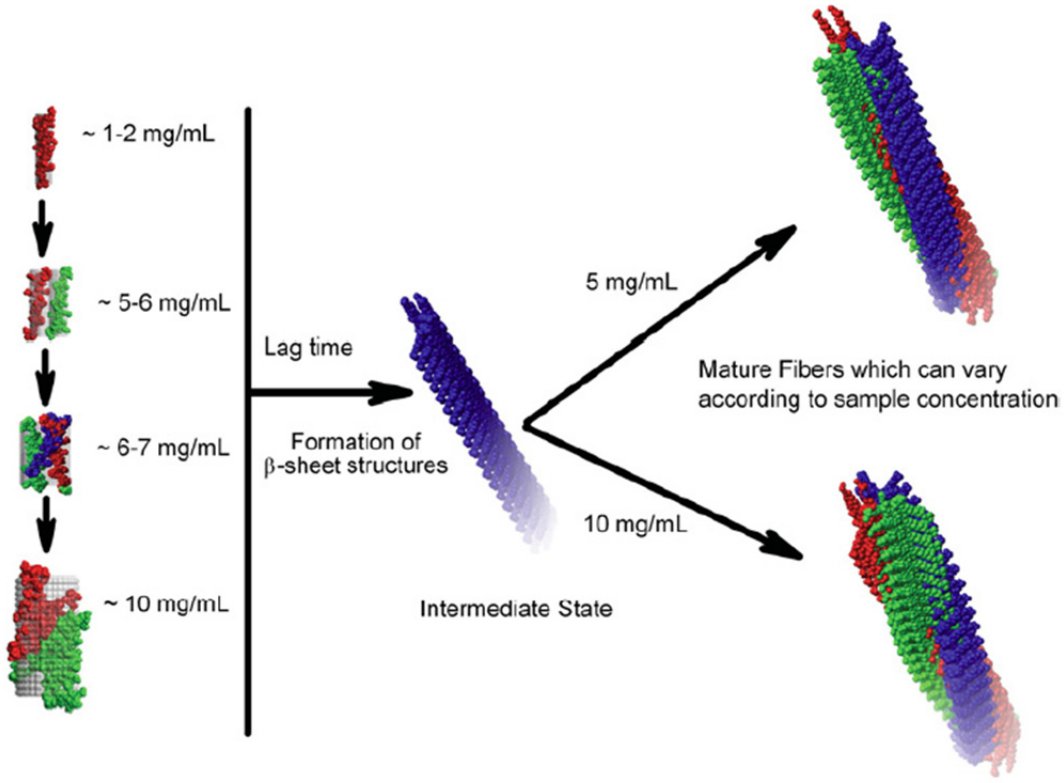

Fig. 2.14 Examples of fibrillisation pathways that are dependent upon protein concentration as a function of time [78].

2.8 Amyloid fibrils-dye interactions

One of the most commonly used methods to detect mutations in proteins and to monitor the formation of amyloid fibrils involves staining with organic chromophores. Unlike studies of DNA-dye interactions, chromophores are not considered as molecules that can be used for targeting specific regions of the genome so as to inhibit cell growth and block the progress of some disease. However, in studies with biological materials, binding molecules share certain properties relevant to their use *in vivo*, i.e., low cytotoxicity, high photostability, long half-life, high quantum yield, and large Stokes shifts upon binding. One approach to monitoring the formation of amyloid fibrils could be the fusion of a protein that forms amyloids with, for example, green fluorescence protein (GFP)[79] or covalently attached molecules, such as the Alexa family of dyes[80]. An alternative strategy is to use dyes that tend to bind *via* electrostatic

interactions and display high affinities for specific protein conformations, such as fibrillar aggregates, which are characteristic of amyloidogenic proteins. Two histological dyes, Congo Red (CR) and Thioflavin T (ThT) [Fig. 2.15], are commonly used, although CR lacks distinct specificity for the fibrillar state. ThT undergoes a red-shift in absorption upon binding to amyloids and exhibits enhanced fluorescence[81]. ThT is a sensitive probe of local environmental changes, and in response (for example) to geometrical confinement, it becomes brightly fluorescent. The underlying mechanism is reminiscent of molecular rotors, in that upon photo-excitation ThT enters a fluorescent, locally excited state and then through internal rotation around the single bond to 90° of the benzothiazole moiety and dimethylaniline group, which breaks the conjugation of the molecule and relaxes it into the nonfluorescent twisted internal charge transfer state (TICT) state. When ThT binds to the amyloid fibril, steric hindrance makes it relatively rigid and prohibits twisting. Thus, the TICT state is prevented and the enhanced fluorescence properties are maintained. The main drawback associated with the use of ThT is that misleading false-negative results may be obtained if no increased emission occurs upon binding to some types of amyloids. Moreover the emission profile of ThT overlaps with the intrinsic fluorescence of cellular components, such as flavins and reduced NAD(P)H[82]. Furthermore, ThT usually competes with polyphenols or curcumin for binding sites (if they are present), thereby reducing the ability of the chromophore to detect fibrillar states. Even though staining of amyloids with organic dyes is not particularly novel, there is an urgent need for new probes that can be used to monitor the kinetics of fibrillation and that avoid the problems associated with the intrinsic fluorescence of cellular components. One of the main goals of research on amyloidosis is to develop synthetic molecules for diagnostic purposes. An interesting perspective would be to implement nonlinear optical tools for probing aggregation using staining agents. As mentioned in the previous chapters, these advanced techniques increase the depth of penetration and decrease the unwanted intrinsic fluorescence from cellular components in the background. Also these techniques are less invasive and more precise in context of diagnostic application. However, the number of water-soluble organic dyes that have reasonable nonlinear optical properties is limited, as the vast majority of standard chromophores exhibit rather weak 2PA and thus have weak excitation properties. Two types of amyloid markers are of potential interest in applications involving the visualisation the fibrillar states: metal-organic compounds [Fig. 2.11 b, c], and a large class of derivaties of stilbene, e.g., Stilbene 420 [2.15 b].

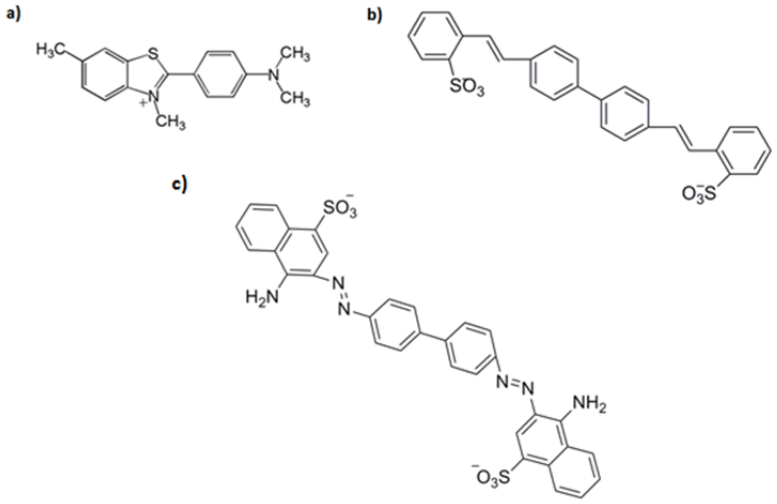

Fig. 2.15 Structures of a) Thioflavin T, b) Stilbene 420, and c) Congo Red.

Many metal-organic compounds possess the unique property of expressing the "light-switch" effect, which is of particular interest in studies of biomolecules. Ruthenium complexes are quenched in a polar medium, whereas they become luminescent in a nonpolar environment. This is the case for DNA, as well as amyloid fibrils, as reported by Cook and co-workers concerning monomeric $[Ru(bpy)_2dppz]^{2+}$ [Fig. 2.11a]. The principle mechanism in the case of amyloids is similar to that for DNA, whereby the planar dppz moiety becomes protected from water molecules upon interaction with the fibrils. The microenvironment around the nitrogen atom at dppz is changed, and luminescent state is favoured. Together with strong nonlinear optical properties and long lifetimes, these are excellent candidates for both detecting and monitoring the formation of fibrils. A second proposed class of molecules based on stilbene is interesting owing to its broad range of possible modifications. Thus, apart from the reasonable nonlinear properties that can be enhanced by elongation of the molecular structure, these compounds can be easily modified with respect to the size and shape of the type of amyloid fibril. It may be possible to increase the affinity and specificity for various conformation states of proteins through structural modifications of these chromophores. In particular, Stilbene 420 [Fig. 2.15 b] is promising, since it has a chemical structure that is similar to that of the well-known amyloid probe Congo Red [Fig. 2.15 c].

3. Methodology

3.1 Linear spectroscopy

Linear spectroscopic phenomena arise from the interaction of a molecule with one photon at a time. Electromagnetic radiation of wavelength λ can be thought of as a wave that is propagating at the speed of light *c* with an electric and magnetic field component oscillating in phase at the frequency ν. The amount of energy carried by a single photon, hν, (where h is Planck's constant) is inversely proportional to the wavelength: $\nu = c / \lambda$, which means that low-energy photons have longer wavelengths and high-energy photons have shorter wavelengths. In this thesis, linear spectroscopy refers to one-photon measurements.

3.2 Absorption and emission of light

Absorption is a process through which matter captures electromagnetic radiation and converts the energy of photons to internal energy of matter. In simplified terms, energy is transferred from the radiation field to the absorbing species. A change in the energy of the absorber, occurring as a transition (an excitation) from a lower energy level (ground state, typically termed S_0 in organic molecules where the lowest state has a zero spin) to a higher energy level (excited states, S_1, S_2…S_x) can be simply described as an energy difference between the two states, such that $\Delta E = h\nu$. Since the energy levels of matter are quantised, only the light of the energy that can cause a transition from one level to another will be absorbed. For molecules in condensed phases the electronic energy levels are, however broadened due to the contributions of vibrational and rotational energy. In practice, transitions between electronic of the most molecules states correspond to the absorption of ultraviolet and visible light, whereas absorption of light at longer wavelengths (infrared) corresponds to transitions between vibrational or rotational states. The discussion of linear spectroscopy in this thesis is focused exclusively on the impact of UV-Vis light irradiation on molecules and their electron distribution following the absorption of photons, in the context of structural and environment (dielectric constant) changes.

In studies on nucleic acids, absorption spectroscopy is often the method of choice to confirm duplex formation by oligonucleotides. The melting or hybridisation of DNA results in distinct changes in the absorption at around 260 nm of DNA, in a phenomenon termed

hyperchromism or hypochromism, respectively. Furthermore, spectroscopic techniques can be used to study biomolecules that bind in different environments, such polymeric matrices, and to determine how this binding is affected by local changes. In general, the absorption can be quantified as the logarithm of light intensity (I_0) before it enters the sample, (the incident light intensity) divided by the intensity of the light of specified wavelength λ that has passed through the sample (transmitted light intensity), expressed as mathematical quantity - absorbance (optical density) as follows:

$$A = \log \frac{I_o}{I} = \varepsilon c l \qquad (1)$$

The absorbance A in the above equation is also also expressed by the Beer-Lambert law, and is thus assumed proportional to the thickness of the sample (optical path length, l), concentration (c) of the absorbing species in the sample, and the extinction coefficient of the molecule (ε).

Further detailed descriptions of the absorption and emission processes are found in the Jabłonski diagram [Fig. 3.1]. After the molecule has absorbed light (i.e., became excited to a higher energy level), there are a number of pathways through which it can return to the ground state. Initially, the molecule rapidly relaxes to the lowest vibrational level of the excited electronic state. Thereafter, the molecule may return to the ground state S_o *via* either radiative or non-radiative processes. The former process is accomplished either by emitting fluorescence in a direct relaxation from the singlet state (a process occurring with no change of spin) or by undergoing intersystem crossing to the triplet excited state (T), which in an analogical way relaxes to the lowest vibrational level and can further convert to the ground state by emitting phosphorescence. A process in which the spin is changed, thus disallowed by selection rules which results in long liefetimes of phosphorescence compared to those of fluorescence [Fig. 3.1]. The diverse pathways for emission allow investigation of different processes, mainly because they are relatively slow in comparison to absorption and any deviation from standard relaxation to the ground state will have an impact on the overall behaviour. In general, the rate of these processes is dependent upon the magnitude of energy gaps between the states and whether the transition is spin-allowed or not. Thus, fluorescence provides a broad range of opportunities to study, for example, molecular interactions or local environmental changes around biomolecules. All the required information can be obtained by

versatile experimental methods based on fluorescence, such as Forster Resonance Energy Transfer (FRET), or by studying the environment-dependent quenching or anisotropy.

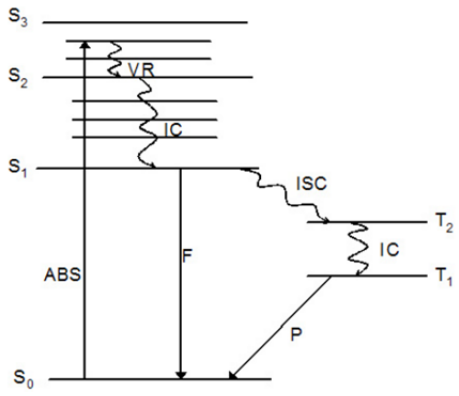

Fig. 3.1 The Jabłonski diagram illustrating the fundamental photophysical processes that occur as molecules undergo excitation by absorption of light (ABS), vibrational relaxation or internal conversion to vibrational ground state.(VR, IC), intersystem crossing (ISC,); fluorescence (F) or phosphorescence (P).

3.3 Photophysical properties of coordination complexes

The photophysical features of metal-organic chromophores can be categorised in terms of two distinct regions of absorption: those due to so-called intra-ligand charge transfer (ILCT), and those due to metal-to-ligand charge transfer (MLCT) transitions. The absorption spectrum is dominated by strong $\pi \rightarrow \pi^*$ (ILCT) transitions, which lie in the UV region, and the spectrum also contains weaker bands at longer wavelengths, which often determine the colour of the metal-organic complexes and which are directly related to $d \rightarrow \pi^*$ (MLCT) transitions. Thus, ruthenium compounds, for example, exhibit a characteristic orange colour. The most striking feature of some of the water-soluble ruthenium complexes [Fig. 2.11] is the “light switch” effect, which relates to quenching in polar solvents and long-lived luminescence in non-polar environments. The explanation offered for this effect is fast hydrogen bonding to the un-coordinated aza nitrogens of the dppz ligand in the excited state. When the dppz moiety slides between the DNA bases into the interior hydrophobic part of the helix, the accessibility to water is restricted and the complexes become more emissive. Exploiting the environmental sensitivity of this phenomenon, information about the binding geometry, as well as local distortions of the DNA helix can be obtained.

3.4 Polarised spectroscopy in studies of biomolecules

Simple absorption measurements provide only limited information about biomolecules and their interactions with chromophores. The use of polarised light of light using the appropriate optics has led to the development of more sophisticated spectroscopic techniques. Among these are linear and circular dichroism, which are based on differences in light absorption for different light polarizations (described in greater detail below). In general, polarised-light spectroscopy yields valuable information about organic molecules (i.e., transition dipole moments) or biomolecules (orientation and conformation of the DNA or amyloid fibrils). It can also be used to investigate biomolecular interactions and to understand biomolecule geometry and how this undergoes changes when the environmental conditions are varied.

3.4.1 Linear dichroism in polymer systems and flow solutions

Linear dichroism (LD) is primarily used to study the structure and functions of orientable macromolecules. LD is defined as the difference in absorbance between light that is linearly polarised parallel ($A_{\parallel}$) and light that is linearly polarised perpendicular ($A_{\perp}$) to the macroscopic axis of orientation.

$$LD = A_{\parallel} - A_{\perp} \qquad (2)$$

Thus, before LD spectroscopy can be applied, the sample must be orientated to some degree. Otherwise, in an ideally isotropic sample, the LD is essentially zero. A non-zero LD is recorded when the transition dipole moments of molecules are somehow anisotropic. The higher the degree of orientation, the larger is the difference between the absorption in parallel and the absorption in perpendicular, which determines the magnitude of the LD signal. If the orientation is not spontaneous, as it is in the case of liquid or solid crystals, some method to induce macroscopic orientation has to be applied. Extensively used are polymer films that can be stretched, thereby indirectly aligning the molecules; alternatively, electric or magnetic fields or flow orientation in Couette cells may be used [Fig. 3.2].

Only a few polymers are available for aligning molecules. For solubilisation of non-polar organic molecules, polyethylene films (PE) are often used. Droplets of the compounds dissolved in chloroform are deposited on the surface of the PE film either before or after

stretching. For slightly more polar molecules, water-insoluble polyvinyl chloride (PVC) can be used instead. Molecules can be also associated with the polymer matrix and polyvinyl alcohol is often used to form composites. This approach is taken when studying polar molecules that are soluble in water or biomolecules, such as DNA, that can be mixed with a viscous PVA solution and then casted onto glass to prepare the film sample. The baseline in such experiments is determined using PVA without loaded sample. PVA, which is a universal host that is transparent at UV wavelengths >200 nm, as well as in the visible region of the absorption spectrum, is ideal for investigating the properties of biomolecules. In this thesis, PVA and the flow orientation method were used for studies of DNA and amyloid fibrils, as well as their interactions with binding chromophores. Briefly, PVA of low molecular weight can be mixed with biomolecular samples, poured on a glass slide, and left to dry (2 days at room temperature in a dust-free environment), so as to form dehydrated PVA sheets. The sheets are further assembled into a stretching device and hydrated into humid films by exposing them for 30 minutes to distilled water or other buffer (see Table 1) in a closed chamber at 100% r.h. at room temperature, which is equivalent to 50% water content in the film. Hydrated films are stretched under the same controlled humidity conditions to a predetermined stretching ratio of $R_s = d_{\parallel}/d_{\perp}$ between the lengths of the long and short axis of the film. In comparison to the Couette cells used for the orientation of long polymers based on the shear gradient between an outer rotating and an inner fixed quartz cylinder, PVA is difficult to use and the method is time-consuming. However, as will be shown in the *Results* section, the PVA method has an advantage over most commonly used flow orientation techniques in that it allows for alignment of short synthetic DNA sequences, thereby opening up new versatile research opportunities for LD applications, since oligonucleotide sequences can be easily designed for the desired type of experiment. Overall orientation can be controlled *via* the stretching ratio, whereas the in-plane transitions of DNA bases are almost perpendicular to the helix axis in fully hydrated films (100% r.h.), and this results in the B-DNA conformation in a polymer environment, similar to what is observed in flow solution experiments. In studies of the interactions between biomolecules and binding dyes or drugs, LD spectra provide information on the orientation of the bound dye relative to the biomolecules axis[83]. However, unlike the Couette cell experiments, in which small molecules cannot be oriented, PVA can align small organic dyes. Thus, competition between the biomolecule and PVA for binding drugs may occur. On the one hand, this entails a serious

limitation for DNA-drug studies in PVA, since most of the dyes are confined in the polymer matrix rather than stacked in intercalation pockets. On the other hand, an unexpected advantage is that drug behaviour can be kinetically monitored by LD when subtle changes are introduced into the system (i.e., a change in the rate of hydrophobic interactions or ionic strength). A viscous polymer environment efficiently slows the response to external variations, and repetitive LD measurements can be used to monitor the behaviour of the DNA and drug with respect to the helix. Dissociation cannot be monitored at an early stage for weakly bound dyes, since the amount of time needed for humidification and making the film elastic in preparation for stretching precludes alignment of the sample in a short time-scale. With stronger binding dyes ($K > 10^{-6}$ M^{-1}), the dissociation process is slowed and it can be monitored by LD. While the first-order dissociation model of $\alpha=1 - e^{-t/\tau 1}$ failed to describe accurately these data, a two-step process describes satisfactorily the LD data[20]:

$$\alpha = \alpha_1 \left[1 - e^{-\frac{t}{\tau 1}}\right] + \alpha_2 \left[1 - e^{-\frac{t}{\tau 2}}\right] \qquad (3)$$

In this equation, α is the total dissociation rate of the dye from the intercalation pockets as a function of time. The α_1 term is the first step of dissociation amplitude, although it usually occurs faster than the experimental delay. Notably, the need for the α_1 term does not stem from the free dye being present at time zero, rather in this case of binding molecules with high K values it means that more than 99% of the dye is bound in solution with polymer before the film is cast. Under such conditions, α is assumed to be zero. The second step (α_2) presents the highest dissociation rate, which is related to the equilibrium of the system, which is reached when the film is undergoing humidification for a certain time period and the dissociation process is most pronounced.

From a technical perspective, a potential problem is one of reproducibility in obtaining films of the same thickness, although this risk could be easily overcome by calculating the reduced linear dichroism (LD^r), which in its simplest case is the LD divided by the isotropic absorption (A_{iso}). A dimensionless quantity, named reduced linear dichroism(LD^r), which depends only on the geometric arrangement of the transition moments relative to the orientation axis and path length (in the case of polymer films, the thickness of the film sample), is no longer taken into consideration.

$$LD^r = \frac{LD}{A_{iso}} = \frac{3 \cdot LD}{A_{\parallel} + 2A_{\perp}} \qquad (4)$$

This holds true for molecules with a uniaxial orientation distribution, e.g., biomolecules aligned in PVA matrix. That the orientation is uniaxial is reflected in the fact that the films are thick (40 µm for a dry film) relative to the helix diameter (2 nm).Thus, LD^r is a product of the orientation factor S and an optical factor O (Note: $A_{iso} = (A_{\parallel}+2A_{\perp})/3$ only holds true for uniaxial orientation).

$$LD^r = S \cdot O = \frac{3}{2} S(3cos^2\alpha - 1) \qquad (5)$$

The optical factor *O* is related to the angle α between the helix axis and the light-absorbing transition moment of the actual chromophore, which could be a DNA base or a DNA-bound dye. The orientation factor $S = ½(3\langle\cos^2\theta\rangle - 1)$ corresponds to the average orientation of the DNA helix in the PVA film, where θ is the angle between the macroscopic stretching direction and the local helix axis of a particular molecule, and where the average applies to all the DNA molecules in the sample (note: the relation $S = ½(3\langle\cos^2\theta\rangle - 1)$ assumes uniaxial orientation distribution for PVA films whereas it is not valid for a flow orientated molecules where a more complex definition with two angular coordination is required to describe the system[4]). The degree of helix orientation *S* is usually calculated from the LD^r values at 260 nm using the average angle α_{DNA} =86° for the DNA bases[84]. The binding angle α_{dye} for a dye with respect to the DNA helix axis can then be calculated from the LD^r value in the visible region of its absorption spectrum.

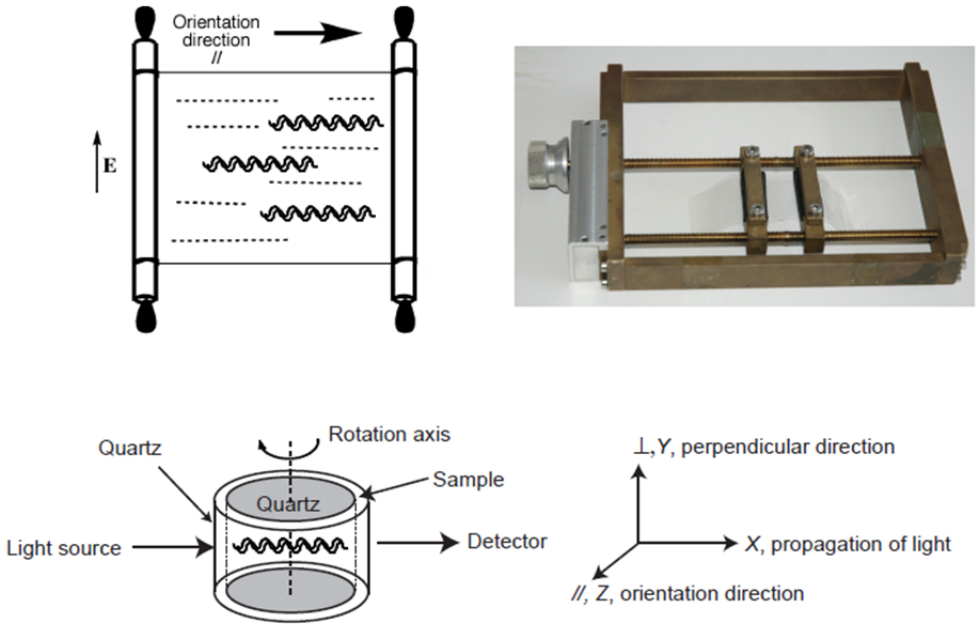

Fig. 3.2 Schematic of a stretched PVA film with a DNA sample and a stretching device (top). The Couette cell for flow orientation experiments [X, Y, Z] is shown, together with a schematic showing how the LD data is collected with respect to light propagation[4].

3.4.2 Circular dichroism

In principle, circular dichroism (CD) is similar to LD, although the output reflects the difference between the absorption of the left (A_L) and right (A_R) circularly polarised light:

$$CD = A_L - A_R \qquad (5)$$

CD spectroscopy is used in a wide range of applications. In studies of biomolecules, it is often used when probing the secondary structures of proteins or nucleic acids. It is also possible to implement UV/Vis CD to investigate charge-transfer transitions, and near infrared (NIR) CD can be used to study geometric and electronic structures by probing metal d→d transitions. Recently, vibrational CD has attracted attention as a technique to study the structures of small bio-related molecules. CD is used more commonly than LD in research laboratories, mainly because there is no need to use complicated orientation systems prior to the measurements. The popularity of CD in the biomolecular field is related to the fact that most biomolecules are chiral, and this is a principle of CD spectroscopy. During measurements in circularly polarised light, the direction of oscillation of the electric field rotates around the propagation

direction, and the tip of the electric field vector is continuously tracing out any chirality in the system. Interestingly, chirality can be induced also in molecules that are originally non-chiral. For example, while isolated DNA bases are achiral, upon formation of the helical structure there is strong CD, the shape of the spectrum of which is dependent upon the DNA conformation, since left-handed or right-handed helices absorb circularly polarised light differently. Another example is amyloid- or DNA-binding drugs, which are often small organic molecules. When free in solution, the CD should be zero, but when an interaction with a chiral biomolecule occurs an induced CD signal (ICD) in the chromophore band should appear. Thus, CD can be used as a direct test for biomolecule-dye interactions and it can complement the LD technique. Regarding binding mode to DNA, ICD can also to some extent distinguish between groove binding and intercalation, as the former exhibits a signal that is an order of magnitude stronger than that of the latter. The formation of dimers or sandwich structures can lead to strong exciton-coupled CD with a typical bisignate-shaped spectrum. Unfortunately, CD is limited to solution-based experiments, and it cannot be applied to polymeric systems, most notably due to the presence of crystalline structures that perturb the light during transmission through the film sample. However, since polymer systems can align short oligonucleotides and small amyloid structures (i.e., prions), LD in combination with CD performed for experiments in solution is a powerful methodology for further bimolecular studies. Another class of molecules that bind to DNA or amyloid fibrils are metal-organic compounds, which can exist in two enantiomeric forms, which are themselves chiral and for which even in the pure non-bound form, it is possible to record CD spectra. If both enantiomers are mixed in racemate then the CD should be zero, and this could be a simple test for the purity of these compounds. Metal-organic chromophores are relative large molecules compared to standard intercalators or groove binders, and they have strong transition dipole moments that overlap with DNA bases. CD is therefore a good method for studying geometrical changes when ruthenium complexes interact with DNA. Threading usually results in strong perturbation of DNA bases in the UV region and a strong positive CD signal in the visible band, whereas external binding or groove binding does not significantly influence the DNA secondary structure[52c,85].

3.5 Emission kinetics in threading intercalation studies

The dimer ruthenium complexes considered here are known to have a high binding constant for DNA owing to their tetravalent charge. However, since these molecules are large

compared to classical intercalators, the DNA duplex has to unwind in order to allow one bulky moiety to pass through the helix. This unique type of DNA intercalation by threading is an extremely slow association process and it is difficult to study by other techniques, such as NMR or crystallography. Since the emission profiles of ruthenium complexes are directly related to the presence of water molecules in the neighbourhood of the nitrogens at dppz, the binding mode can be monitored by continuously exciting the sample and measuring repetitively emission spectra. For ruthenium complexes, it was discovered at an early stage that these chromophores are binding to DNA either externally or in the groove[52a]. However, a threading interaction for dimeric molecules was discovered much later. More recently, slow rearrangement into the final threading mode for dimmers has been investigated in terms of structural modifications, rigidity, and the length of the threading part of the complex[86].The slow association and geometrical rearrangement of the complex from the groove to threading makes this system difficult to control and describe. Even though the CD analysis follows a mono-exponential law, the more sensitive emission kinetics analysis fails to describe the process and it follows a rather multi-exponential law. Detailed examination has shown that the whole rearrangement process is a mixture of different redistributions of the threaded complex over the entire length of the DNA duplex[85]. Thus, it is important to study the interactions of ruthenium(II) complexes with oligonucleotides of defined sequences. Emission kinetics studies have been mostly performed with AT-containing oligonucleotides or mixed sequence DNA species, whereas GC-rich polymers are not used, as the compact structure of GC pairs in DNA probably precludes threading. In particular, in the presence of GC, the emission level is several orders of magnitude lower that that observed for AT-rich sequences. Emission kinetics together with polarised spectroscopy methods (CD and PVA-LD) can provide valuable data for detailed analyses of metal-organic dyes that interact with DNA.

3.6 Gel electrophoresis

Electrophoresis is the motion of dispersed particles relative to a fluid under the influence of a spatially uniform electric field. The migration of positively charged particles is called cataphoresis, while that involving negatively charged particles is called anaphoresis. That particles can migrate when a field is applied was first observed by F.F. Reuss already in 1807. Subsequently, the technique was developed and gel electrophoresis found broad applications in bio-related research for the separation of charged biological macromolecules, such as nucleic acids and proteins. The quality of the separation, i.e., the mobility of the

biomolecules, relies on three important features: the applied force (and thereby the field strength); the overall charge of the biological macromolecules; and the relationship between the size and shape of the molecules and the density of the electrophoretic gel. For long biopolymers, such as DNA, the most commonly used gels contain agarose at different concentrations, chosen so that the gel pores are of the appropriate size for good separation. As short synthetic oligonucleotides are too small to be resolved by agarose gel electrophoresis, polyacrylamide or MetaPhor agarose gels are used instead. To visualize the DNA bands in the gel, fluorescent intercalators are used. One approach is to stain the DNA before loading the sample onto the gel; in this case, dyes with high binding affinities for DNA, such as YO-PRO and YOYO, should be used, to minimise the high dissociation rate. An alternative method is to soak the entire gel in electrophoretic buffer that contains ethidium bromide. Some dyes, such as Cy3, Cy5, and members of the Alexa group, can be covalently attached to oligonucleotides without influencing the DNA secondary structure, as happens in the case of intercalation. Gel electrophoresis has found many interesting applications, including nanotechnologies based on nucleic acids. It has been shown that using this method it is possible to distinguish between different DNA nanoconstructs based on hexagons[87]or DNA-gold/quantum dot nanostructures[34b]. Gel electrophoresis is especially useful in preparation procedure for DNA-gold nanoconjugates. Due to the plasmon resonance of the gold, the DNA does not need to be stained at all, and depending on the nanoconstruct structure or the number of strands bound to the spherical Au nanoparticles, different red bands in the gel can be easily distinguished [Fig 3.3].Furthermore, electrophoresis can be used for the separation of DNA-based nanostructures. This is also a simple and fast method to check the efficiency of hybridisation processes and the yields of formed nanoconstructs. Such analysis can be performed using specialised software (i.e., Gel Analyzer).

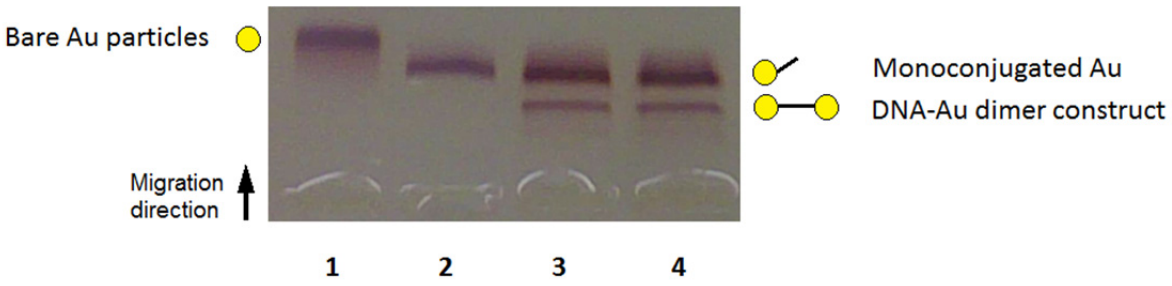

Fig 3.3 Example of gel electrophoresis experiments with DNA-gold samples, showing that the bands for the unconjugated (bare) gold particles (1) have higher mobility than the bands for the DNA-Au monoconjugate (2) and the DNA-Au dimer nanoconstructs (3, 4).

In the work of this thesis, electrophoretic gels were used for two purposes:1) to separate DNA-gold conjugates for further spectroscopic analysis; and 2) to confirm duplex formation by oligonucleotides, which was performed in conjunction with melting experiments.

3.7 Nonlinear spectroscopy

Nonlinear optics (NLO) describes the behaviour of light in nonlinear media, i.e., media in which the dielectric polarisation responds nonlinearly to the electric field of the light. The nonlinearity is typically observed at very high intensities of light, such as those generated by femtosecond-pulse lasers. The availability of appropriate equipment enables studies of light-matter interactions through nonlinear spectroscopy (NLS)[88], in which multiple light-matter interactions can be used to correlate different spectral features and to dissect complex spectra. Thus, NLS-assisted interpretation of the dynamics or the relaxation processes of molecules is possible. NLS provides a way to resolve some of these aspects, as it uses multiple light fields with independent control over the frequency or time-ordering to probe correlations between different spectral features.

In general, NLS is used to refer to cases that fall outside the scope of linear spectroscopy, including: (1) observation of the response of matter subjected to interactions with two or more independent incident fields; and (2) cases in which linear response theory is inadequate for examining how the material behaves, as in the case of very intense incident irradiation[88].

3.8 Principle of the Z-scan technique and experimental setup

Reliable methods for determining the nonlinear optical properties of solid and liquid materials (i.e., nonlinear absorption and nonlinear refraction) have been developed for a wide range of applications, including optical limiting, multi-photon polymerisation, and optical switching. One of the most commonly used techniques is Z-scan, which was introduced in 1989 and subsequently developed by Eric Van Stryland and coworkers[89]. It has become a standard method for measuring nonlinear effects and it is constantly under development. The Z-scan technique is performed by translating a sample through the beam waist of a focused beam and then measuring the power transmitted through the sample. There are many possible configurations of the basic technique, including EZ-Scan, White Light Z-scan, and Excite-Probe Z-scan. In this thesis, only the standard open-aperture (OA) and closed-aperture (CA) Z-scan systems will be discussed [Fig. 3.4]. The two measurable NLO effects detected by Z-scan are nonlinear refraction (NLR) and nonlinear absorption (NLA). The parameters characterizing these effects are associated with the imaginary and real part of the third-order nonlinear susceptibility, respectively, and provide important information about the properties of the material. Z-scan experiments have been carried out using a laser system that consists of a Quantronix Integra Ti-sapphire regenerative amplifier operating as an 800-nm pump and a Quantronix Palitra-FS BIBO crystal-based optical parametric amplifier. This system delivers wavelength-tuneable pulses of ~130 fs in length. For the NLO experiment, the liquid samples are placed in a 1-mm path length Starna glass cuvette, stoppered, and sealed with Teflon tape. Results obtained for the cells that contain solutions are always calibrated against Z-scan measurements performed on a fused silica plate and compared with the measurements carried out on an identical glass cell filled with the solvent alone. The output from the Palitra apparatus in the range of 460 nm to 1100 nm was appropriately filtered using wavelength separators and colour glass filters, to remove unwanted wavelength components, attenuated to the μJ/pulse range, and used as the excitation source for simultaneous recording of standard OA and CA Z-scan traces. In the case of biological materials or water-soluble chromophores, the measurements were performed at wavelengths up to 1100 nm, since at higher wavelengths water-based buffers absorb the light. Briefly, in the standard measurement [Fig. 3.4], the laser beam was focused to provide a focal spot in the range of $w_0 \approx$ 25–50 μm (giving the Rayleigh range, which was always well in excess of the total thickness of the cell and the reference silica plate) and the cuvette was made to travel in the *z*-direction, typically from -20 mm to 20

mm. The data were collected using three InGaAs photodiodes to monitor the laser input, the OA signal, and the CA signal, respectively. The outputs were fed into three channels of a digital oscilloscope and the data were collected using Labview software designed for that purpose. The traces of the CA and OA scans obtained by dividing each of them by the laser input reference were analysed with a custom fitting program[90]. The real and imaginary parts of the second hyperpolarisability, γ, of the solutes were computed with the assumptions that the nonlinear contributions of the solvent and the solute were additive and that the Lorentz local field approximation could be applied[91]. To handle the data from the Z-scan measurements, the results have been extrapolated to a pure material, excluding nonlinear effects from the solvents. In this thesis, the focus is on measuring the nonlinear absorption coefficient using the OA. The calculated values for two-photon absorption cross-section are qualitatively compared. A useful comparison of the merits of various nonlinear absorbers can be obtained by scaling the two-photon absorption cross-section using the molecular weight M, i.e., by comparing the σ_2/M values.

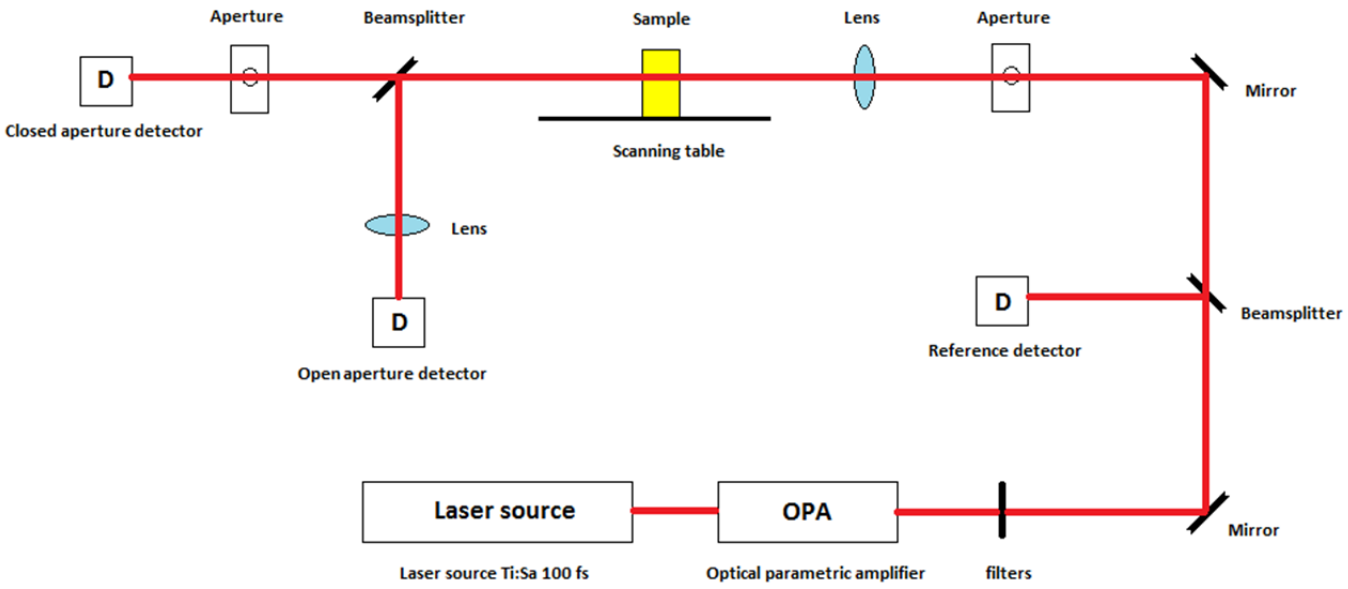

Fig. 3.4 Experimental setup for Z-scanning to measure the open-aperture and closed-aperture signals.

3.8.1 Closed- and open-aperture Z-scanning

The standard "closed-aperture" Z-scan apparatus determines the nonlinear refractive index of the medium, n_2. The transmittance of the sample through the aperture is monitored in the far field as a function of the position, z, of the nonlinear sample in the vicinity of the linear optics

focal position. The required scan range in an experiment depends on the beam parameters and the sample thickness, L. A critical parameter is the diffraction (Rayleigh) length, z_0, of the focused beam, which is defined as $\pi w_0^2/\lambda$ for a Gaussian beam, where w_0 is the focal spot size (half-width at the $1/e^2$ maximum in their radiance). Here, only thin samples are considered and the mean thickness of the glass cuvette L is less than the Rayleigh length, $L \leq z_0$. Thus, the sample in the intense laser beam starts self-focusing or self-defocusing depending on its position with respect to the lens and the third-order effect of nonlinear refraction is either positive or negative. The normalisation is performed in such a way that transmittance is unity for the sample far from a focus where no nonlinear response can be detected (i.e., for $|z| >> z_0$). The positive lensing in the sample placed before the focus moves the focal position closer to the sample, resulting in greater far-field divergence and reduced aperture transmittance. In contrast, with the sample placed after the focus, the same positive lensing reduces the far- field divergence, allowing for increased aperture transmittance. The opposite phenomenon is noted for a self-defocusing nonlinearity, $\Delta n < 0$. A typical closed-aperture Z-scan output for a thin sample that exhibits nonlinear refraction is shown in Figure 3.5A. To simplify the data analysis while accurately determining the nonlinear coefficients n_2 and β (the nonlinear refractive constant and the nonlinear absorption coefficient), some assumptions are necessary. Considering only thin samples in this thesis, we can assume that neither diffraction nor nonlinear refraction affect the beam profile during the measurement. This simplification establishes an equation for calculating the refractive index n_2:

$$\Delta\Phi = \Delta n(I)L \qquad (6)$$

where L is the propagation depth in the sample, and for third-order nonlinearities:

$$\Delta n = n_2 I \qquad (7)$$

Where n_2 is the nonlinear refraction index and *I* denotes the intensity of the laser beam within the sample.

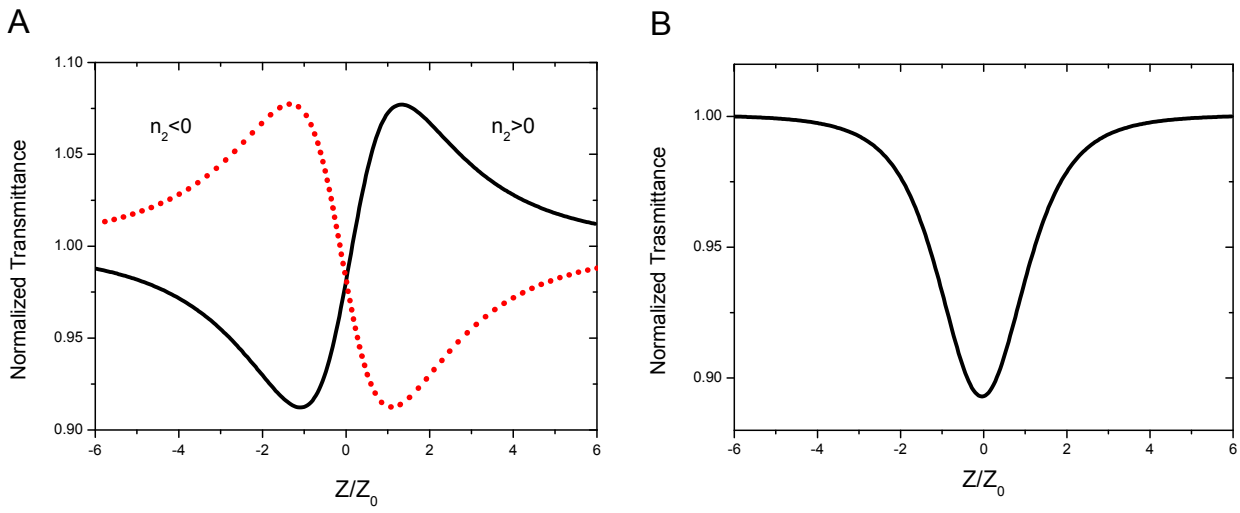

Fig. 3.5 A) A typical closed-aperture Z-scan for positive (solid line) and negative (dashed line) third-order nonlinear refraction coefficient n_2; and B) an example of an open-aperture Z-scan.

In the case of aperture absence or if the aperture is completely open, all the light is transmitted and collected by the detector (aperture transmittance S=1), which entails insensitivity to any nonlinear beam distortion due to nonlinear refraction. Such a scheme is referred to as an "open-aperture" Z-scan [Fig. 3.5B], and it is used for measuring the nonlinear absorption (Δα) of a sample.

$$\frac{dI}{dz'} = -\alpha(I)I \qquad (8)$$

where α(I) generally includes linear and nonlinear absorption terms, and for third-order nonlinearities (Δα) this gives:

$$\Delta\alpha = \beta I \qquad (9)$$

where β denotes the third-order nonlinear absorption coefficient, which for ultrafast NLA is mostly due to two-photon absorption (2PA), but in general can also contain contributions from higher-order absorption and from absorption saturation (SA) or reverse saturation (RSA).

3.9 Two-photon absorption

Two-photon absorption (2PA) follows the principle described previously for one-photon processes (OPA). The only difference in the Jabłonski diagram is that instead of one-photon absorption the excited state is reached upon the simultaneous absorption of two photons of identical or different frequencies. The energy difference between the involved lower and upper states of the molecule is equal to the sum of the energies of the two photons. Two-photon absorption is a third-order process that is dependent upon the square of the light intensity, and it is usually much weaker than linear one-photon absorption. In the simplest 2PA process, if the same excited state can be reached by both OPA and 2PA, the wavelength of absorption in the case of 2PA is shifted towards longer wavelengths by a factor of two. While the nonlinear phenomenon of 2PA was originally predicted and explained in theory by Maria Göppert-Mayer, it was only confirmed experimentally a few decades later when the first lasers were applied with sufficient power. The strength of 2PA is typically expressed as a two-photon absorption cross-section having units of cm^4s $photon^{-1}$ or GM.

3.10 Two-photon excitation and emission processes

The term two-photon excitation refers to process that is in principle two-photon absorption, but in this type of experiment the goal is to measure emission that results from this absorption. Upon excitation with two or more photons and depending on the wavelength, the sample emits a photon of fluorescence. Emission may be recorded by a detector positioned perpendicularly to the excitation beam. When the laser power (and thus, the light intensity) is sufficiently high, an amplification of emission can occur, which can be described as a cascade of emission from dye molecules in the excited state that are stimulated by the spontaneous emissions linked to the decay of other molecules from an excited state. Thus, it is not purely spontaneous phenomenon, but rather involves spontaneously emitted photons that are amplified by further coherent, stimulated emission. The amplification substantially changes the emission spectrum, which no longer resembles one-photon emission but rather is very narrow and sharp.

4.Results and Discussion

4.1 The structure of DNA in PVA (Papers I , II, III)

DNA incorporated into PVA has been already studied extensively by others. Polymer matrix has been used to align long and sonicated DNA for linear dichroism studies in which the structure and conformation were carefully analysed[19,83-84,92].

In this thesis, a similar system was used to study DNA alignment using repeating linear dichroism as a function of time under conditions of different ionic strength. Aligned DNA exhibits negative LD with a maximum around 260 nm, depending on the conformation. Figure 4A shows how the corresponding LD spectrum evolves over time after the humidified PVA film was stretched to R_s = 1.5 at a low salt content of 2 mM NaCl (note: the salt concentrations shown are for the PVA solutions, not the films). That the LD has a negative value indicates that the DNA helix axis is more or less aligned with the direction of film stretching, in agreement with previous reports[92].Figure 4A also shows a slight shift in the position of the LD minimum, starting at 261 nm after 5 minutes and reaching a final position at 258 nm at the end of the equilibration. This observation confirms that the DNA secondary structure converts at an early stage from the A-form in the partially hydrated PVA film to the B-form DNA in the fully humidified films[84]. PVA itself exhibits a positive LD value as the films are stretched [Fig. 4D]. The amplitude is one order weaker than that measured in samples with DNA. Relative humidity, ionic strength, and stretching do not affect the shape of the LD spectrum nor its amplitude [Fig. 4D]. Nevertheless, to obtain pure DNA signal spectra from samples with DNA, the spectrum of PVA itself is always subtracted. In Figure 4C, the solid circles represent the amplitude of the PVA-LD (at 350 nm, a wavelength that DNA does not absorb), which increases over time post-stretching, and the solid squares represent the amplitude of the (negative) DNA LD at 258 nm, which evolves over the same time span. The LD amplitudes of the PVA and DNA [Fig. 4 C] increase essentially in parallel over tens of minutes, and they reach their final level about 40 minutes after the film is stretched. Figure 4C also shows the corresponding LD spectrum of DNA when the PVA film contains 17 mM NaCl. The spectrum is virtually time-independent, as compared with the changes seen at 2 mM NaCl (Fig. 4A). Furthermore, the LD minimum reaches 258 nm already after a few minutes. A plot of the LD amplitude at 258 nm versus time (open squares

in Fig. 4C) confirms this time-constancy, and a plot of the LD for the PVA matrix (open circles) reveals that it is as constant as the LD of the DNA. These results indicate that DNA has the ability to respond quickly to external conditions in the polymer matrix if the ionic strength is sufficiently high [Fig. 4B]. However, it is important to note that the LD of DNA at 17 mM NaCl is about five-fold lower than the final LD of DNA at 2 mM NaCl. These preliminary observations suggest that a viscous PVA matrix is an interesting system for studying the kinetics of DNA alignment. As shown in Figure 4A and B, ionic strength plays crucial roles in DNA stability and order of orientation. In low-salt concentrations, DNA is stiffer and its persistence length is greater, so it adjusts more slowly to the stretched matrix. In addition, a conformation change from A-form to B-form DNA is observed with time of hydration, which confirms that the amount of water in the hydration shells around the DNA changes when the film sample is exposed to an environment of high relative humidity. At higher salt concentrations, the DNA is more elastic and it responds almost immediately to stretching and hydration. It seems that a sufficient number of water molecules are rapidly attracted, and the intermediate state of the A-conformation is not detected under conditions of dehydration; a stable LD signal at 258 nm indicates that the B-form of DNA is immediately adopted. In conclusion, it can be stated that lower ionic strength retards the kinetic changes in the PVA matrix, thereby making it easier to monitor, whereas the eventual outcome appears to be the same as that obtained in a high-salt environment with the B-type of DNA conformation.

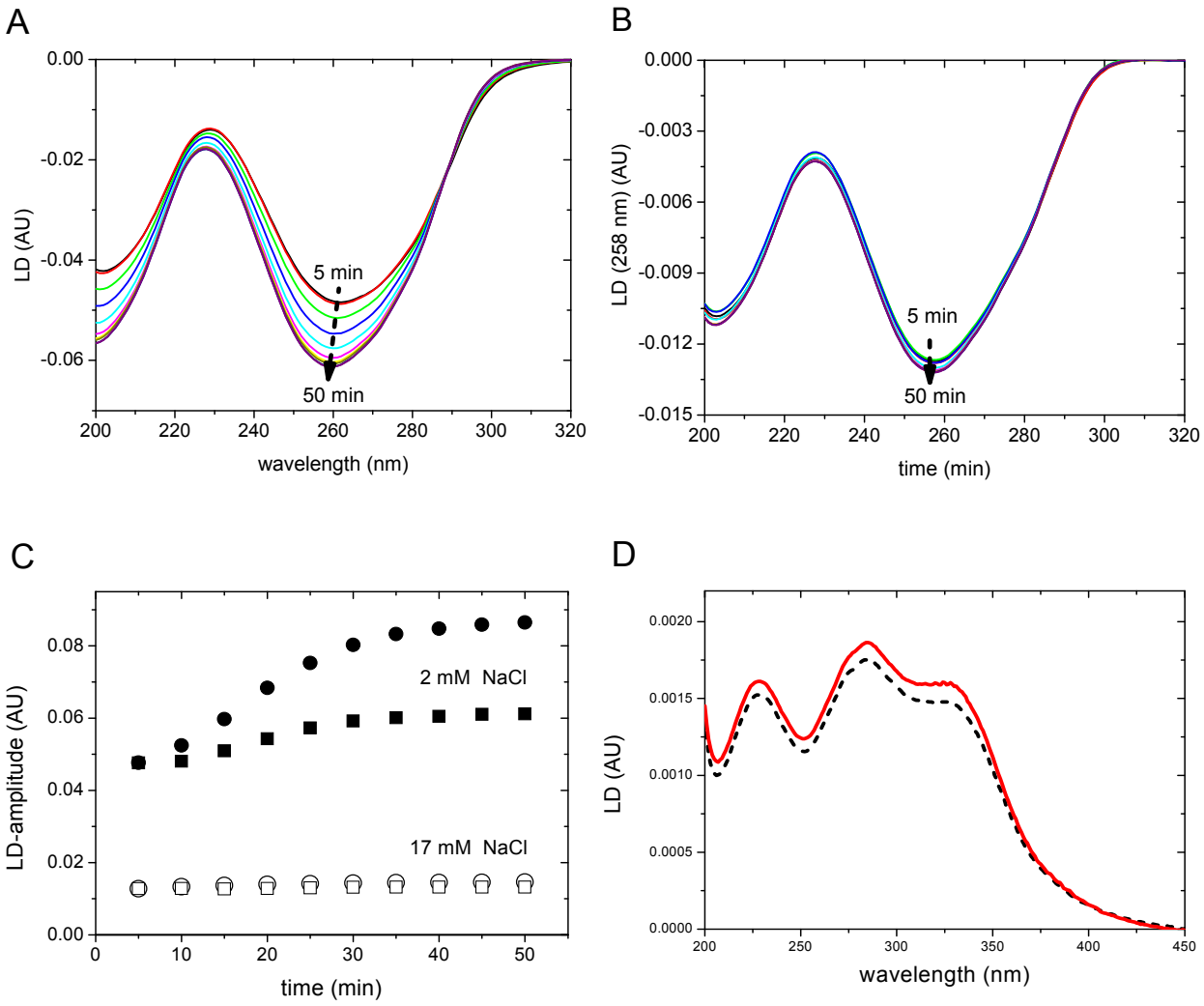

Fig. 4 Time-dependence of DNA alignment in stretched PVA films. The initially dry films were humidified for 15 minutes and then stretched to R_s = 1.5 (at time zero). The PVA-DNA solution samples contained A) 2 mM NaCl and B) 17 mM NaCl; C) LD amplitudes versus time in the PVA-DNA samples that contained 2 mM NaCl (solid symbols) or 17 mM NaCl (open symbols). The squares show the amplitude of the (negative) LD of DNA at 258 nm, and the circles show the amplitude of the (positive) LD of PVA at 350 nm, scaled to coincide with the LD of DNA at time zero. (D) LD of stretched PVA, which was itself equilibrated at two different relative humidity levels. 100% r.h. (red solid line) and 75% r.h. (black dashed line), showing a positive peak at 280 nm and resistance to hydration conditions.

In the next step, studies of the properties of DNA in PVA were carried outusing short oligonucleotides. A set of single-stranded (ss) and double-stranded (ds) oligonucleotides of mixed sequence and of various length (range, 10–60 bases) was used. The ssDNA or dsDNA

was incorporated into PVA and stretched either at 100 % r.h. or 75% r.h. in a closed humidity chamber in which various saturated salt solutions were placed at the bottom (see Table 1). All the samples for LD measurement were dissolved in 2 mM NaCl, since 1) ionic strength is an important factor stabilising the DNA secondary structure in PVA, and 2) in low-salt situations, slow subtle structural rearrangements can be recorded and monitored by LD.

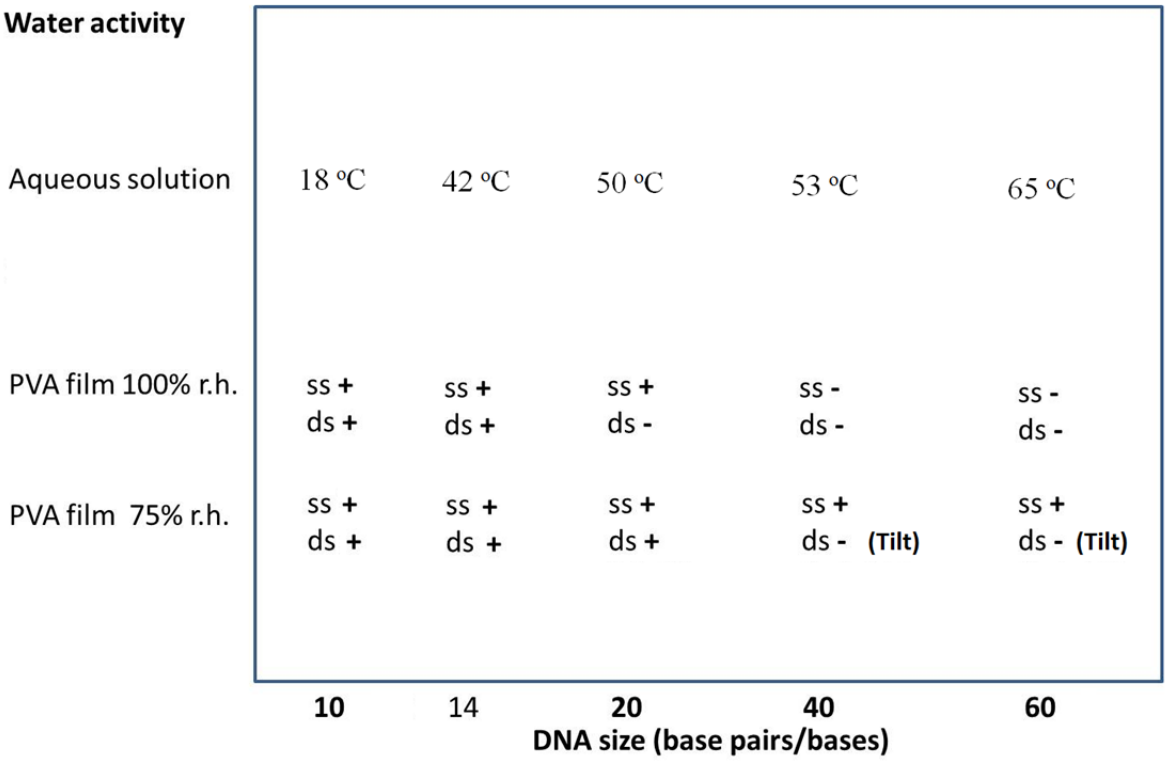

Fig. 4.1 Overview of LD results (LD sign: + or - ; and indication of base tilt) of single-stranded (ss) and double-stranded (ss) oligonucleotides in a stretched humid PVA matrix that contained low-salt conentration (2 mM NaCl in PVA-oligonucleotide solution), at 20°C and r.h. of 100% or 75%. The melting temperatures in 2 mM NaCl aqueous solution are also indicated.

In this low concentration of salt, the shortest 10-mer oligonucleotide is probably denaturated already in solution at room temperature. Indeed, the LD of PVA experiments showed positive signals for both dsDNA and ssDNA, confirming the lack of helical structure already in the PVA solution. The LD results indicate that each nucleotide is oriented independently in line with the polymer chains, more or less resembling the orientation observed in PVA samples

that contained pure nucleobases[93]. Interestingly, similar spectra with positive LD peaks were obtained in the case of the longer 14-mer oligonucleotide, which is more stable due to its high GC content (64%) and the fact that (unlike the 10-mer duplex) it does not melt in a low-salt solution. However, the LD of PVA results indicate the presence of destacked nucleobases, which probably occur during the early stages of film sample preparation when the PVA-14mer DNA sample is cast on the glass slide and the environmental conditions are changing drastically. Elongation of the DNA strands to 20 bp results in negative LD values, as in the case of long calf thymus DNA in a stretched PVA or in a flow oriented solution[4]. The threshold minimum length for orienting oligonucleotides as duplexes in PVA appears to be 20 bp. The calculated LD^r indicates that the helix is in the B-conformation. In contrast, the single-stranded 20-mer oligonucleotide has a positive LD signal, similar to those recorded for the 10-mer and 14-mer oligonucleotides, indicating base separation and strongly tilted bases. A possible explanation for the structural disruption of DNA with strands shorter than 20 base pairs is the low melting temperature, with instability probably also contributed by the lower effective relative dielectric permittivity of PVA (28), as compared with water (78), which affects both the intermolecular and intra-helical interactions of nucleic acids. As a consequence of decreased π-stacking between the bases, which normally provides the hydrophobic environment required for strong inter-base hydrogen bonds, the hydrogen bonds between the bases are breaking up in PVA and the DNA structure is collapsing. Competitive hydrogen bonding to the oxygen molecules in PVA is another destabilising factor.

Longer oligonucleotides were investigated in terms of the stability of the duplex when the water activity was gradually decreased by lowering r.h. in a closed chamber (Table 1). Initially, 40 ssDNA and dsDNA were exposed to 100% r.h. for a specified time period. The LD in both cases showed negative values, indicating that π-stacking between the bases in the 40-mer was sufficiently strong to retain the helical structure in both the ssDNA and dsDNA. These results were confirmed for a 60-mer ss DNA [Fig. 4.2 D, black solid curve] under the same r.h. conditions as used for the 40-mer DNA. To obtain a clearer picture of the situation at 100% r.h., at which the water activity is the highest (50% water content in PVA) and of the structural stabilities of the 40-mer and 60-oligomers, film samples were further exposed to conditions of dehydration.

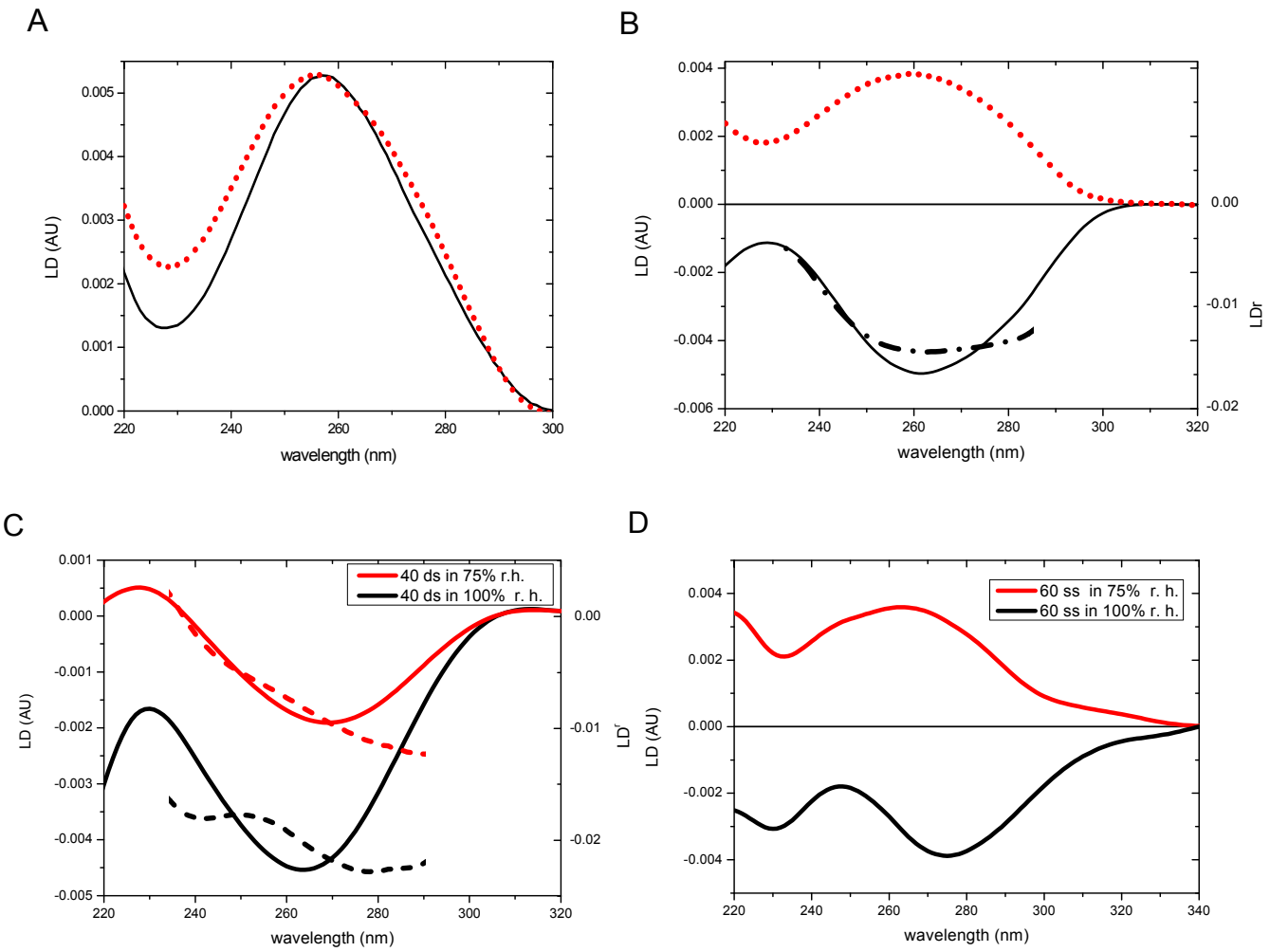

Fig 4.2 LD spectra of single-stranded (ss) DNA and double-stranded (ds) DNA in a stretched humid PVA matrix at 100% r.h. in 2 mM NaCl. A) ssDNA (dotted line) and dsDNA (solid line) of 10 bases/base-pairs; B) ssDNA (dotted line) and dsDNA (solid line) of 20 bases/base-pairs and the LD^r values (calculated from Eq (4); dashed line). C) 40-mer dsDNA in PVA films at the indicated r.h. levels and 2 mM NaCl: 75% r.h. (red solid line); 100% r.h. (black solid line); and LD^r (dashed line). D) LD of a single-stranded 60-mer oligonucleotide at 100% r.h. (red solid line) and 75% r.h. (black solid line).

Negative LD spectra were recorded for the 40-mer dsDNA (Fig. 4.2 C) equilibrated at 75% r.h. The shape of the LD^r for the 40-mer dsDNA at 100% r.h. is similar to that of the long DNA and 20-bp dsDNA in PVA, which suggests a B-type conformation with the nucleobases preferentially oriented perpendicular to the helix axis, while at 75% r.h., the LD^r has wavelength consistent with the A-form of DNA. The negative peaks for dsDNA are

significantly suppressed at 75% r.h., as compared with those at 100% r.h., indicating also a less preferential orientation in addition to the conformational change from the high relative humidity condition. An important message here is that in the case of longer oligonucleotides, the helical structure appears to be retained in a dehydrated environment. However, dehydration clearly affects the structures of single-stranded oligomers that are aligned in PVA [Fig. 4.2 D]: while the single-stranded 60-mer shows negative LD at 100% r.h., and thereby exhibits base stacking perpendicular to the direction of orientation, at 75% r.h. the LD is positive, indicating that the bases are unstacked and oriented in a more parallel fashion with the direction of stretching. In conclusion, the LD spectra of the single-stranded 40-mer and 60-mer DNA species change signs from negative at 100% r.h. to positive when the r.h. is decreased to 75%,and this is due to secondary structural changes induced by the presence of the PVA and the lower water activity [Fig. 4.2 D].

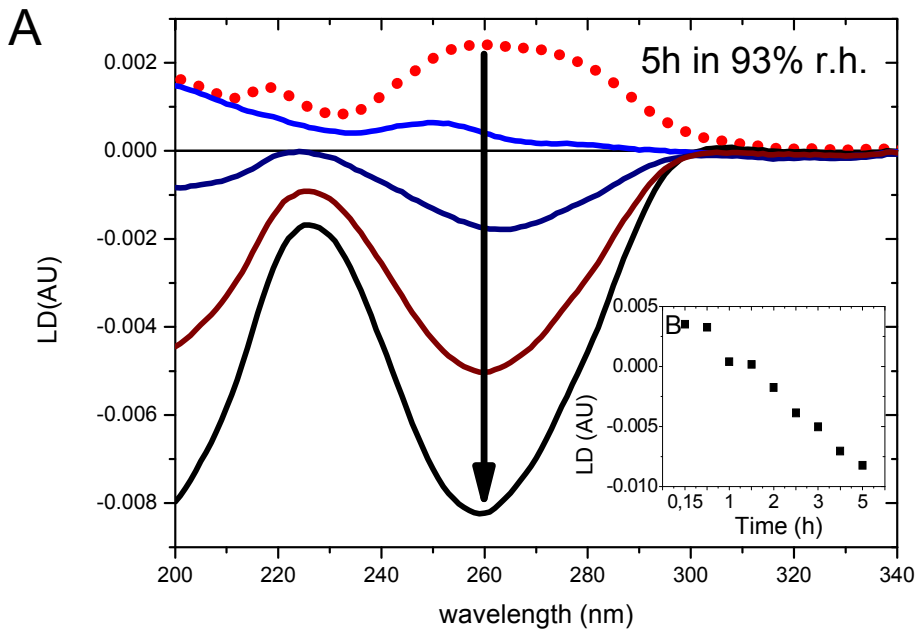

Fig. 4.3 A) LD of a PVA film that contains a 20-mer dsDNA, showing positive LD when equilibrated at 90% r.h. (dotted line) and negative LD when the r.h. was readjusted to 93% and the sample was equilibrated at 93% r.h. for 15, 30,120 and 300 minutes (solid lines), indicating slow rearrangement and renaturation of the double-helix DNA structure. B) Kinetics of reformation of the B-form DNA over a period of 5 hours.

The fact that short oligonucleotides are highly susceptible to the water activity and high viscosity of the PVA matrix permits slowing of the kinetics of reorientation and thereby, monitoring of the conformation changes by LD. This raises the interesting questions as to what is the minimum number of water molecules needed to maintain the DNA in a helical structure in PVA, and whether the transition from double helix to denaturated nucleobases can by recorded using LD. Obviously, while all of the information required to address these questions cannot be obtained directly from LD spectroscopy, much can be learned by combining LD with the Raman and X-ray studies reported by Rupprecht and Franklin[94] on DNA at different relative humidities. For this purpose, the shortest (20-bp) DNA that can be aligned in PVA was examined. Interestingly, the negative LD spectrum obtained at 100% r.h. started to change to a positive spectrum already when the sample was equilibrated (at just below 93% r.h.). Further lowering of the relative humidity and equilibration at 75%, 80%, and 90% r.h. did not make any difference, and all the spectra continued to display a dominant positive LD band with maximum around 260 nm. This is clear evidence that the nucleotides are no longer perpendicular to the DNA helix axis but are instead tilted in the PVA. However, when the r.h. in the closed chamber was readjusted to 93%, the nucleotides reoriented themselves, and the LD spectrum returned from the positive to the negative shape within a few hours [inset B in Fig. 4.3]. This suggests that in the presence of water, the hydrophobic stacking forces force the bases to undergo 'renaturation' into a structure in which their planes are preferentially perpendicular to the direction of the fibre. The sign-flip observed for the LD spectrum of the double-stranded 20-mer at reduced humidity shows how the number of water molecules directly influences the secondary structure of the B-form duplex. Within the range of 75%–90% r. h., the A-form has been reported for long DNA in PVA[95], dehydrated films[96] and fibres[94b]. The observed lack of the A-conformation for the 20-bp oligonucleotide, especially at r.h. levels >80% r.h., where the primary hydration shell around the helix is expected to be fully formed[97], is thus surprising and shows once again that cooperative base-base stacking over a minimum number of bases is a prerequisite for a defined secondary structure, whether it is B-like or A-like. On the one hand, 25 water molecules per nucleotide pair, including the 17 claimed to be bound tightly[96], form a layer that ensures separation from the polymer environment. On the other hand, the PVA matrix may enthalpically wrench off some water molecules that may form hydrogen bonds with OH groups of the PVA. Entropy of dissociation leads to removal of water molecules that are bound less strongly to DNA. In

addition, interactions with the hydrophobic crystalline regions of the polymer can influence the DNA properties and lead to nucleotide separation, as observed in case of oligonucleotides that are <20 bp in length.

When the humidity in the closed chamber is adjusted to 93% r.h. there is a slow (over several hours) reorientation of the nucleotides, consistent with the change in LD sign from positive to negative [Fig. 4.3]. The catalyst for this rearrangement is the number of water molecules present in the system. For pure, humid DNA fibres, according to Rupprecht, there is an average 30±3 water molecules per base pair in the r.h. range of 93%–95% for B-DNA in its primary hydration shell[94a]. These results, together with our present observations, indicate that an increase of 4–6 water molecules per base pair, from 25±2 at 80% r.h. to 30±3 at 93% r.h., may trigger the reformation of the protection layer around the DNA, thereby facilitating further re-hybridisation. Thus, the water structure may be relocated within the system, as the polar and negatively charged sugar-phosphate backbone, which attracts electrostatically Na^+ ions, starts to form a secondary hydration shell, which in presence of 2–4 mM NaCl contains 5–7 water molecules per nucleotide pair[94a]. In total, there are 37±3 water molecules in both shells per base pair at 93% r.h., according to Rupprecht[94a]. Although the exact number of water molecules may vary depending on how it is estimated, the conclusion reflects the lowest number of water molecules required to retain the secondary structure of short DNA in PVA.

Another important aspect is the rate at which the effects of hydrophobic interactions caused by PVA appear. The interactions becoming stronger when fewer water molecules are present in the matrix, and the increased effects of intermolecular (mostly hydrophobic) forces in dehydrated films may explain why A-form DNA is not observed in PVA but instead there is a direct transition from the B-like DNA to the molten form as the r.h. drops below 93%. It is highly probable that dehydration causes reorientation of the phosphate group relative to the helix axis, with as much as 25° between the B and A conformations in humid films of pure DNA[98]. Thus, the balance in the hydration shells could be disturbed and the nucleotides, especially those in short DNA sequences which seem to be more sensitive to hydrophobic interactions with PVA, may start to interact directly with the polymer. The water molecules in the secondary shell are removed and closed in the PVA clusters. In conclusion, the transition from the B-form of DNA to molten oligonucleotides can be induced directly by PVA if there is not enough water present. In this way, the change of solvent from water to the

less polar but still somewhat hydrophilic PVA influences the structural properties and stability of the DNA helix.

As shown previously, the stability of oligonucleotides in PVA increases with the length of the DNA. However, a second crucial factor is water activity. Since the 20-bp DNA was very sensitive to water content variations in PVA, it was interesting to investigate longer DNA sequences under conditions of dehydration. The nucleotides in a 40-bp oligonucleotide remained perpendicularly oriented at 75% r.h., suggesting that the helical stacked structure is adopted also in the dehydrated polymer environment, even though the primary hydration shell is not complete at that r.h. level[94a,97a]. The wavelength dependence of the LD^r calculated for short oligonucleotides is similar to that of long DNA in the dehydrated condition, and this is clear evidence of the presence of the A-conformation of DNA in the PVA, with the nucleobases tilted at an angle of about 20° [84,95], according to the gas model. This indicates that DNA responds to conditions of dehydration by forming stable A-type DNA, while the intramolecular interactions have to be at least equal to or stronger than the competitive dispersion forces of the PVA. Therefore, it seems that the sum of the π-stacking interactions and hydrogen bond formation between the bases creates a net stabilising energy within the double helix of a 40-bp oligonucleotide but not within that of a 20-bp oligonucleotide. Thus, the strength of the intramolecular forces increases with oligonucleotide length, and the last question is whether hydrogen-bond interactions and π-stacking are equally important for helix stability in PVA.

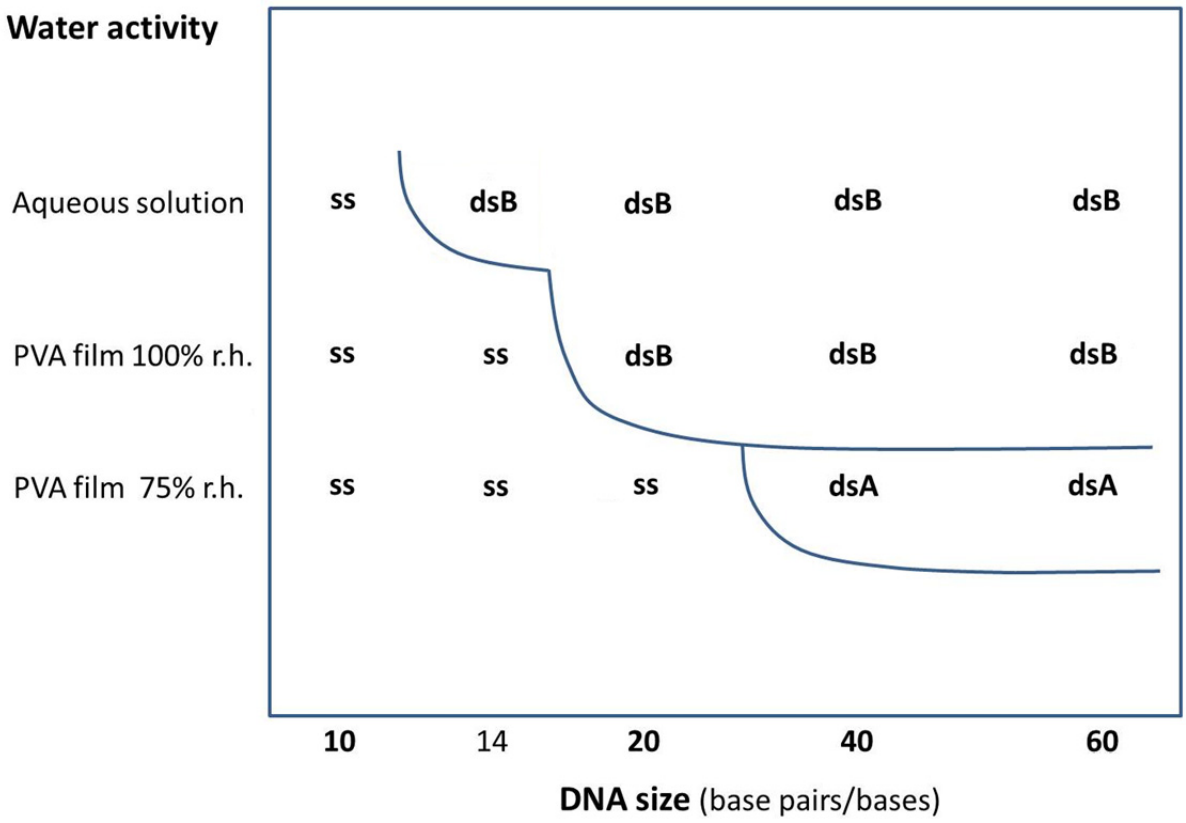

Fig. 4.4 "Phase diagram" illustrating how DNA conformation in the PVA environment depends on water activity and oligonucleotide length. Oligonucleotides at 20°C in 2 mM NaCl.

In order to gain insight into this matter, and to understand the role of stacking interactions in which no hydrogen bonds are present between the DNA bases, a single-stranded 60-mer was aligned and studied. A positive LD was recorded for the 60-base ssDNA at 75% r.h. [Fig 4.2 D], which can be explained by the tilting of the bases due to dehydration leading to partial denaturation[98]. In contrast, a negative LD was observed at 100% r.h., showing that a pile of bases, created by π-stacking, can restrain the helical structure of a single-stranded sequence (even without a complementary strand) if there is sufficient bulk water to contribute a significant hydrophobic stacking effect. Overall, these results indicate that the secondary structures of the oligonucleotides are strongly dependent upon both the length of the DNA and the conditions in the surrounding environment, as schematically shown in the "phase diagram" (Fig. 4.4). This schematic shows that the behaviours of oligonucleotides are similar to that of long DNA in a flow solution or in PVA. An important finding here is that an oligonucleotide as short as 20 bp may be aligned and studied by LD in humid PVA. This

discovery is important because it could open up new opportunities for analysing specific DNA sequences or oligonucleotide-dye/drug interactions, analyses which to date have only been possible with non-specific long DNA[99].

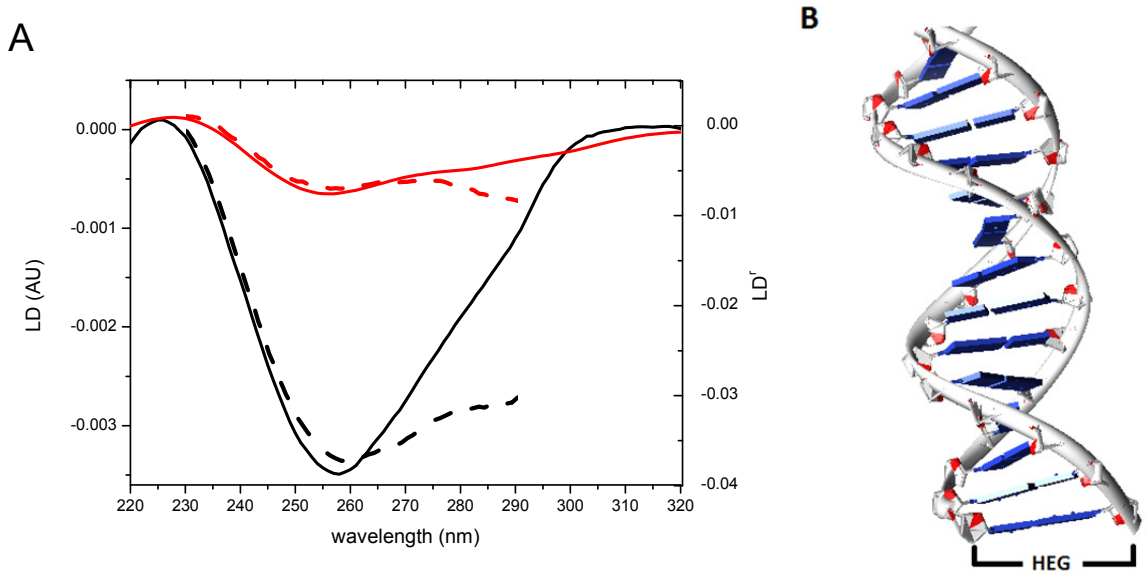

Fig. 4.5 A) LD and LD^r of free GC HEG-linked oligonucleotides in PVA at 75% r.h. (black solid line and black dashed line, respectively) and at 100% r.h. (red solid line and red dashed line, respectively). B) Illustration of hairpin oligonucleotides functionalised with hexaethylene glycol (HEG).

However, to take full advantage of PVA-LD and to be able to study the interactions of defined short DNA sequences with dyes under conditions of lower water activity, the shortest oligonucleotides (20±2bp) that can be aligned must be additionally functionalised and thereby stabilised, so as to retain the helical structure under conditions of low relative humidity. For the purpose of functionalisation, hexaethylene glycol (HEG) was incorporated at the end of the helix, to avoid the fraying ends and thereby improve stability [Fig. 4.5].As a result, the LD showed a negative sign also for the 22-bp GC-containing DNA at both 100% r.h. and 75% r.h. Surprisingly, the LD amplitude was much larger under lower water activity conditions, possibly reflecting the fact that a helix built exclusively of GCs seems to prefer to exist in the A-conformation[12]. In additional, it is a natural response of DNA to adopt the A-form under dehydration conditions, as shown above for long and short DNA sequence in the PVA matrix. However, it is difficult to explain what happens to the HEG-linked oligonucleotide at 100% r.h., bearing in mind that its orientation is several-fold weaker than that of the non-functionalised, mixed 20-bp DNA sequence. Nonetheless, the main goal, demonstrating that

even oligonucleotides as short as 22 bp are amenable to study by polarised light spectroscopy under conditions of low water activity, was achieved.

As for the attempts to utilise and study oligonucleotides that were stabilised by attaching gold particles to each end using multiple thiol anchors[100], it is described in the *Methods* section how such dimeric constructs, with one double-stranded,73-bp DNA and two spherical Au particles, can be made, with each single-stranded construct being purified by gel electrophoresis [Fig. 3.3]. Furthermore, attempts were made to incorporate the dimeric construct into the polymer matrix. Using the standard approach with drying PVA on a glass slide led to aggregation of the gold particles and spontaneous orientation of anisotropic aggregates. In order to retain a random, isotropic distribution of DNA-gold conjugates over the entire PVA matrix, a freezing/thawing[14c] method for PVA deposited on top of a polyethylene (PE) film was developed to prevent complete drying of the polymer with a loaded sample. The PVA layer on PE was successfully applied for orienting the DNA, although the gold particles remained virtually isotropic and no LD was recorded in the visible range of Au absorption. Thus, the PVA/PE system resolves the problem of crystalline domain formation in PVA due to complete dehydration of the polymer upon preparation and it enables investigations of the structure and conformation of an oligonucleotide upon interaction with gold nanoparticles, which can act as anchors in a viscous environment (Hanczyc and Norden, unpublished data).

4.2 DNA-dye binding in a polymer matrix (Papers II and III)

Before presenting the results regarding the interactions of dye molecules with specific sequences on short oligonucleotides, it is necessary to understand how dyes and DNA-dye complexes behave in a PVA matrix. For this purpose, we used a set of cyanine dyes, YO^{+}, YO-PRO-1^{2+}, and $YOYO^{4+}$, which are similar in structure and photophysical properties but have increasing charge and thus, increasing affinity for DNA. The first step was to investigate the chromophores alone in PVA and to discover the influences of the polymer matrix on the photophysical properties of the dyes. The absorption spectra of YO and YOYO were also measured in a 10% aqueous solution of PVA, which was intended to represent a PVA environment that lies between water and the humid PVA films [Fig. 4.6]. Then, measurements were conducted on humid PVA films. In the cases of YO and YO-PRO (Fig.

4.6A), there was a clear tendency towards red-shifting of the absorption maximum when the PVA solution was compared with the humid PVA film. The absorption spectrum of YOYO [Fig. 4.6 B] was more strongly affected by the PVA matrix. In the PVA solution, the spectrum was similar to that of YOYO dissolved in water[41], whereas in the humid PVA film, YOYO exhibited a reversed spectral shape similar to that observed when the dye was stacked between DNA bases. This indicates that PVA itself affects the dye properties, so more detailed studies using LD are necessary to investigate the binding mode and dynamics.

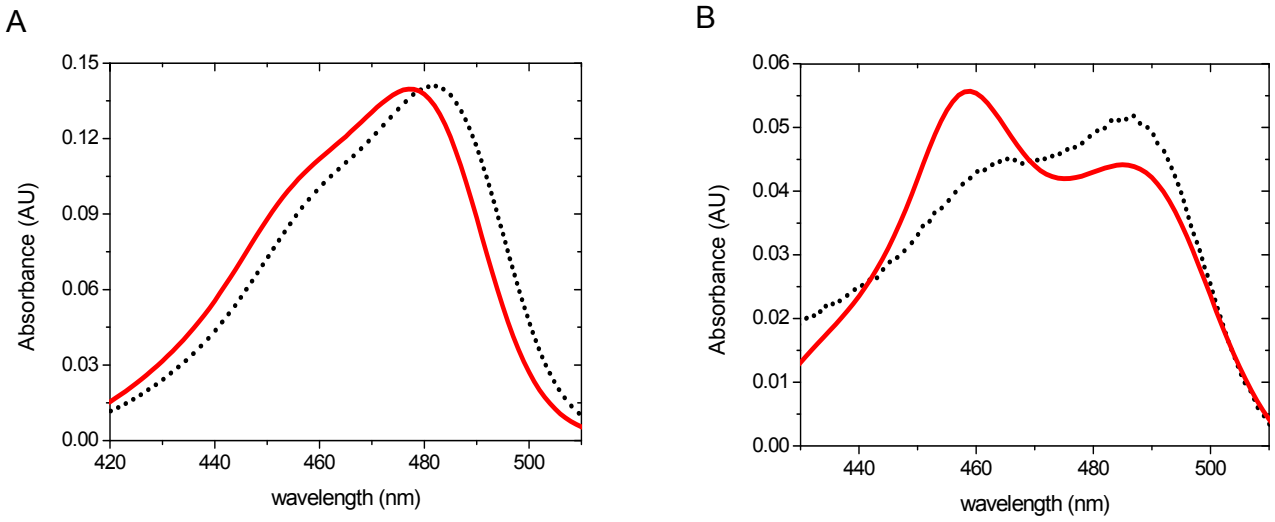

Figure 4.6 Absorbance spectra of A) YO and B) YOYO (no DNA) in a humid PVA film (dotted line) or in a 10% w/v PVA solution (solid line). For the purposes of comparison, the spectra are normalised to have the same peak height.

To investigate the DNA-dye interactions, the complex was aligned in PVA and LD experiments were performed. DNA-YO [Fig. 4.7] was analysed first because it has the lowest binding constant to DNA, which is on the order of those of common staining agents, such as ethidium bromide (10^6 M^{-1}). A positive LD sign in the main absorption band indicates that the long axis of the YO chromophore is aligned preferentially in parallel with the stretching direction. The fact that the long axis of the dye is more or less parallel to the DNA helix and perpendicular to the orientation of the bases means that YO is no longer bound to the DNA in the PVA. If YO had been intercalated between the base pairs its long axis would be perpendicular to the helix axis and its LD would have a negative sign[41]. The positive-sign LD

is instead due to the interaction of YO with PVA; a control experiment with YO alone (no DNA) aligned in PVA also revealed a positive LD in the dye absorption, perfectly overlapping with that of the DNA-YO sample. Repeated measurements showed that there was no change in the LD spectrum of the YO-DNA sample over time.

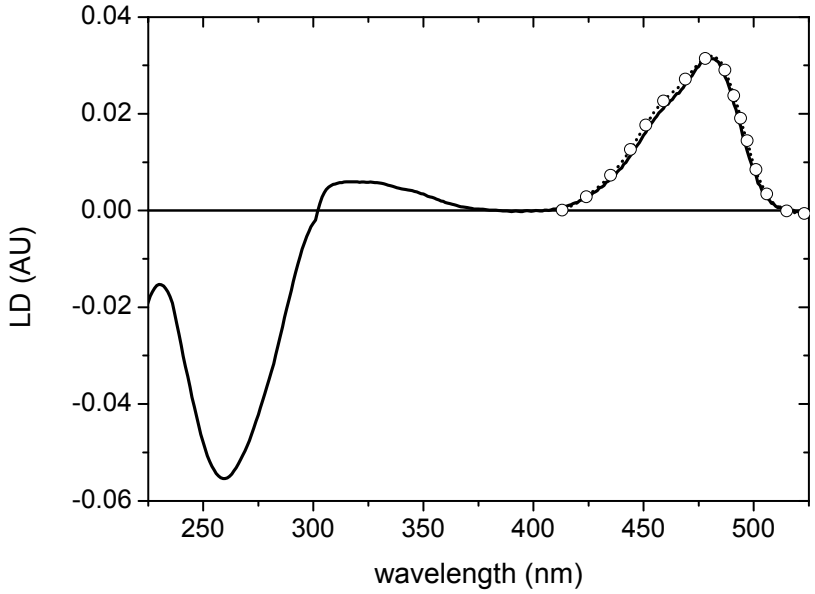

Fig. 4.7 LD spectra of YO/DNA (solid line) and YO alone (dotted line in the visible region of absorption overlapping with DNA-YO band) in a humid PVA film stretched to R_s = 1.5 in 2 mM NaCl.

In contrast to the behaviour of DNA-YO [Fig.4.7], the LD spectrum of YO-PRO in the presence of DNA changed dynamically over time. Figure 4.8 shows the LD spectra recorded after identical DNA-YO-PRO samples had been equilibrated in three separate PVA films for 15 minutes, 1 hour, and 24 hours, respectively. The spectrum recorded after 15 minutes shows a negative LD in the main dye absorption band, which indicates that most of the YO-PRO molecules are still bound to the DNA at this time-point. However, when the same DNA-YO-PRO sample was allowed to equilibrate for 1hour before the film was stretched, the dye LD turned mostly positive, indicating that most of the YO-PRO molecules had dissociated from the DNA in a manner analogous to that of YO [Fig. 4.7]. After 24 hours of equilibration, the LD was fully positive, suggesting complete dissociation, although it should be noted that the dye part of the spectrum still differed slightly from that of YO-PRO alone in the stretched

PVA film. Figure 4.8 also shows that the (negative) LD signal of DNA at 258 nm had increased in amplitude by about 25% after 1 hour. A possible explanation is that due to dissociation of the dye molecules, the helix has to adjust once again to the polymer environment and the bases become oriented more perpendicularly. The complete kinetics of the YO-PRO dissociation was recorded by repeated LD spectra of one and the same humid PVA film as a function of time.

Figure 4.8 B (main panel) shows the fraction (α) of free YO-PRO versus time, as obtained by resolving the measured LD spectra within the first hour into the contributions from the bound and free dye spectra shown in the same figure. Although it is clear that the amount of free YO-PRO increases with time, it is also evident that the time delay in our present protocol (about 15 minutes before the first spectrum) prevents us from monitoring the early stages of the dissociation. The results indicate that the fraction of free YO-PRO dye increases in a two-step fashion, since a mono-exponential decay of bound dye fails to describe the data, whereas a bi-exponential fit works satisfactorily. The two-step mechanism indicates that YO-PRO initially dissociates from the DNA molecule and binds/interacts with the PVA polymers in its vicinity (whereby the dye becomes aligned with a positive LD), and thereafter, the dissociated YO-PRO is transported into the remainder of the PVA film, making available those interaction "sites" in the part of the PVA matrix that lies close to the DNA molecule. Although the first step occurs too rapidly to be monitored by LD, it seems reasonable because it take seconds or less for YO-PRO to dissociate from the DNA in aqueous solution[40]. The diffusion into the rest of the PVA film can be expected to be retarded by the steric or attractive YO-PRO/PVA interactions, which are evident from the alignment of dissociated YO-PRO, so a time-scale of 30 minutes is not unreasonable. The inset of Figure 4.8 B shows that the data can be analysed using a two-step dissociation model according to equation 3 (see the *Methods* section). The fitted parameter values [see caption to Fig. 4.8] reveal that the second step has an amplitude that is twice as large as the first step and occurs with a time constant of about 30 minutes. Together, the two processes contribute a total amplitude of 0.75 to the fraction of free dye, suggesting that a considerable fraction of the YO-PRO remains bound to DNA even after incubation for a long time in PVA. The dissociation of YO-PRO molecules takes hours, and it is a much slower process than that for YO, which is fully dissociated already after 15 minutes [Fig. 4.7]. An important aspect is that dissociation of YO-PRO is not an effect of film stretching *per se*, as the same spectral signs for YO-PRO

dissociation are observed if the LD is measured either on one and the same stretched film over a period of time [Fig. 4.8] or on different films that were equilibrated for different times before being stretched [Fig. 4.8]. The derived LD spectrum of bound YO-PRO in PVA indicates that this dye binds DNA through intercalation. The negative-sign LD excludes other modes, such as groove binding, and is consistent with intercalation. Moreover, comparison of the spectral shapes of free and bound YO-PRO indicates that the vast majority of the dye is bound at the beginning, since it has a more marked shoulder region than the free form.

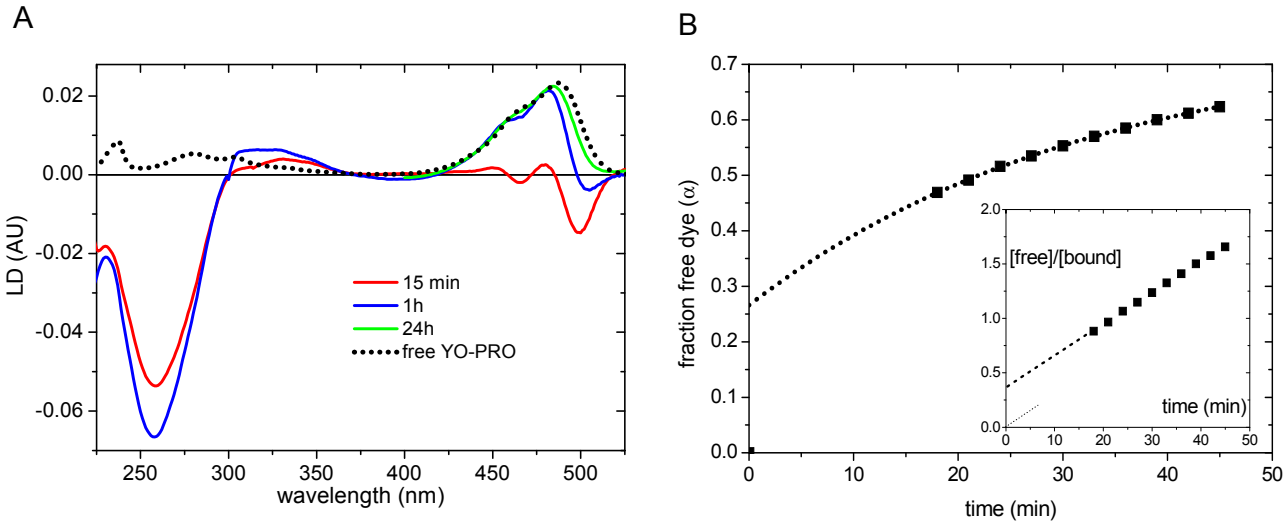

Fig. 4.8 A) LD spectra of DNA/YO-PRO after the indicated times (solid line) and of YO-PRO alone (dotted line) in a humid PVA film stretched to R_s = 1.5 in 2 mM NaCl. B) Fraction α of free YO-PRO versus time, obtained by resolving the spectra repeated every 3 minutes within the first hour.

The last investigated binding chromophore was the tetravalent homodimer YOYO. Figure 4.9 shows the LD spectra of DNA-YOYO and YOYO alone in a stretched, humid PVA film. Free YOYO has a positive LD in the dye absorption band, in agreement with what was previously shown for free YO [Fig. 4.7] and YO-PRO [Fig. 4.8]. When DNA is present, the YOYO dye exhibits a negative LD in the visible region of absorption. Figure 4.9 also includes the LD^r spectrum of the DNA-YOYO sample, and it is evident that although the LD^r varies with wavelength in the DNA band, it is essentially constant in the dye absorption band. The overall LD^r level in the DNA band is clearly less-negative than the LD^r of the dye, as previously

observed for the DNA-YOYO complex in aqueous solution[36]. As discussed below, these observations support the notion that YOYO is intercalated in the DNA in the PVA matrix.

In contrast to that of YO-PRO [Fig.4.8], the LD spectrum of DNA-YOYO (Fig.4.9) was essentially constant over 1 hour. The behaviour of the DNA-YOYO complex over 20 hours was studied by recording the LD spectra on a PVA film, and Figure 4.9 A shows the resulting spectra in the dye absorption band at the indicated times. The observed decrease in LD amplitude over several hours suggests that YOYO eventually dissociates from the DNA, although this dissociation is slow compared to that of YO-PRO. Even after 18 hours, there were no signs of the positive LD of the free dye seen with YO-PRO already after 1 hour. Figure 4.9D shows the relative LD amplitudes versus time, at 258 nm for DNA (spectra not shown) and at 491 nm for YOYO. The LD of the DNA was essentially constant over time, showing that the helix alignment conferred by the stretched PVA matrix does not change appreciably over 20 hours. In contrast, there was a clear decrease in the LD amplitude of YOYO (491 nm) over the same time period. Since there was no change in the alignment of the DNA helix to which YOYO was bound, this decrease in LD at 491 nm can be ascribed to loss of the bound dye. The curve in Figure 4.9 D shows the best fit of the dissociation to a bi-exponential decay. The fitted amplitudes show that a major fraction of the initial LD signal (about 75%) remains at the later time-points.

The high-level stability of the DNA-YOYO complex allowed us to study how the binding of YOYO to DNA depends on the degree of film stretching. Figure4.9B shows the LD spectra of DNA-YOYO when the R_s was increased stepwise from 1 to 2. The amplitudes of the DNA band (around 260 nm) and YOYO (centred at 491 nm) increased as the stretching of the film increased, which was as expected since both the DNA helix and its complex with YOYO should have become better aligned. Binding by intercalation also explains why the amount of bound YOYO increased in parallel with the degree of DNA alignment, since the affinity of intercalators increases when the DNA molecules are stretched mechanically[101]. The peak position of the DNA band remained at 258 nm throughout the stretching experiment, so the degree of helix alignment (S) could be calculated from the LD^r values measured at 258 nm, using $\alpha(DNA) = 86°$ [102] in equation 5. The inset of Figure 4.9B (open symbols) shows how the obtained S-values increase and level off as the film is progressively stretched.

Also included in the inset of Figure 4.9B (solid symbols) is the ratio of LD(491) to LD(258), which increases and levels off with increasing R_s in parallel with the DNA orientation (S,

open symbols). The LD signal at 491 nm is dependent upon how many dye molecules are bound to the DNA, as well as on how well the target DNA helix is aligned. Dividing the LD signal at 491 nm by the LD signal at 258 nm compensates for the latter effect, so the LD ratio can be taken to reflect the amount of bound YOYO. Therefore, the observation that the LD ratio increases with increasing R_s indicates that the amount of DNA-bound YOYO increases as the film is stretched. The data shown in Figure 4.9 were collected over a period of 2 hours, so it is worth noting that any YOYO dissociation that might have occurred in that time span would affect the LD ratio in the opposite direction.

Taken together, the dissociation rates and final LD spectra suggest that the affinity for DNA in PVA increases in the same order as in aqueous solution: YO < YO-PRO < YOYO (Table 2). However, in the polymeric environment, competitive binding of the dye to the PVA affects the noncovalent interactions between the dyes and double-stranded DNA. The estimated equilibrium fraction of PVA-bound dyes (100%, 75%, and 25% for YO, YO-PRO, and YOYO, respectively) indicates that dye affinity for PVA increases in the following order: YOYO < YO-PRO < YO, and it is inversely proportional to that dye affinity for DNA. The binding constant of 10^6 M^{-1} for YO means that more than 99% is bound in aqueous solution at the used DNA and dye concentrations, in contrast to the 100% of YO that is DNA-dissociated and instead bound to PVA in the polymer environment. A similar destabilisation of the DNA complexes with YO-PRO and YOYO in PVA is evident in that both dyes dissociate and start interacting with the polymer to a substantial degree in the films (75% and 25%, respectively), despite their higher binding affinities to DNA in aqueous solution (Table 2).

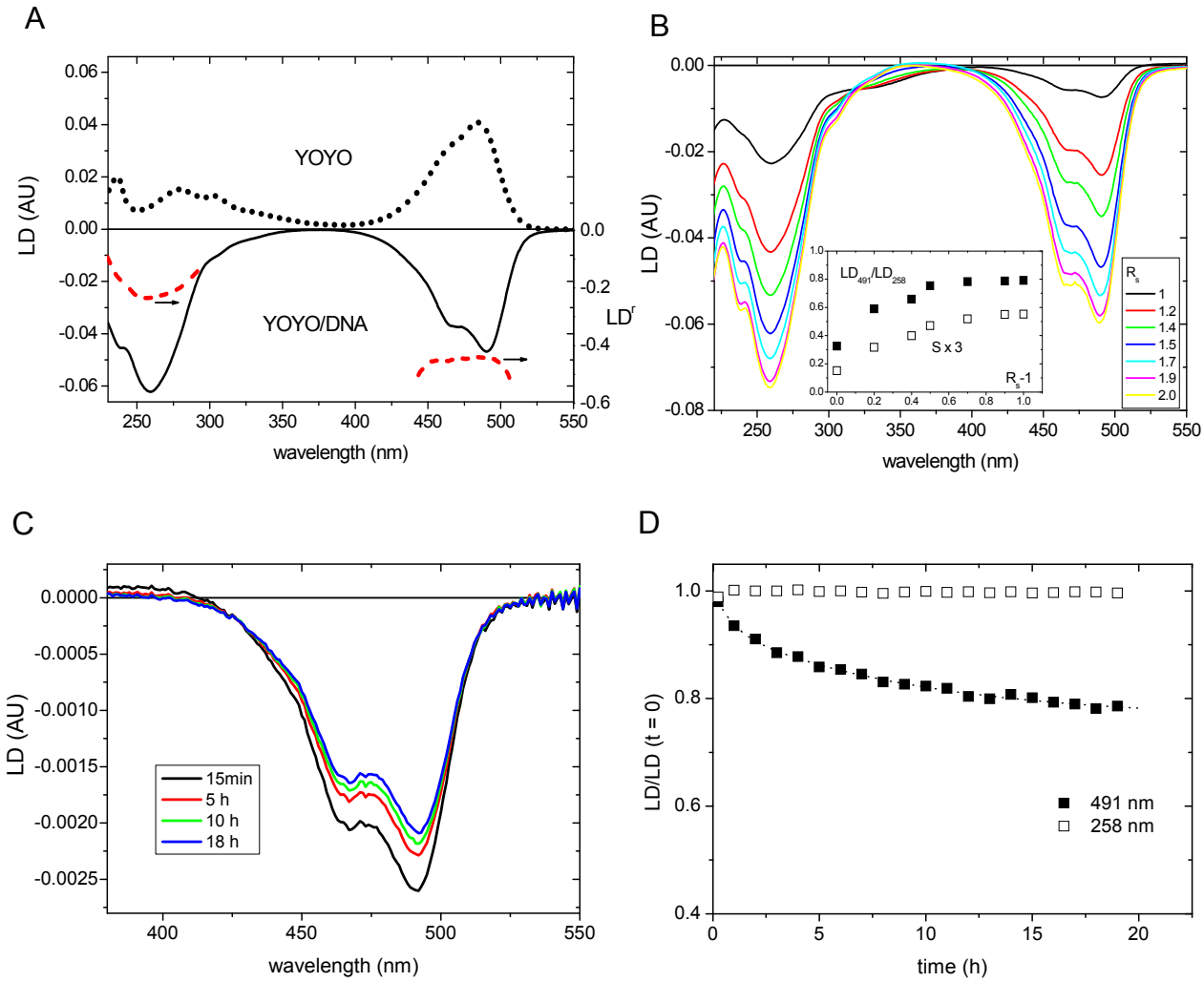

Fig.4.9 A) LD spectra of YOYO/DNA (solid line) and YOYO alone (dotted line) in humid PVA, with the LD^r spectra in the main dye and DNA absorption bands (red dashed line). B) LD spectra of YOYO/DNA in a humid PVA film at the indicated stretching ratios R_s. C) LD spectra of YOYO-DNA in PVA at the indicated times after the film was humidified and stretched to R_s = 1.5. D) Normalised LD values at 258 nm and 491 nm as a function of time after the film was maintained at100 % r.h., showing the DNA helix stability over time and the time-dependent dissociation of YOYO.

Dissociation of the YO-type dyes from DNA in humid PVA films may be due to: 1) a reduction in the forces that drive the dyes to bind DNA in the first place; and 2) dye-PVA interactions that compete with the DNA binding.

All three dyes become aligned when they were present alone in the stretched films (dotted curves in Figures 4.7, 4.8, and 4.9), which suggests that they interact with the aligned PVA

matrix. A possible explanation for this is steric (repulsive) confinement of the dye molecules between the PVA chains as the film is stretched. It is known that viscous solvents increase the quantum yield of free YOYO[41] in a way that is similar to what we observe with free YOYO in humid PVA films. However, the overriding type of dye-PVA interaction seems to be attractive: Figure 4.8 shows that YO-PRO molecules become aligned even if they enter the PVA matrix after it has been stretched, and in Boltzmann terms it is unlikely that the dye becomes oriented by entering a repulsive cage. Attractive PVA-dye interactions also explain the enhanced quantum yield of free YOYO in PVA, since binding to PVA is expected to restrict the intra-dye rotation, which is known to quench YO fluorescence in an aqueous solution[41]. If present, such attractive dye-PVA interactions would contribute to the observed destabilisation of the DNA-dye complexes.

The PVA environment may also reduce the attractive interactions that drive YO-type dyes to bind DNA. That YO and YO-PRO are both red-shifted in their absorption spectra compared to the same free dyes in water indicates that the PVA matrix is a less polar environment, since a similar redshift is observed when the two dyes enter the hydrophobic interior of the DNA helix from water. The behaviour of free YOYO supports this scheme because the shape of its absorption spectrum is in fact a sensitive probe of the dielectric environment. In aqueous solution, YOYO exhibits a reversed spectral shape compared with those of YO and YO-PRO [Fig. 4.6] (the shoulder of YOYO is on the blue side of its maximum), which has been ascribed to stacking of the two YO chromophores of YOYO in water[41]. Figure 4.6B shows that in humid PVA films, the YOYO spectrum instead has the shoulder on the red side of the maximum, similar to the shape in less polar solvents, such as ethanol[41]. Interaction with the hydroxyl groups of the PVA matrix is a possibility, since glycerol has a similar effect on the YOYO spectrum[41] as the PVA films, although this seems unlikely because YOYO exhibits the same reversed spectral shape in an aqueous solution of PVA (Fig. 4.6B) as in pure water[41].Taken together, these observations indicate that the humid PVA film presents an environment that is less polar for the YO-type of dyes than an aqueous solution.

The reduced polarity of PVA films is likely due to lower water activity than a pure aqueous solution, perhaps because water molecules can hydrogen bond to the PVA chains. At any rate, one consequence is a lower effective dielectric constant in the PVA environment, which strengthens the electrostatic attraction that is known[39] to be important to drive the cationic dyes to bind DNA at a low ionic strength, as was used here. However, the reduced water

activity would also strengthen the hydrophobicity of PVA matrix and weaken both the stacking interactions and the hydrogen bonding between the bases in the DNA. All these forces are essential for the secondary structure of short DNA sequences in PVA [Fig. 4.2], as well as for intercalation. However, since the LD of PVA is the only way to align oligonucleotides and it is possible to study DNA interactions with tetravalent dyes, it is interesting to look closer at the metal-organic group of chromophores, specifically the ruthenium binuclear complex $[(11,11'\text{-bidppz})(\text{phen})_4\text{Ru}_2]^{4+}$ [Fig. 2.11c] and its two enantiomeric forms, ΛΛ and ΔΔ, which are known to thread intercalate long DNA sequences, although the interactions with short oligonucleotides of defined sequence are not so well-studied. A preliminary investigation was performed by P. Nordell and colleagues[103] in which AT sequences of different length were used in emission kinetic experiments. To have a better overview, it is essential to study the interactions of ruthenium(II) complexes with both short AT and GC sequences. Of particular interest is the case of GC, for which the mechanism of interactions with oligonucleotides has not been explored at all.

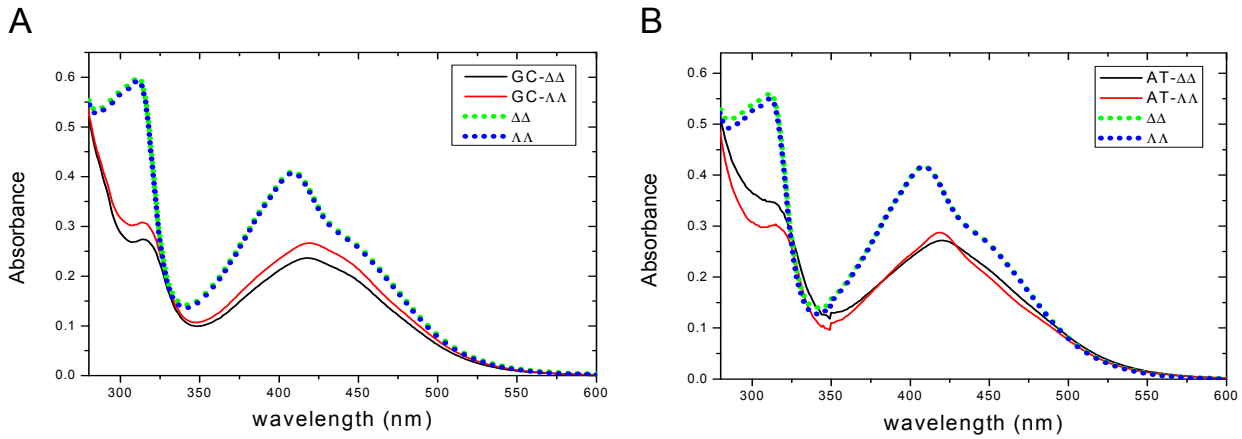

Fig. 4.10 Absorption spectra of ΔΔ and ΛΛ in 25 mM NaCl in water solution (dotted green and blue lines) and in the presence of A) a GC oligonucleotide (solid red and black lines) and B) an AT oligonucleotide (solid red and black lines) after heating at 37°C.

Here, AT oligonucleotides were mostly used to confirm and to allow reference to the previous kinetic studies performed by Nordell[103]. To prove in a general way that the interactions between ruthenium(II) complexes and oligonucleotides indeed occur, the absorption spectra of ΔΔ and ΛΛ were measured and the procedure was repeated after the addition of either AT or GC oligonucleotides. A distinct decrease in absorbance (hypochromism) was observed for

the intraligand $\pi \rightarrow \pi^*$ transitions of the bidppz ligand and the MLCT region of absorption following the addition of either AT- or GC-containing, HEG-linked oligonucleotides [Fig. 4.10].These results provide evidence of close interactions between the chromophores of the probe and the nucleobases. The hypochromicity for ΔΔ and ΛΛ was almost identical in the case of the AT sequence, whereas there was a slight difference in the absorption amplitude upon interaction with the GC oligonucleotide. However, it is clear that both enantiomers interact strongly also with the GC-containing sequence. The first impression based on simple absorption measurements is not surprising because previous LD studies of ΛΛ and ΔΔ $[(11,11'\text{-bidppz})(\text{phen})_4\text{Ru}_2]^{4+}$ in the presence of a long DNA sequence, either a mixed sequence (calf thymus DNA) or alternating polynucleotides $[\text{poly(dAdT)}]_2$ or $[\text{poly(dCdG)}]_2$ aligned in a Couette flow cell, indicated that the binuclear complexes could indeed thread-intercalate all three DNA contexts[52c]. Since oligonucleotide length seems to a crucial factor for threading and no such mode has been observed for the shortest oligonucleotides in NMR studies and emission kinetics, the binuclear complexes with HEG-linked short oligonucleotides composed of either AT or GC sequences were mixed with ΔΔ and ΛΛ in an approximately 1:1 ratio and further incorporated into PVA. This allowed for alignment of the DNA-dye complex and investigation of the system using LD. In this type of study, the LD of PVA has an advantage over emission or NMR techniques in that it can distinguish the binding mode and position of the complex with respect to the DNA helix. Of special importance is that both the aligned complex itself and the DNA-metal complex in PVA show some LD signal. The free metal complex aligns preferentially with its longest dimension, in parallel with the direction of polymer stretching [Fig. 4.11, dotted line], whereas when it is bound to DNA it orients preferentially perpendicularly to the direction of stretching of the polymer matrix [Fig. 4.11, solid line]. Experiments in which humidity control was imposed on the DNA-drug revealed improvements in the stabilities of the AT and GC oligonucleotides in the PVA in the presence of the binuclear ruthenium complex. This outcome is not surprising, since the lower water activity should strengthen the hydrogen bonds between the dye and DNA.

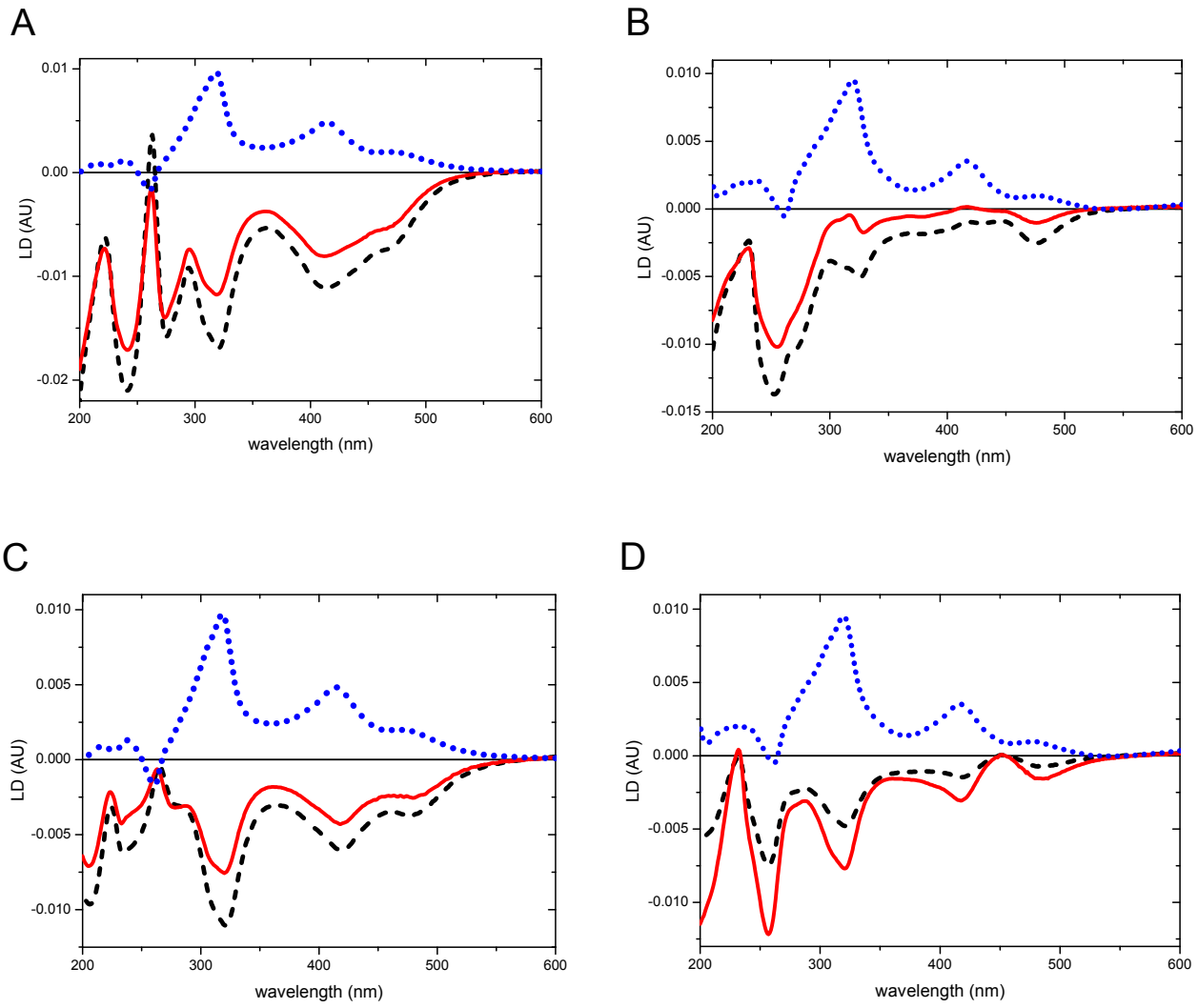

Fig. 4.11LD spectra of AT and GC oligonucleotides interacting with ruthenium(II) complexes at two levels of PVA hydration, whereby the PVA film equilibrated at 100% r.h.(red solid line) and 75% r.h. (black dashed line), respectively, in the following order: the 22-bp GC oligonucleotide with A) the ΔΔ enantiomer; and B) ΛΛ enantiomer, showing a difference in LD shape between 100% r.h. and 75% r.h. due to the dissociation and alignment of the free complex in PVA; and the 32-bp AT oligonucleotide with C) the ΔΔ enantiomer, and D) the ΛΛ enantiomer. In all the graphs, free ΔΔ and ΛΛ complexes oriented alone in PVA are shown for comparison (within margins of measuring errors, the spectra are identical; blue dotted lines). The samples were incubated in 25 mM NaCl.

Analysis of the LD spectra confirmed threading intercalation of both ΔΔ and ΛΛ into the HEG-linked AT sequence. The ruthenium complexes exhibited characteristic absorption spectral shifts upon interaction with DNA, which could be distinguished in both the absorption and LD spectra. The position of the bidppz bridging ligand at around 320 nm, which originated from a $\pi \rightarrow \pi^*$ transition polarised parallel to the long axis of the bidppz ligand, which is responsible for the intercalation, was, as expected, parallel with the plane of the DNA bases [Fig. 4.11 C, D]. Decreasing the relative humidity in the closed chamber, and thereby reducing the water activity inside the film, did not appear to affect the bidppz band, This indicates that the DNA-drug complex is stable and that the hydrogen bonding between the DNA and dye is even stronger due to the lower water activity in the PVA, despite the lower dielectric constant of the surroundings. From the LD^r spectra calculated by dividing the LD with the isotropic absorption of the same film sample, ΔΔ was found interestingly to align more perpendicularly to the helix axis in the dehydrated state than its counterpart enantiomer, ΛΛ. At 100% r.h., the orientations of the two enantiomers were similar [Fig. 4.12 A].

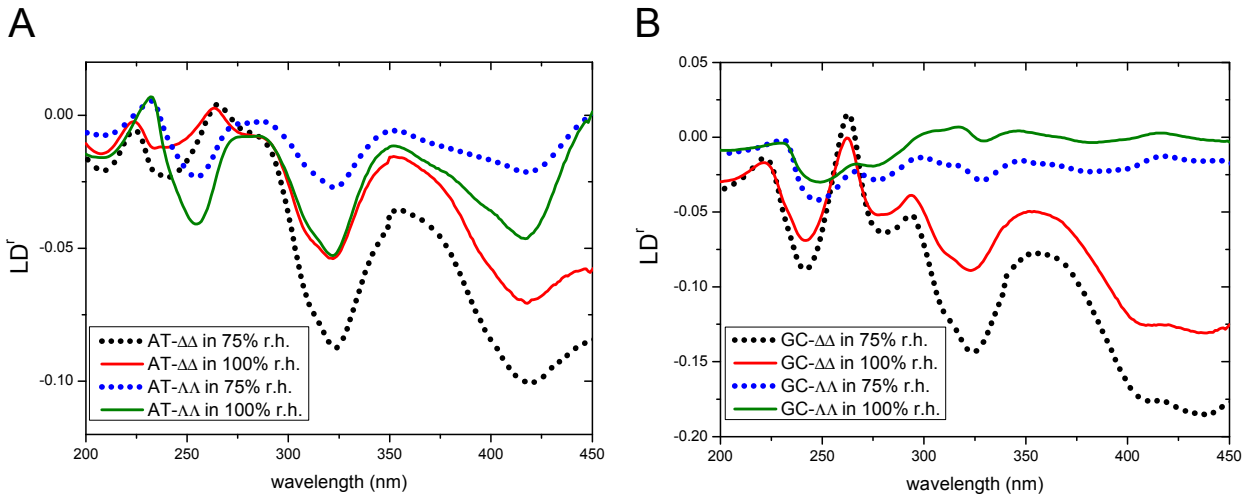

Fig. 4.12 LD^r curves of ΔΔ and ΛΛ in 75% r.h. (dotted line) and 100% r.h. (solid line) in the presence of A) the AT oligonucleotide, and B) the GC oligonucleotide.

In addition, a 22-bp HEG-linked GC oligonucleotide was studied. In this instance, both enantiomers of the binuclear complex exhibited distinct hypochromism in the dppz and MLCT absorption bands, indicating some degree of interaction. To confirm the binding mode, the advantage of the LD of PVA system was exploited. With the GC oligonucleotide, only the

ΔΔ complex exhibited a strong negative LD in the dppz region. In the case of ΛΛ, the LD was negative under low water activity conditions but became more positive at 100% r.h. [Fig. 4.11 A, B]. Furthermore, the shape of the LD at the peak at 320 nm changed with increasing water content of the film. There was a clear tendency to red shifting and the spectrum came to resemble that of the free ΛΛ complex in PVA. This indicates dissociation from the DNA due to the increasing water content of the polymer film. From a linear combination of the LD spectrum of the free complex in PVA with that of the complex in the presence of DNA at 75% r.h., it can be concluded that about 25% of the complex is dissociated and aligned instead in parallel with the PVA polymer chains in the film with high water content. Fast dissociation is deemed to be a result of the external binding mode on DNA, possibly involving groove binding. However, it is difficult to estimate the binding angle between the DNA and the ΛΛ complex due to overlap of the transition dipole moments of the nucleobases and monomeric units in the dimeric ruthenium complex.

In conclusion, the LD of PVA results indicate that ΔΔ intercalates GC by threading, while ΛΛ is virtually externally bound to the double helix [4.11 A, B]. When repeating the AT experiments at various r.h. levels, it is important to remember that the external binding mode of ΛΛ is very sensitive to the water activity in the polymer matrix. In contrast, the threading intercalation of ΔΔ remains robust both at low and high humidity levels. Changing the r.h. affects the dielectric constant of PVA. The lower the hydration level, the lower is the dielectric constant. This will decrease the hydrophobic interactions and thereby decrease the binding affinity of the hydrophobic metal complexes for DNA. However, in the case of tetravalent intercalators, electrostatic interactions are more important and one would expect the opposite phenomenon, i.e., that a lower dielectric constant would provide weaker electrostatic shielding and thereby, stronger binding to DNA and improved stability of short DNA sequences in PVA. This fits well the results obtained for ΛΛ, whereby an increase in the r.h. (with a consequent increase in the dielectric constant) led to destabilisation of the DNA-drug complex. This behaviour is the opposite of that observed for monovalent and divalent cations, where the predominant hydrophobic interactions with PVA abrogate the binding to DNA and result in an orientation parallel with the PVA chains, even in case of hydration at 100 % r.h.

Another interesting feature of the PVA system is the possibility to monitor dissociation of the metal complex from the DNA based on the gradually changing shape and amplitude of the LD

spectrum, progressing from negative to (eventually) positive as the ruthenium complex instead aligns itself parallel with the PVA chains. Thus, the ΛΛ enantiomer is observed to rearrange upon increases in the water content of the film. Each LD spectrum can be reproduced as a linear combination of the extreme LD spectra showing a two-state behaviour with the ruthenium(II) complex either bound to DNA or free. The $\pi \rightarrow \pi^*$ transitions are shifting towards a shorter wavelength and the LD becomes more positive and finally attains the shape of the LD spectrum of free ΛΛ aligned in PVA. Regarding the competition for binding between PVA and DNA, the water activity is obviously a key factor that affects the intermolecular interactions. The binding affinity for DNA is stronger under dehydration conditions, and a larger fraction of the metal complex is then interacting with the DNA [Fig. 4.11 B]. However, when more water molecules are introduced into the system by increasing the r.h. in the closed humidity chamber, the affinity for DNA becomes weaker and ΛΛ starts to dissociate. According to a linear combination fit designed to reproduce the shape of the LD spectrum, approximately 25% of the metal complex is free and aligned with PVA chains, and the process possibly continues until the equilibrium between the free and bound form is reached.

The concluded specific interaction of the binuclear complex with short GC sequences is surprising because it has been previously found that in a bulk water solution, ruthenium complexes with GC oligonucleotide exhibit a relatively low quantum yield. This has previously been interpreted in terms of groove binding. However, based on the results presented in this thesis, threading is indeed the ultimate mode of ruthenium complex binding to DNA stretches that are GC-rich. In summary, threading intercalation is the final binding mode for the ΔΔ and ΛΛ enantiomers upon interaction with AT-containing HEG-linked hairpin oligonucleotides. With GCDNA, only the ΔΔ enantiomer is thread-intercalated, whereas the ΛΛ enantiomer is externally bound to the DNA.

Another interesting observation is that intercalation of the binuclear complex is associated with an increase in the orientation factor (S) of the DNA, as compared with the free hairpin oligonucleotide aligned in PVA [Fig. 4.5]. One possible explanation for this is that the ruthenium complex once it is threaded between the DNA bases acts to stabilise the stacking of neighbouring bases by neutralising the repulsion between phosphate groups, thereby decreasing any wobbling or fraying dynamics that may be caused by the decreased dielectric constant of the surroundings. The ruthenium complex may act as a staple at the position of

threading and, together with HEG at the end of the helix, may prevent the strands of the duplex from separating transiently, thereby somehow zipping up the duplex. Although its existence is currently speculative, such an electrostatically "zipped" DNA would be consistent with the current conclusion that the DNA-ruthenium(II) complex is more stable at low humidity, while free oligonucleotides are vulnerable to variations in water activity in the PVA and changes in the hydration shell around the DNA.

In general, the PVA system is very convenient and effective for LD studies. In addition to the advantage of allowing the alignment of short oligonucleotides, both in free form and in the presence of tetravalent chromophores that tend to interact by electrostatic attraction, it is also a very stable system. The orientation can be easily restored when PVA that contains DNA is once again humidified, and in the case of organic chromophores, alignment in the dry film orientation can be maintained for more than 30 years with an S factor as high as almost 1.

4.3 Enantioselective binding of nonlinear absorbers (Papers III and IV)

The LD of PVA system, even though it is powerful, needs to be supported by complementary techniques. The binuclear complex $[(11,11'\text{-bidppz})(\text{phen})_4\text{Ru}_2]^{4+}$ and its two enantiomeric forms, ΔΔ and ΛΛ, were studied in detail for the first time in the presence of short oligonucleotide composed exclusively of GC. The experiments were also performed with an AT oligonucleotide as a reference to the data in the existing literature.

To confirm and characterise the phenomenon of threading intercalation of the AT and GC hairpin oligonucleotides, as shown for the first time using the LD of PVA system, CD experiments were performed. The asymmetry of the interactions is designated as "Perturbation CD" (PCD), which is defined as the differential between the CD spectrum of a pure enantiomeric ruthenium complex (since enantiomers are themselves chiral) and the spectrum observed when the complex is in the presence of DNA. This differential spectrum represents in part an induced CD, due to the chiral arrangement of nucleobases providing a non-degenerate rotational strength in the absorption active transitions, and in part it is due to the change in absorption intensity, which correspondingly scales (symmetrically) the CD of the complex. Different shapes of the perturbation spectra for opposite enantiomers are expected: the induced CD will have the same sign provided that the orientation of the chromophore relative to the DNA bases is the same, for example, positive for a transition

moment aligned along one of the grooves[104]. However, hypochromism will decrease the CD of an enantiomer (thus, with opposite signs for the two enantiomers). If the degree of interaction for the two enantiomers differs, the latter mechanism will add further to the difference between the PCD spectra.

Initially, the CD of the pure enantiomers were measured, and subsequently, either the AT or GC oligomer was added. The PCD results indicate strong interactions with AT sequences for both enantiomers [Fig. 4.13A]. Similar observations made by Westerlund et al.[105] were interpreted in terms of threading intercalation of long poly $(dAdT)_2$ sequences.

However, with a GC sequence, only the ΔΔ was thread-intercalated, such that the DNA band in CD was significantly influenced. The ΛΛ enantiomer revealed only minor changes in the DNA region, suggesting a relatively small impact of the complex on overall DNA secondary structure and minor perturbation of the double helix [4.13 B]. This is suggestive of an external binding mode, possible in one of the DNA grooves.

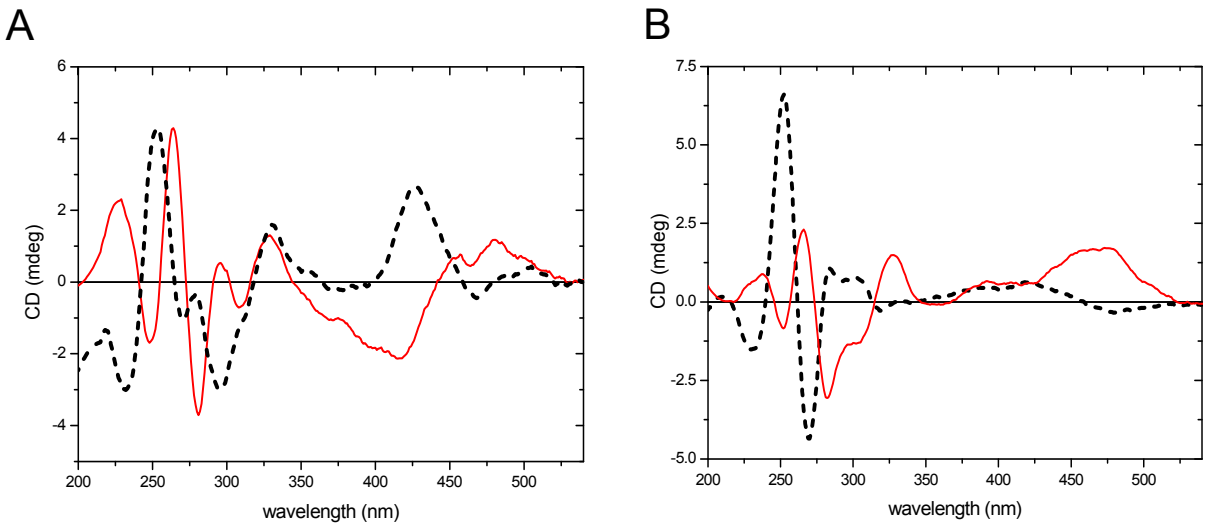

Fig. 4.13 PCD spectra, defined as the DNA-metal complex CD minus the CD for the pure complex, for: A) ATDNA with ΔΔ (solid red line) and with ΛΛ (dashed black line); and B) GCDNA with ΔΔ (solid red line) and with ΛΛ (dashed black line).

In addition to the CD study of molecules in free solution, the emission kinetics was measured [4.14]. As previously reported[106], the present class of ruthenium complexes, which are known to interact with DNA by threading intercalation, are quenched in aqueous solutions but

become brightly luminescent upon binding to DNA – the "light switch" effect – proving that a dppz moiety is indeed deeply inserted among the stacked bases making it inaccessible to water. This large difference in luminescence intensity enables sensitive kinetic study of threading intercalation through constant monitoring of the luminescence changes at 650 nm. Figure 4.14 shows the kinetic traces of enantiomers ΔΔ and ΛΛ when they interact separately with DNA at 37°C. The emitted luminescence gradually increased after addition of the GC oligonucleotide, with approximately two-fold stronger intensity being noted for ΔΔ than for ΛΛ. Further addition of poly(dAdT)$_2$ resulted in a strong enhancement of luminescence intensity. The equilibrium was reached relatively quickly for ΛΛ, which indicates an external binding mode, since only rapid dissociation from HEG-linked GC can explain the rapid subsequent intercalation into poly(dAdT)$_2$. In contrast, ΔΔ dissociated very slowly, reaching an equilibrium of threading intercalation between the GC oligonucleotide and poly(dAdT)$_2$ after about 3 hours. This observation is in good agreement with the LD and CD data, which show enantioselective threading intercalation of sufficiently long GCDNA stretches. Even though the emission was not as high as in the presence of AT, which was previously interpreted in terms of groove binding and accessibility of water that would strongly quench the emission, threading can indeed occur also in GC DNA and the quantum yield is not negligible, reaching ~20% of that in the presence of poly(dAdT)$_2$. Taken together, these results indicate that threading is indeed the final binding mode also for short GCDNA sequences of ≥20 nucleotides.

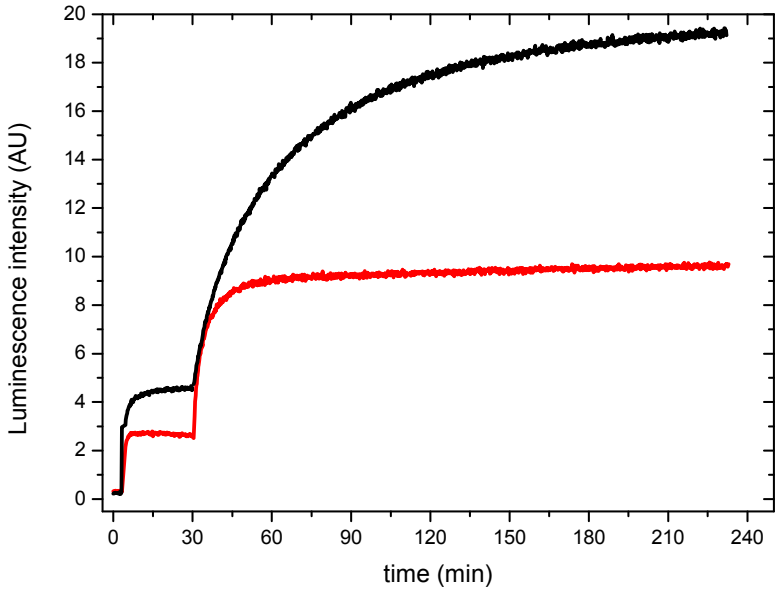

Fig. 4.14 Kinetics of dissociation of GCDNA with ΛΛ (red line) or ΔΔ (black line), measured as change in luminescence upon addition of extra poly(dAdT)$_2$. All measurements were performed at 37°C in aqueous solutions with 25 mM NaCl.

Undoubtedly, enantioselective threading intercalation of metal-organic ruthenium(II) complexes points the direction for designing more-specific chromophores for targeting dysfunctional regions of chromatin, e.g., drugs that target specific DNA sequences and inhibit the growth of cancer cells without affecting non-cancerous cells. Importantly, this should lead to the use of decreased doses of drugs, thereby further lowering the risk of toxicity. However, these applications will require more-sensitive detection tools. In this context, the unique "light switch" effect and strong luminescence upon binding to biomolecules are very promising features, since non-bound complexes will not emit light. In terms of potential bio-imaging applications *in vivo*, it is important to perform spectral analysis of the ruthenium(II) complex [(11,11′-bidppz)(phen)$_4$Ru$_2$]$^{4+}$ across a broad spectral range, to investigate chromophore sensitivity to light in the longer wavelength regions of NIR and IR. Simultaneous absorption of two or more photons can occur in the high- intensity region of a focused laser beam. In that process, normal absorption is moved to longer wavelengths, although this does not necessarily follow the simple principle of a multiplied single-photon spectrum. Thus, it is important to base the analysis on data collected over a broad range of wavelengths. The complex [(11,11′-bidppz)(phen)$_4$Ru$_2$]$^{4+}$ exhibits the strongest two-photon absorption properties [Fig. 4.15], with

the maximum at 540 nm (5000 GM), which is in the ILCT region of absorption. Open- and closed-aperture Z-scan measurements at that wavelength are presented in Figure 4.16. In the MLCT region, the absorption is lower (700 GM at 710 nm) but these are still the highest reported values obtained for these types of DNA-binding compounds. Among the studied compounds, the binuclear $[(11,11'\text{-bidppz})(\text{phen})_4\text{Ru}_2]^{4+}$complex seems particularly promising and may represent a new generation of DNA probes based on advanced multiphoton techniques. The 2PA cross-section values recorded between 600 nm and 650 nm, where two dppz moieties are absorbing, are between 1000 GM and 2500 GM. In addition, some signals were recorded at higher wavelengths, so these planar DNA threading ligands exhibit the character of three-photon absorption at 900 nm (σ_3=2.0 × 10^{-78} cm^6s^2). The high values observed for the cross-sections can be directly attributed to extension of the π-conjugated system upon dimerisation and the effect of symmetric charge transfer in ligands focusing in the centre of the dimeric molecule. An important aspect is the substitution position on the phenyl rings on dppz, which retains bridging ligands in the planar conformation so that the phenanthroline moieties cannot rotate. Furthermore, it could be that symmetric charge transfer from the ends to the centre of the conjugated dimeric orbital system occurs to enhance the NLO response. However, this is not the case for the MLCT band, probably because the interaction between the two ruthenium atoms of the dimer is negligible, so no enhancement of the nonlinear response can be expected.

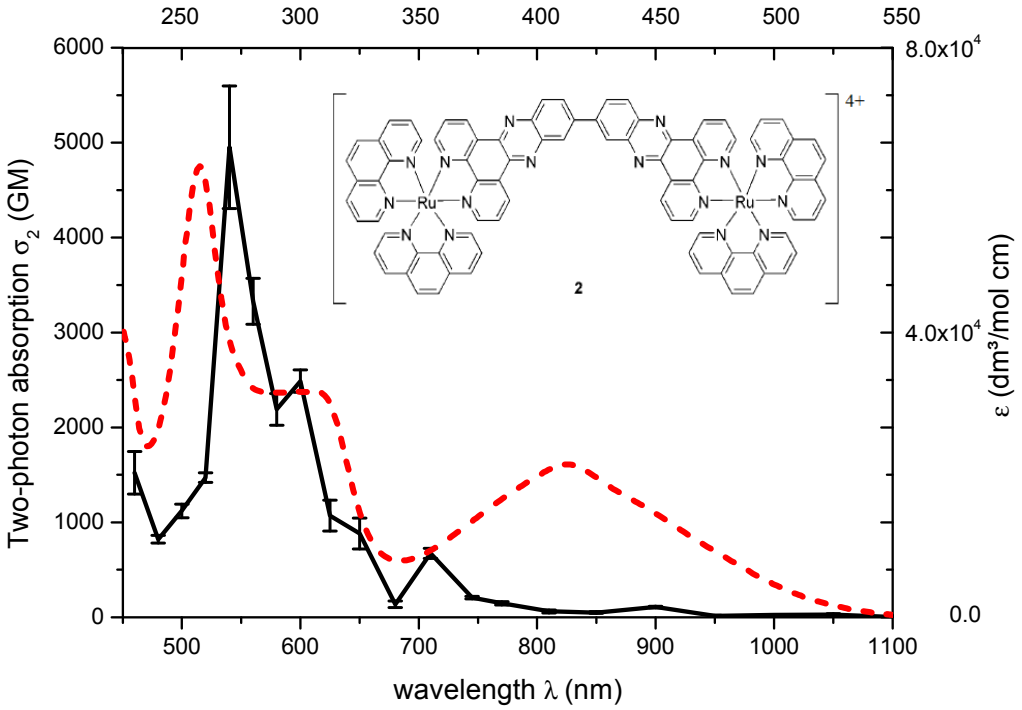

Fig. 4.15 Two-photon absorption spectrum of dimeric ruthenium(II) complexes with maximum in the shorter wavelength of ILCT at 540 nm. The inset shows the structure of ruthenium compound $[(11,11'\text{-bidppz})(\text{phen})_4\text{Ru}_2]^{4+}$. For the purpose of comparison, the one-photon spectra are plotted with wavelength multiplied by a factor of two and normalised to the same peak height (red dashed line).

In the next chapter, the nonlinear properties of different ruthenium complexes, as well as organic intercalating drugs, will be compared, discussed, and analysed. However,the $[(11,11'\text{-bidppz})(\text{phen})_4\text{Ru}_2]^{4+}$complex with its enantioselectivity towards specific sequences of DNA and strong nonlinear absorption properties, seems to be most promising candidate for further *in vitro* and *in vivo* research using advanced multiphoton technology. The binuclear ruthenium complex could be a prototype for a new generation of DNA-binding nonlinear chromophores with wide applications in biology and materials science. The combination of large two-photon cross-sections and selective strong luminescence quantum yields for only intercalated molecules makes these compounds uniquely bright and photo-stable probes for use in two-photon luminescence imaging. Preliminary results indicate that luminescence can be easily detected even upon multiphoton excitation at 1600 nm, which is the longest wavelength at which analysis can be performed using the current femtosecond laser setup.

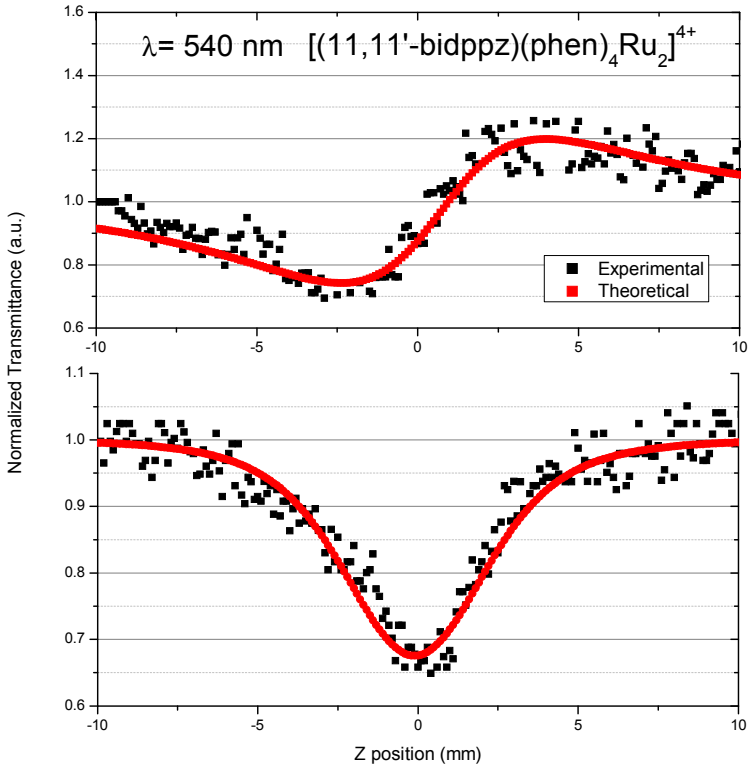

Fig. 4.16 Open- and closed-aperture Z-scans and the theoretical fits for ruthenium complexes at 540 nm for the $[(11,11'\text{-bidppz})(\text{phen})_4\text{Ru}_2]^{4+}$ complex.

4.4 Nonlinear properties of biomolecular labels (Papers IV and V)

To better understand the mechanism of nonlinear absorption in monomeric, as well as dimeric intercalating DNA molecules, ruthenium complexes and standard chromophores, such as ethidium bromide and a homodimer in which the two moieties are connected by an aliphatic linker, were studied in detail. Two-photon absorption spectra for monomeric and dimeric ruthenium(II) complexes known to be particularly promising as biomolecule-staining probes were investigated in the broad wavelength range of 460–1100 nm. Ethidium is one of the most commonly used staining agents in molecular biology. All these compounds provide an interesting overview of how the structure, substitution position in the dimer, and the rigidity of the molecule affect the nonlinear responses of metal-organic and organic probes. Two-photon absorption spectra can be compared with the linear absorption spectra and re-plotted at twice the original wavelength [Fig 4.17]. All the studied ruthenium-based metal-organic

compounds revealed strong nonlinear optical properties. The values for the 2PA cross-section σ_2 of the monomeric complex are the lowest among the explored compounds, although the maximum value in the short wavelength region of the ILCT is as large as ~500 GM at 560 nm (Fig.4.17 A). The values for the MLCT band and the absorption band of the intercalating dipyridophenazine (dppz) ligand, which overlaps with the MLCT, are significantly lower at ~150 GM at 710 nm. The 2PA spectrum of the monomer is qualitatively consistent with the shape of the one-photon spectrum (Fig. 4.17A; dashed red line), which would normally be taken as indication that the same electronic states are reached by the one-photon and two-photon excitations. However, its maximum at around 560 nm appears to be red-shifted relative to the one-photon spectrum, whereas in the MLCT region, it appears to be blue-shifted. Examination of the results obtained for the dimers reveals also certain shifts for the main short wavelength peak of σ_2. The peak magnitudes of the two-photon cross-sections derived for the dimers (Figs. 4.17B and 4.15) can be compared to those of the monomers when proper scaling is used to account for the increased molecular size. While various positive factors might be useful when dealing with two-photon analyses, the simplest way of comparing molecules of similar type is to scale the two-photon cross-section according to the molecular weight, i.e., by comparing the σ_2/M values. Table 3 lists the peak values of the cross-sections that have been scaled in this way.

Table 3.Values for two-photon absorption cross-sections at the maxima of the absorption bands.

	Absorption region	λ_{max} (nm)	λ_{2PA} (nm)	σ_2 (GM)	σ_2/M
(1) $[Ru(phen)_2dppz]^{2+}$	ILCT	262	560	490 ± 30	0.64
	DPPZ[b]	372	710	150 ± 10	0.19
	MLCT	383	710	150 ± 10	0.19
(2)$[(11,11'\text{-bidppz})(phen)_4Ru_2]^{4+}$	ILCT	265	560	4900 ± 600	3.23
	BIDPPZ[b]	320	600	2500 ± 100	1.62
	MLCT	417	710	670 ± 50	0.44
(3) $[11,11'\text{-bipb}(phen)_4Ru_2]^{4+}$	ILCT	285	560	900 ± 100	0.63
	BIPB[b]	320	650	180 ± 20	0.12
	MLCT	460	775	160 ± 20	0.11
(4) Ethidium Bromide	UV	285	605	68 ± 15	0.021
	VIS	480	950	12 ± 3	
(5) Ethidiumhomodimer	UV	300	610	175 ± 15	0.025
	VIS	528	1050	25 ± 5	

The high values for the two-photon and three-photon absorption cross-sections, especially in the absorption band that is sensitive to intercalation, look promising for *in vivo* DNA research.

The σ_2 values of the bipb-substituted complex are highest at 540 nm (~900 GM). Similar values for the 2PA cross-sections are obtained in the MLCT region (~160 GM) and in the absorption band of bipb at 640 nm (~180 GM). There is also a three-photon absorption contribution recorded between 900 nm and 1050 nm, with the $\sigma_3$value ranging from 9.1×10^{-79} to $1.2 \times 10^{-78} cm^6 s^2$.

The lower values of the 2PA cross-sections noted for the dimer [11,11′-bipb(phen)$_4$Ru$_2$]$^{4+}$[Fig. 4.17 B] are likely a consequence of the substitution on the phenyl ring at bipb bringing in the *meta* position, which does not allow the bridging ligands to form a well-conjugated π-electron system, as is in case for *ortho*- or *para*- substituted [(11,11′-bidppz)(phen)$_4$Ru$_2$]$^{4+}$ [Fig. 4.15] Thus, the nonlinear properties do not show much enhancement upon dimerisation. To examine further the effect of molecule flexibility on nonlinear absorption, standard chromophores were investigated and compared. Ethidium bromide and its dimeric derivative showed substantially lower values than the ruthenium complexes and the outcomes could not be directly compared with the results obtained for metal-organic compounds. Again, scaling using the molecular weight could be helpful in normalising the 2PA cross-sections and comparing with other chromophores. The ruthenium(II) complexes have an order of magnitude stronger 2PA, as shown by comparing [Ru(phen)$_2$dppz]$^{2+}$ with ethidium bromide (Table 3). This comparison makes it clear that metal-organic chromophores have significant potential in biomolecular studies using advanced nonlinear optics. For the dimers, both ruthenium(II) and ethidium homodimer show that size does not necessarily enhance the two-photon absorption. Interestingly, a comparison of the scaled 2PA of ethidium bromide and its homodimer, as well as a comparison of the ruthenium monomer and its *meta*-substituted dimer showed that flexible dimer compounds exhibit nonlinear absorption values that are very similar to those of monomers. Thus, even though dimeric molecules are larger, their nonlinear responses are not more effective than those of monomers. This has implications for biomolecular studies using two-photon excitation because dimeric molecules self-quench the emission owing to the short distance between the moieties. Flexible dimeric molecules are thus less useful for those kinds of studies. A reasonable strategy for developing good multiphoton absorbers is to focus on the rigidity and extension of conjugated π-electron systems that show a few-fold stronger nonlinear absorption, e.g., [(11,11′-bidppz)(phen)$_4$Ru$_2$]$^{4+}$(Table 3).

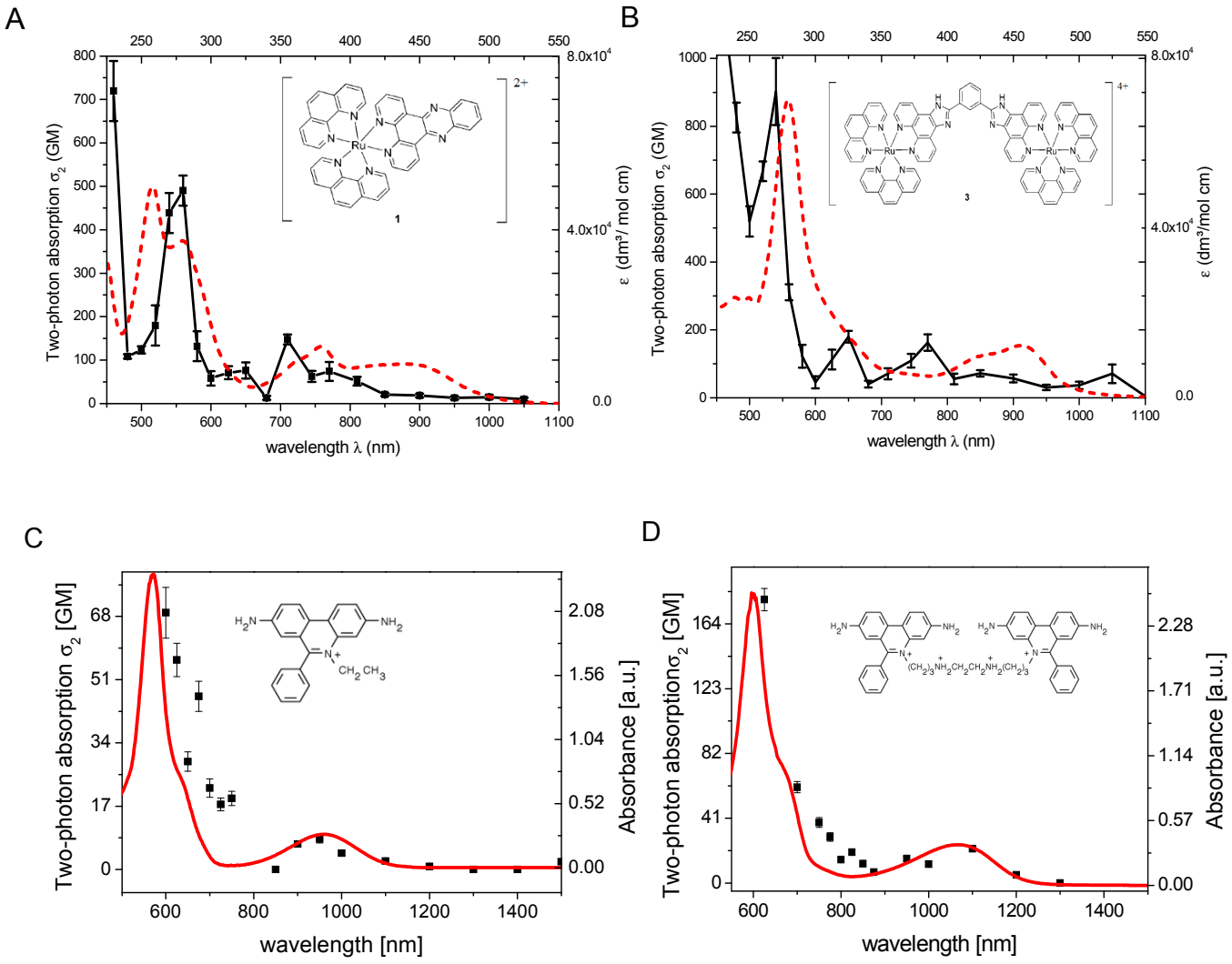

Fig 4.17 Two-photon absorption spectra of dimers and monomers. A, B) Metal-organic ruthenium(II) complexes. C, D) Ethidium bromide with homodimer derivative. The structures of the chromophores are presented in the insets. One-photon spectra (red lines) are plotted with the wavelength multiplied by a factor of two and normalised to the same peak height for the sake of comparison.

4.5. Amyloid fibrils interactions with metal-organic and organic chromophores

Fibrillisation of peptides or polypeptides leads to the formation of amyloid structures[74]. This process is promoted by certain mutations that affect protein folding, which may result in erratic structures, such as self-assembled, isolable aggregates, which are believed to lead to amyloidosis and as a consequence, serious diseases[75]. One of the most commonly used methods to detect amyloids *in vivo* and *in vitro* is staining with organic dyes, such as those mentioned in the *Introduction* [Fig. 2.15]. New chromophores that are more effective, specific, and have good photophysical properties are in demand for studies of fibril structure recognition. Since binuclear ruthenium(II) complexes represent a class of molecules with strong potential for the bio-imaging, the amyloid-ruthenium(II) interactions were investigated. Amyloids formed by insulin or lysozyme can be oriented in flow LD, which provides an opportunity to understand the mechanism underlying the interactions between chromophores and fibrils. Rigid $[(11,11'\text{-bidppz})(\text{phen})_4\text{Ru}_2]^{4+}$ and flexible $[\mu\text{-C4(cpdppz)}(\text{phen})_4\text{Ru}_2]^{4+}$ complexes [Fig. 2.11 b,c] were studied in terms of binding and accessibility for multiphoton detection. LD showed that both complexes interact with amyloids, although there were no distinct shifts in absorption similar to those detected in the presence of DNA. Since binuclear complexes are relatively large, it seems unlikely that they can thread-intercalate amyloid filaments. Besides, the diameter of amyloid is 8–10 nm, which is 4–5-times larger than that of DNA (2 nm), which means that a perpendicular arrangement of the binding compound with respect to the orientation of the amyloid (even in the case of a complex with a flexible aliphatic linker) is sterically prohibitive. According to the LD results, the orientation of the ruthenium(II) complexes is parallel to the tyrosines, so that they are in macroscopic alignment with the overall orientation of the fibrils. Especially interesting are the positions of the dppz moieties at around 320 nm for a rigid complex and at 370 nm for one with an aliphatic linker. A positive LD indicates that both dppz moieties are parallel to the direction of orientation, which should entail rapid dissociation of the complex; however, the results suggest that the strong electrostatic attraction of the dimeric molecules to negatively charged amino acids predominates and that some binding indeed occurs. Moreover, the flexible dimer resembles the parental monomers, for which strong interactions with fibrils have been reported[107]. It is clear then that both complexes are bound externally to the fibrils and that the dppz moieties are not inserted between the filaments. The question as to what is the exact position of the dppz (and thus, the entire complex) remains to be resolved. The relatively weak orientation of

the compound with flexible linker, as compared with the rigid dimer, suggests close proximity to the magic angle of 55° (at which the LD is 0).

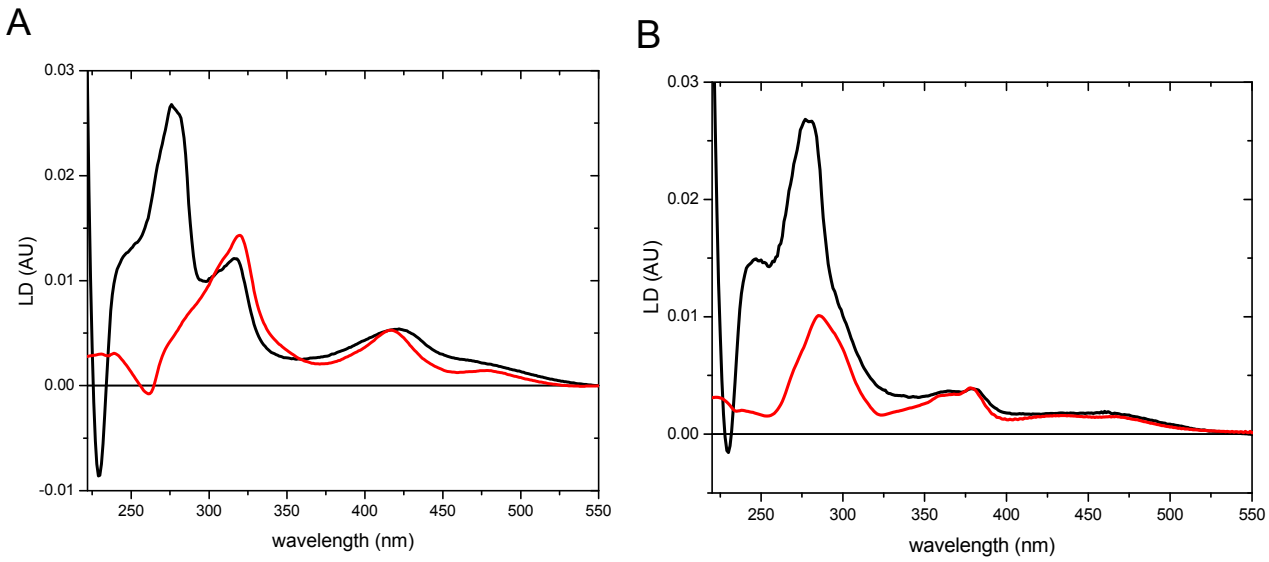

Fig 4.18 LD spectra of: A) $[(11,11'\text{-bidppz})(\text{phen})_4\text{Ru}_2]^{4+}$ free-aligned in PVA and in the presence of insulin fibrils aligned in a flow; and B) $[\mu\text{-C4(cpdppz)}(\text{phen})_4\text{Ru}_2]^{4+}$ free-aligned in PVA and with insulin fibrils aligned in a flow.

To obtain more information about the interactions between amyloids and binuclear ruthenium(II) complexes, the emission spectra were recorded in the presence of insulin fibrils and free in solution. A large difference in emission intensity was noted between the rigid and flexible chromophores upon the addition of fibrils, indicating that the rate of interaction is related directly to the dimer structure. A rigid complex is stiff and cannot bend, whereas a complex with an aliphatic linker has some degree of freedom and thus has the possibility for adjustment among the monomeric structures of the filaments, thereby better protecting the nitrogens from the hydrophilic solvent environment that quenches emissions. The intensity is not as important in the one-photon process as when the sample is excited by two photons. The rigidity of the metal-organic complexes leads to π-conjugation, and it is a prerequisite when dealing with multiphoton spectroscopy. However, in the presented case, no emission was observed for the rigid dimer due to strong quenching. In contrast, the flexible dimer showed very sharp and strong peak at 585 nm when excited at 860 nm. A possible explanation of the band narrowing may be the emission amplification due to strong laser power. Similar effects

were previously observed in polymer films that were doped with dyes and biomolecules, such as DNA[108] and DNA-CTMA[109], although those experiments were conducted in polymer films rather than in solution.

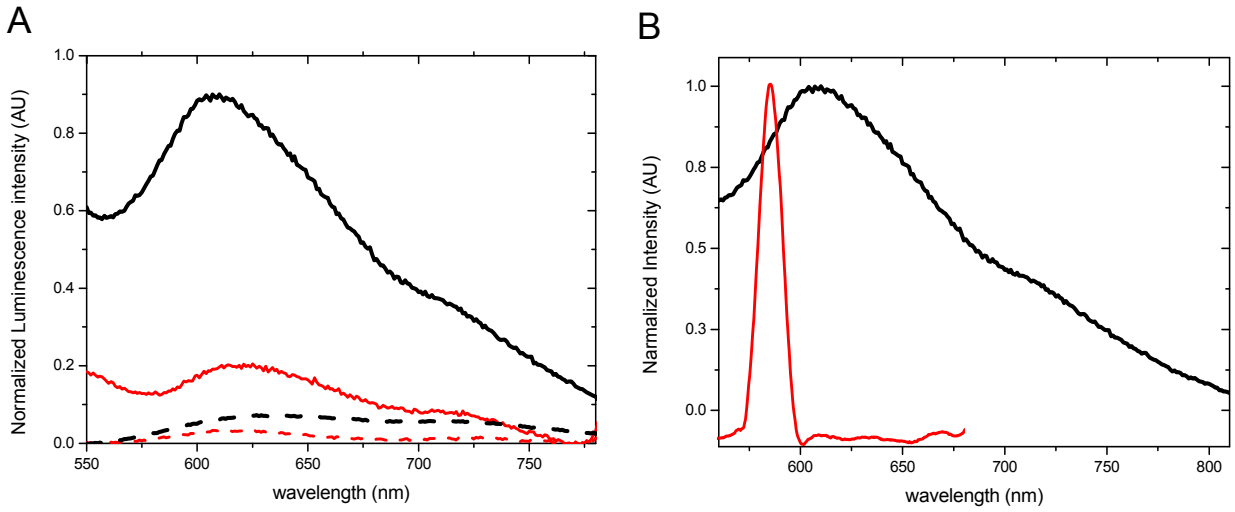

Fig. 4.19 A) Emission spectra of: $[(11,11'\text{-bidppz})(\text{phen})_4\text{Ru}_2]^{4+}$ free in solution (red dashed line) and in presence of insulin fibrils (red solid line); and flexible $[\mu\text{-C4(cpdppz)}(\text{phen})_4\text{Ru}_2]^{4+}$ free in solution (black dashed line) and with insulin fibrils (black solid line); B) One-photon spectra of $[\mu\text{-C4(cpdppz)}(\text{phen})_4\text{Ru}_2]^{4+}$ with insulin fibrils excited at 435 nm (black solid line) and excited by two photons at 860 nm (red solid line).

In this thesis, two important discoveries are reported. The emissions from binuclear ruthenium(II) complex can be recorded, which is direct proof that advanced multiphoton spectroscopy (and potentially also microscopy methods) can be applied to amyloid fibril-dye adducts. It seems unlikely that emission peak is produced only due to the ruthenium(II) complexes themselves, since similar experiments with DNA have been performed and have shown identical emission spectrum shapes to those recorded in one-photon excitation experiments (results not shown). It is thus necessary to show that the fluorescence band narrowing phenomenon is directly related to the properties of amyloids. Therefore, it is reasonable to carry out experiments with a dye that is a standard marker for amyloid and that upon binding exhibits enhanced emission. Experiments with Thioflavine T bound to insulin fibrils were performed and showed the same effect as seen for amyloid interacting with the

binuclear ruthenium(II) complex. The band was very narrow when compared to the standard one-photon spectrum in the dye band, the maximum was red-shifted to around 40 nm. Thus, it is clear that emission spectrum shape is directly related to the structure of the amyloid fibrils and dye acts rather as an antenna enhancing the process. A possible clue lies in the material properties of fibrils that determine dye confinement, similar to that observed for the polymer matrix, since as Smith reported, the mechanical shear stiffness, persistence length, and mechanical rigidity of insulin fibrils are similar to those of silk[77]. But that hypothesis needs to be further confirmed by other experiments.

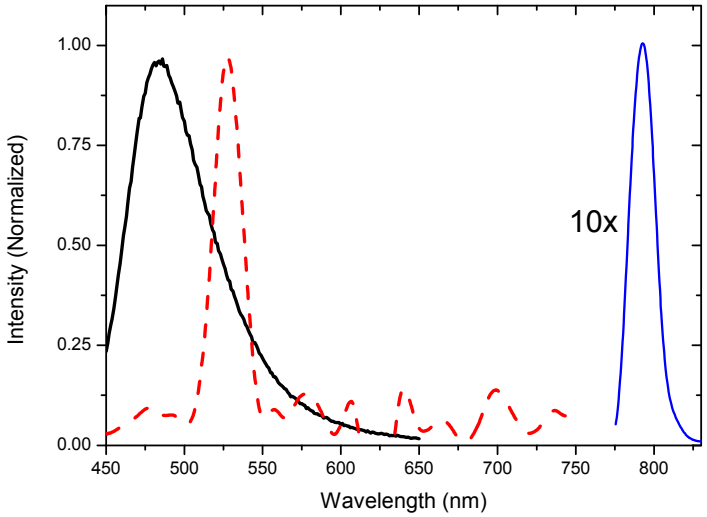

Fig. 4.20 Emission profile of Thioflavine T bound to insulin fibrils excited at 400 nm (black solid line) and the same sample excited by two photons at 800 nm (blue solid line), and the emissions collected with maximum at 525 nm (red dashed line).

In the context of nonlinear properties, stilbene dyes are often the candidates of choice [Fig. 2.15 b]. Stilbene and its derivatives are often used as a gain medium in lasers, so it is interesting to know the dye can form a stable adduct with amyloid fibrils, as this would prevent dye aggregation and even distribution of the dye over the binding sites in the amyloid filaments. This would significantly improve the efficiency of the dye as a gain medium, for example in bio-lasers. On the other hand, stilbene can be an interesting type of dye for amyloid probing when using multiphoton techniques because it is very often used to extend π-conjugated systems, so as to enhance the nonlinear properties. A simple structure makes it easy to modify and tune the optical properties. The structure of a derivative, Stilbene 420, is

similar to that of Congo Red, which is a well-known fluorescent marker that is used in amyloid diagnostics [Fig. 2.15 b,c]. All these properties make Stilbene 420 a promising new-generation chromophore for probing amyloid with multiphoton-based technologies, e.g., two-photon excitation microscopy. However, linear spectroscopy methods were used to investigate whether there is indeed an interaction between Stilbene 420 and amyloid fibrils. The experiments included analyses of absorption, LD, and one photon excitation.

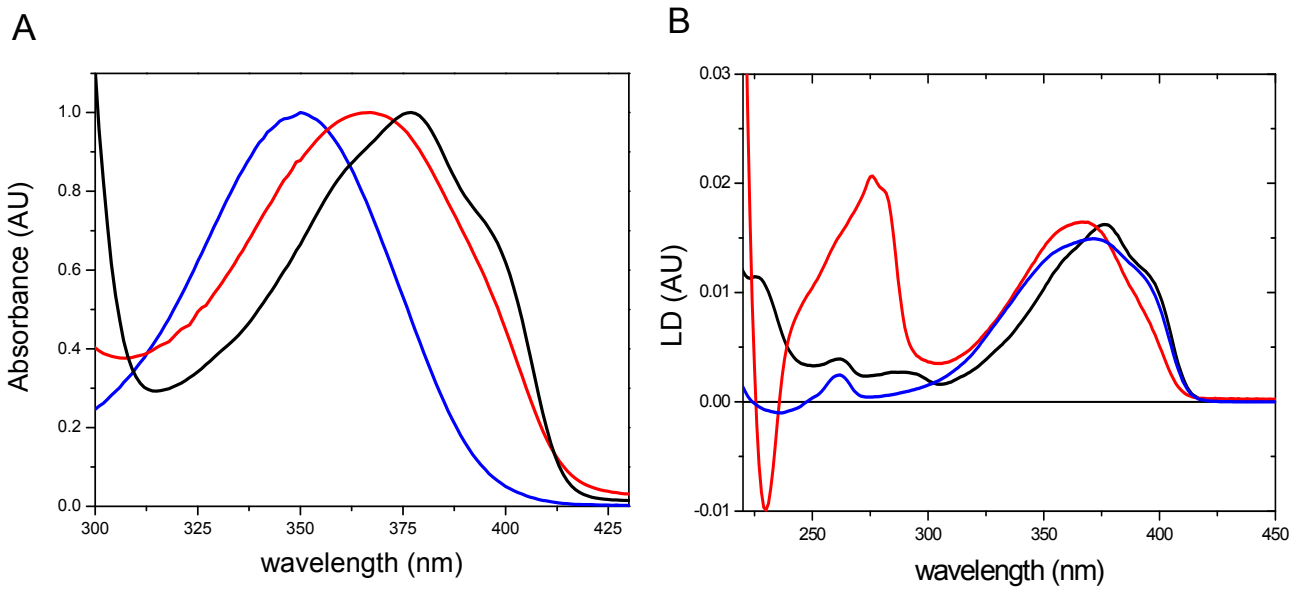

Fig. 4.21 A) Absorption spectra of Stilbene 420 dye in water (pH 2) and in the presence of either insulin fibrils (red solid line) or lysozyme fibrils (black solid line). B) LD spectra recorded under the same conditions as in the absorption experiment and showing alignment of fibrils with bound stilbene to the insulin fibrils(red solid line) or lysozyme fibrils (black solid line) and the dye itself aligned in PVA.

The absorption measurements of samples with Stilbene 420 in the presence of different fibrils, either lysozyme or insulin, showed red-shifting compared with the dye alone in a solvent. In the case of lysozyme, the shape was also different, with a marked shoulder above 400 nm. Since Stilbene is sensitive to environmental changes, in both cases there was an indication of some interaction between the dye molecules and the amyloid fibrils. Additional LD experiments confirmed that Stilbene was indeed bound to both types of fibrils, showing a distinct peak in the dye absorption band, although the shifts in LD did not follow the red-shifting trend recorded in the absorption experiments when the spectrum was compared with that of the pure dye aligned in PVA. One possible explanation for this is the sensitivity of the

stilbene dye to the dielectric properties of the material, as well as the pH. Thus, it would be reasonable that the shapes of the LD spectra also would differ from each other. A final test was made by collecting the emission spectra for the dye itself, the dye with native proteins, and the dye with fibrils. No change in emission intensity was recorded upon addition of the dye to native insulin or lysozyme. However, in the presence of the fibrils, there was strong enhancement of the emission intensity, especially with the insulin fibrils. Since the fluorescence properties of Stilbene mostly rely on isomerisation, whereby the *cis* form is non-fluorescent and the *trans* form is fluorescent, Stilbene must be interacting with the fibrils in the *trans* form, whereas the dye in a solution is probably a mixture of *trans*-*cis* and *cis*-*cis* forms[110]. Interestingly, there was a large difference in the emission intensities between lysozyme and the insulin fibrils, which means that the amyloid structure is a factor that has to be taken into consideration when discussing amyloid-Stilbene adducts. A possible explanation is that insulin fibrils that form well-ordered β-sheet structures determine also the geometry of the binding mode, and in this exact case, the fibrils influence the planarity of the compound. This explanation would also account for the lower emission intensity observed for the lysozyme fibrils, which are less-ordered than the insulin fibrils. In addition, some random coils can appear in the fibril structure, allowing some degree of rotational freedom to the bound dye. The degree of planarity is an important factor that determines the optical properties of Stilbene 420[111]; increased planarity upon binding would provide a more extensive conjugated electron distribution in the dye molecule and thus enhance the emission properties.

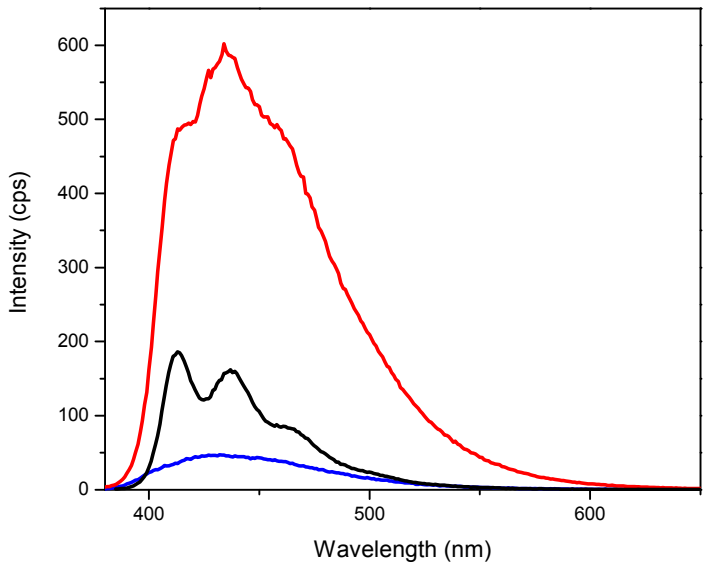

Fig. 4.22 Emission spectra recorded upon excitation at 350 nm for the free Stilbene dye (blue solid line) and in the presence of insulin fibrils (red solid line) or lysozyme fibrils (black solid line).Note the excitation at 370 nm due to the large shift in absorption upon binding to the fibrils.

In summary, linear spectroscopy analysis confirmed the binding of Stilbene 420 to amyloid fibrils. This binding may be similar to that of Congo Red dye, which is similar in structure to Stilbene 420. In the next step, multiphoton excitation of a Stilbene 420-amyloid adduct will be studied. However, before that can occur, the nonlinear properties of the amyloid fibrils are analysed and described in the next chapter, since the interaction may influence not only amyloid, but also the dye properties, as has been shown for the ruthenium(II) complex and the standard amyloid marker Thioflavine T.

4.6. Nonlinear absorption profile of amyloid fibrils (Paper VI)

Serious diseases, such as Alzheimer's, Parkinson's and Creutzfeldt-Jakob diseases, are generally a consequence of amyloidosis, which by definition refers to a variety of conditions in which normally soluble proteins undergo misfolding and changes in secondary structure to become insoluble and deposited in the extracellular spaces of various organs or tissues, thereby disrupting normal functions. It is possible to recognize the regions in which amyloid fibrils are deposited by staining with organic dyes. It is a widely used strategy to visualise and quantify the presence of amyloid fibrils, both *in vitro* and *in vivo*. However, labelling with organic dyes[112] is cytotoxic and is not always the best approach for *in vivo* applications. Thus,

it is important to find new diagnostic and treatment methods for amyloidosis. In this thesis, a completely new strategy for detecting amyloid fibrils is presented. The discovery that amyloid fibrils exhibit remarkably enhanced multiphoton absorption properties and that this is directly related to the fibrillisation opens up new research opportunities as well as applications in many fields, especially for the development of diagnostic tools for amyloidosis.

The parameters that characterise nonlinear absorption were determined in a fashion similar to that used for the dyes in Chapter 4.4, at wavelengths in the range of 530–950 nm, and the fibrils were compared with native proteins. Three kinds of fibre-forming proteins were investigated, all of which were found to exhibit non-linear properties only in the fibrillar state. Pure two-photon absorption was only observed at the shortest wavelengths (525–600 nm), as judged by the criterion of fit between the experimental open aperture Z-scan and theoretical line shapes. [Fig. 4.16 shows an example of fits for ruthenium(II) complexes similar to those obtained for fibrils]. Figure 4.23 shows the wavelength dependence of exponent n, defined formally as if describing the absorption according to a Boguer-Lambert-Beer type of law: $dI/dz = -kI^n$ where I is the light intensity impinging on the sample and z is the propagation distance. It can be seen that two-photon absorption is dominant in the range of 530–600 nm, while a three-photon process appears to dominate in the range of 700–750 nm, which is in agreement, for example, with the position of the lowest single photon transition of tyrosine at 275 nm. At the longest wavelengths, the value of n needed to fit the experimental data is close to 5, indicating that the system exhibits a multi-photon behaviour.

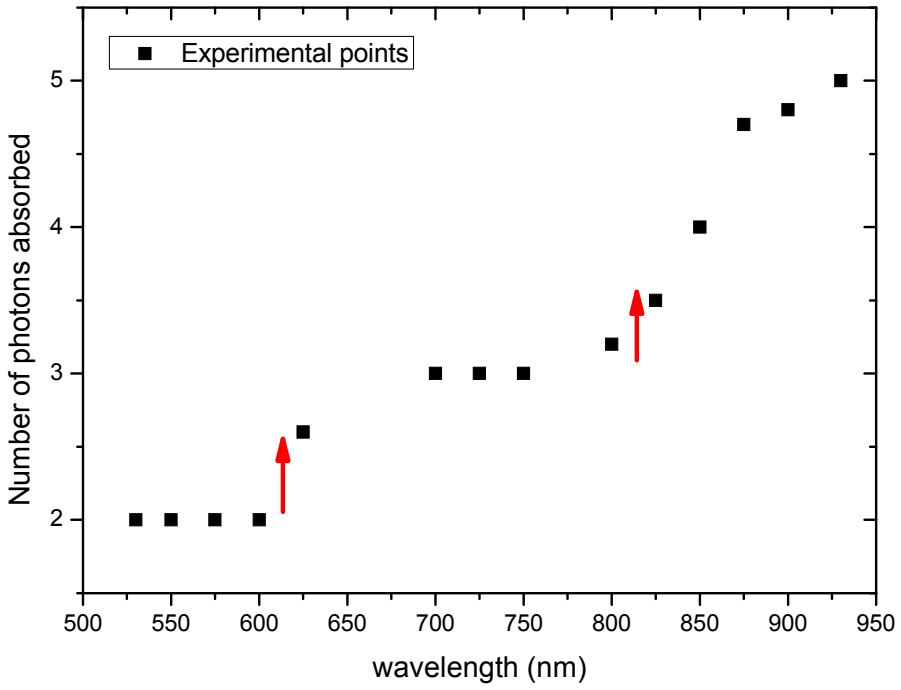

Fig. 4.23 Apparent number of photons taking part in the nonlinear absorption process versus the wavelength of the light. Note the steps marked with vertical arrows: <625 nm, two-photon absorption; and <850 nm, three-photon absorption.

Figure 4.24 shows the nonlinear absorption spectra presented as two-photon and three-photon absorption cross-sections versus the wavelength, respectively where appropriate, and as an apparent two-photon cross-section corresponding to the typical light intensity of the measurements (100 GW/cm^2) for regions in which neither clean 2PA nor 3PA behaviour was observed. Within the region in which a two-photon process dominates, there is a prominent maximum at 550 nm, with σ_2 = 2600 GM (calculated per insulin monomer). This is in good agreement with the true linear (one-photon absorption) spectrum re-plotted in the figure versus the wavelength number multiplied by a factor of two.

Table 4. Values of 2PA for three proteins in the amyloid fibril state, including scaling

Amyloid fibril type	Number of aromatic amino acids in monomer unit (Y, F, W)	Molecular weight of monomer unit [g/mol]	2PA max. wavelength	σ_2[GM]	σ_2 / M
insulin	4×Y, 3×F, 0×W	5733,5	550 nm	2600	0.45
lysozyme	3×Y, 3×F, 6×W	14307	570 nm	1640	0.11
α-synuclein	4×Y, 2×F, 0×W	14460	550 nm	5250	0.36

Amino acid designations: Y, tyrosine; F, phenylalanine; W, tryptophan.

Scaling according to the molecular weight of the protein monomer unit allows estimations of the strength of the nonlinear response with respect to already reported molecules. In the case of insulin fibrils at 550 nm, $\sigma_2/M = 0.45$, which is a value three-orders higher than that for pure tyrosine, at $\sigma_2/M = 0.13\times 10^{-3}$ [113]. To confirm the postulate that it is the fibrillar state that is specifically enhancing multiphoton absorption, experiments were performed with lysozyme and α-synuclein fibrils, which have different compositions of aromatic residues. Both fibrils showed enhanced 2PA, although upon scaling lysozyme was found to be 3–4-times weaker as a two-photon absorber than the richer-in-tyrosine α-synuclein and insulin.

In the wavelength range of the dominant three-photon process (700–750 nm), maxima at 725 nm for insulin and at 750 nm for α-synuclein correspond to three-photon absorption cross-sections with $\sigma_3 = 3.3 \times 10^{-77}$ cm^6s^2 and $\sigma_3 = 1.4 \times 10^{-76}$ cm^6s^2, respectively. Some caution is needed when assigning the origin of the effect, i.e., the three-photon active transition, as the data-points corresponding to the 3PA spectrum do not perfectly follow the pattern of the one-photon absorption spectrum wavelength scaled by a factor of three; a substantial blue-shift is seen when comparing the spectra. Note that a blue-shift is predicted for side-by-side exciton models of two-photon absorption. The data in the intermediate region and at longer wavelengths also show appreciable multi-photon absorption. Since the character of the process is $2<n<3$ and $3<n<5$ in those regions, respectively, possibly indicating a mixture of two or more process, quantifying the cross-sections in terms of integer n is not appropriate. Instead, the "effective" σ_2 is used, which is defined as the two-photon cross-section that would give the same number of absorbed photons as the multiphoton process under consideration if both processes were studied at 100 GW/cm^2. It is amazing to realize that the

multiphoton absorption processes actually lead to the fraction of incident photons absorbed being comparable to that expected for strong two-photon absorbers at the same light intensities.

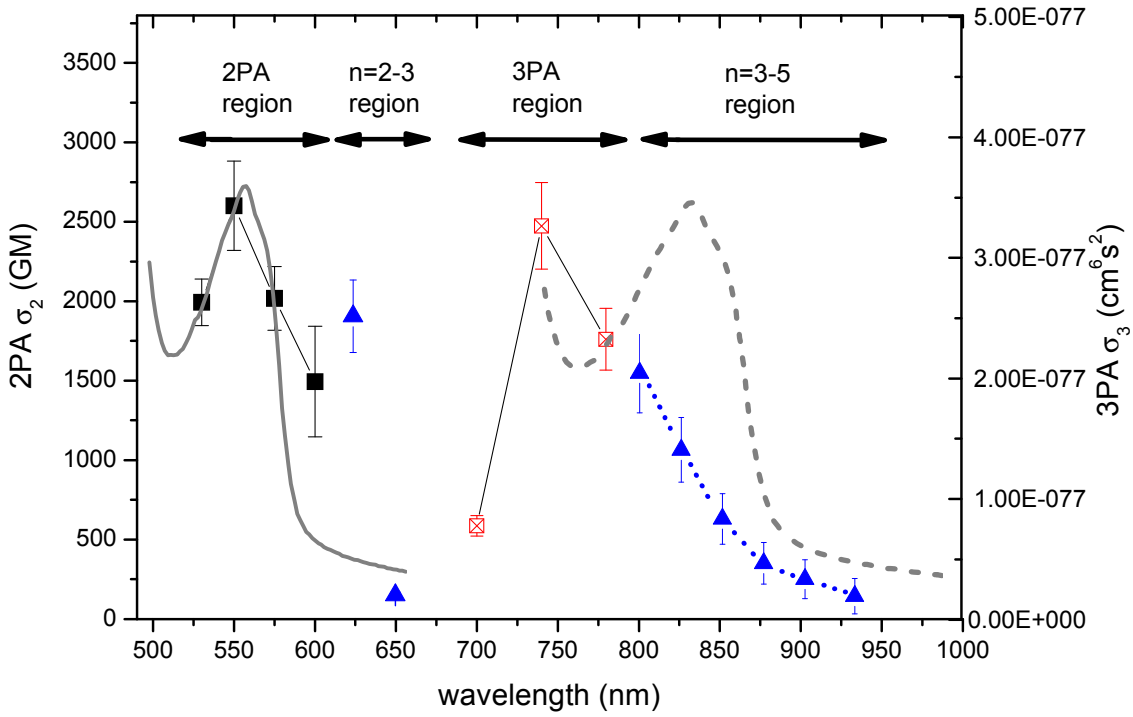

Fig. 4.24 Two-photon absorption of amyloid fibrils (black squares) between 530 nm and 600 nm, together with one-photon spectrum (solid grey line) re-plotted from the normal absorption spectrum with the wavelength multiplied by a factor of two and normalised to the same peak height for comparison. Three-photon absorption (red crossed squares) in the range of 700–750 nm of amyloid fibrils and one-photon spectrum (dashed grey line) re-plotted with the wavelength multiplied by a factor of three and normalised to the same peak height for comparison. The linear absorption data-points for processes between 2PA and 3PA and 3<n<5 in the range of 625–930 nm (cf. Fig 2) are plotted as the "effective 2PA" and denoted by blue triangles.

These results for amyloids are outstanding when compared with natural biopolymers that show usually only modest non-linear optical properties. A Z-scans were performed on DNA[114] or isolated aromatic amino acids[115] with no spectacular effects being seen. Therefore, it is not surprising that proteins in their native states show negligible 2PA[113]. Probably as a result of the relatively low number of aromatic amino acids in the protein sequence, which

would entail large intermolecular separations between the residues in the monomeric protein structure, there is no particular communication between the aromatic amino acids in the non-fibrillised state. However, the influence of protein conformation on 2PA has been considered as an important factor by Meshalkin and Rativa [113,115]. Of particular interest is the observation made by Meshalkin that increasing the number of tryptophan residues in the native protein, together with conformational and structural modifications would enhance the nonlinear effects. The remarkable nonlinear absorption exhibited by the aggregated state of proteins is reminiscent of the nonlinearity enhancements reported for extended π-electron systems, as in dendrimers[116] and porphyrins[117], whereby strong enhancement of 2PA is observed upon progression from the zeroth to the first generation of dendrimer or the conjugation of porphyrins into ladder-type structures. Unfortunately, the complexity of the amyloid fibril systems, as compared to the structurally relatively well-defined dendrimers or porphyrins, together with a general lack of structural information about the internal organisation of chromophores in the fibrils, makes it difficult to deduce the mechanisms and parameters of the proteins that determine the overall non-linear response. However, in contrast to the dendrimers and porphyrins, protein fibrils all lack π-conjugation. Aggregation-induced enhancements of 2PA were recently proposed in terms of the cooperative effects of intra- and inter-molecular charge transfer transitions, and it is plausible that similar cooperative mechanisms are also responsible for the strong enhancement of the non-linear optical response in the compacted structures of amyloid fibrils, generating high nonlinear absorption cross-section values. In addition, sequence composition has to be taken into consideration, and possible modifications to amino acids, such as nitration or phosphorylation, may influence cooperative enhancement. Lysozyme, which contains more tryptophans in a sequence (which dominate the one-photon absorption spectrum), exhibits significantly weaker 2PA than either insulin or α-synuclein. However, this is not surprising since tryptophan itself has only a weak 2PA compared to tyrosine[115] present in larger amounts in insulin and α-synuclein. Thus, the scaled 2PA property indicates that tryptophan-rich amyloids do not show as-effective enhancement of nonlinear absorption as do tyrosine-rich fibril structures. Another aspect to note is the variations in distance between tyrosines in a monomer sequence, although this is of minor importance for a cooperative mechanism that is based on through-space rather than through-bond interactions. Comparing tyrosine-rich amyloids, it is reasonable that the 2PA of insulin is greater than that of α-synuclein, as the tyrosine content

of the former is higher and the monomer unit is almost three-times smaller, allowing denser packing. In summary, the three different proteins in the fibril state, insulin, lysozyme, and α-synuclein, exhibit multiphoton properties that appear to be related to tyrosine content, whereas other aromatic amino acids seem to play less important roles in inducing enhanced nonlinear responses.

The discovery presented here can be helpful in localising the positions along the amino acid sequence at which proteins tend to aggregate, which could prime the development of serious diseases, such as Parkinson's and Alzheimer's diseases. Thus, detecting the specific aggregation using non-invasive nonlinear techniques may represent a breakthrough in diagnostics. The observation of cooperativity in nonlinear absorption opens up several versatile opportunities for tuning the penetration depth by adjusting the number of photons absorbed, for example, in targeting aggregation states with high precision but leaving non-aggregated globular proteins untouched. Envisaging the use of advanced multiphoton technologies, both for diagnostic and therapeutic applications, and even for prophylaxis, sounds exciting but it also brings new limitations and problems. Other fibrillar proteins such as collagen that is inducing second harmonic generation[118] may interfere with detection of amyloids. Thus, further research concerning the sensitivity and background effects has to be performed, and the Z-scan seems to be a relatively direct method to use to resolve important issues, such as detection in "thick" media-like biological tissues or organs or if nonlinear circular dichroism (NLCD)[119] can be measured also for amyloid fibrils aggregates.

5. Concluding remarks

In the work presented in this thesis, I developed a polymer system for aligning short oligonucleotides, which has not been achieved previously through other orientation methods using shear flow or electric fields. Thus, this work represents an advance in the state of the art in spectroscopic studies of modified DNA. It is now possible to perform linear dichroism analyses of designed DNA sequences in the contexts of studying the structures and dynamics of nucleic acids, DNA-based nanoconstructs, and DNA-nanoparticle structures. Furthermore, this polymer system can be used to study DNA-dye interactions and provides a powerful tool for molecular recognition studies on nucleic acids. The present study also has relevance for drug delivery applications in which the drug is exposed to different conditions and forces in the cellular environment before it reaches the nucleus. Moreover, since the polymer environment is much different than the environment in a water solution, these results provide a new perspective, since a dense gel can be considered as a medium that mimics the molecular crowding found in biological systems.

Dyes of the cyanine group YO, YO-PRO-1, and YOYO, which are similar in structure but have increasing affinity for DNA, were first characterised in terms of their binding to long DNA sequences in humid PVA gels. The PVA in the film strongly destabilises the noncovalent interactions between intercalating dyes and double-stranded DNA. The polymeric film environment affects the properties of both the dye and the DNA. This is especially the case for short oligonucleotides, as only synthetic DNA sequences of >20 bp can adopt the helical structure. Low water activity in a highly dense polymeric environment weakens the stacking interactions and the hydrogen bonding in the DNA double helix. In the case of short oligonucleotides, this sometimes leads to denaturation and loss of the secondary structure. This also affects dye binding and promotes attraction between the dye molecules and PVA, which in the case of weaker binders leads to steric confinement of the dye in the polymer matrix. For the YO dye, all the molecules are bound to PVA. Divalent YO-PRO remains partially (25%) intercalated within the double helix, whereas *bis*-intercalation of YOYO predominates (75%) in the films. This leads us to conclude that the binding properties, structural properties, and dynamics of dyes and drugs with affinities for B-DNA $>10^6$ M^{-1} can be investigated in humid elastic gels. The above discussion concerning DNA structure and interactions with dyes in PVA reveals that subtle changes in the system equilibrium can have

serious implications, for example in the drug binding efficiency of chemotherapeutics or the precision of the drug delivery process. In the context of material storage, it is interesting that DNA-drug complexes can be stored in the dry state with PVA and subsequently reformed by rehumidification. The ease with which the hydration levels and long-term stabilities of the films can be controlled allows restraint of the DNA for weeks without any loss of its unique molecular properties.

Once the polymer system had been used successfully to study the interactions between DNA and dyes, the next step was to investigate short hairpin oligonucleotides with the ruthenium(II) complex $[(11,11'\text{-bidppz})(\text{phen})_4\text{Ru}_2]^{4+}$, which shows enantioselective binding modes to DNA sequences that are composed of either ATs only or GCs only. The advantage of the polymer film is that it provides possibilities to align organic chromophores and to monitor the kinetics and binding rearrangements of the dye molecules with respect to the DNA axis through repeated LD experiments over time. Thus, any subtle changes in the binding mode of the chromophore are easily identified. The discovery that only one enantiomer of the binuclear ruthenium(II) complex threads GC-DNA, while the second enantiomer is probably bound to the groove suggests that ruthenium(II) compounds represent a new class of smart drugs that are able to recognize with high-level precision specific regions of the chromatin. Even though the investigated complexes are the precursors of potential drugs that will have to undergo testing in medical trials before they are made available to patients, they appear to be interesting candidate molecules for further research and development. In particular, the ruthenium(II) complexes allow linkages to be drawn between important aspects of DNA molecular recognition and strong responses to laser light irradiation. In the context of drug delivery, progress has been made regarding the release and photo-activation upon light irradiation of drugs, and more advanced multiphoton-based technologies are currently being implemented in biology and medicine. The nonlinear absorption and emission properties of organic chromophores that have potential for cancer therapy, e.g., in photodynamic therapies or in the imaging of degenerated states of proteins as in patients with Alzheimer's disease, are presented in this thesis.

Nonlinear optical experiments performed using the Z-scan technique, as described in this thesis, reveal strong multiphoton absorption properties for the following "light-switch" type of metal-organic coordination complexes that bind to DNA by intercalation: (1) $[\text{Ru}(\text{phen})_2\text{dppz}]^{2+}$; (2) $[(11,11'\text{-bidppz})(\text{phen})_4\text{Ru}_2]^{4+}$; and (3) $[11,11'\text{-bipb}(\text{phen})_4\text{Ru}_2]^{4+}$. The

high values observed for the two-photon absorption cross-sections in the ILCT, and especially in the MLCT (tissue transparent IR region), appear promising for future research on the multiphoton fluorescence properties of these compounds bound to DNA. The increase in rigidity of the dimeric ruthenium(II) complex conferred by *ortho*- or *para*-substitution improves the nonlinear efficiency through π-conjugation and structure elongation. However, when dealing with fluorescent biomarkers, other aspects have to be taken into consideration, such as the availability of intercalation sites in the DNA, the quantum yield of chromophores, and quenching, which is a particular disadvantage associated with dimeric molecules that can undergo self-quenching, as shown in Paper IV. The nonlinear absorption must be sufficiently strong to be detectable using sensitive multiphoton microscopy methods.

The same strategy is presented in this thesis for the detection of amyloid fibrils, whereby amyloid-dye adducts are studied in the context of the implementation of two-photon-based techniques for imaging the degenerated states of proteins. Ruthenium(II) complexes are again used owing to their attractive photophysical properties. In addition, we used stilbene, which is often used to enhance nonlinear absorption and in laser spectroscopy. Importantly, in the optics context, dyes that are bound to biopolymers do not aggregate, are evenly distributed over the binding sites, and usually have enhanced fluorescence properties. However, in the case of amyloid fibrils, many of the fluorophores are not fibril-specific, which means that they often bind to native proteins and show high variability in terms of their photophysical properties.

The results presented in this thesis indicate that both types of chromophores (metal-organic ruthenium(II) complexes and stilbene 420) bind to amyloid fibrils, and their orientations with respect to macroscopic alignment have been determined. However, following two-photon excitation, the emission spectra of the bound dyes become very narrow and sharp. This phenomenon must be directly related to the material properties of amyloid fibrils, and indeed in the final part of this thesis, the multiphoton absorption properties of fibrils are investigated and confirmed. Proteins show strong enhancement of the nonlinear response upon fibril formation. It appears that even though there is a lack of π-conjugation, some cooperativity exists between the aromatic amino acids in the densely packed residues in the protofilaments. It is proposed that this is mainly due to the dipolar coupling between the excited states of the tyrosines, which individually show the strongest two-photon absorption. It is likely that this affects the properties of the bound dyes, which can lead to emission amplification. The

presented results and conclusions regarding the amyloid fibrils and their interactions with dyes indicate that fibrils represent an attractive material for studies involving nonlinear optics. The findings that the fibrils themselves show multiphoton absorption properties and that the structure determines dye behaviour upon laser irradiation underline the potential of amyloid fibrils as self-assembling materials for applications in imaging, photonics, and luminescence devices.

In conclusion, this thesis presents new information regarding the molecular recognition of biomolecules, showing that the strategies for DNA and amyloid fibrils are somewhat similar. Even though DNA and amyloid fibrils are distinct biopolymers the chromophores used as biomarkers for these molecules must exhibit similar properties.

DNA and amyloid fibrils are being tested in technological contexts as both have unique molecular properties, such as chirality or self-assembly, which make them attractive for a broad range of applications, from electronics to molecular nanomachinery. Furthermore, this thesis proposes that organic chromophores as binders of natural biopolymers have significant potential, and that understanding how to improve their photophysical and photochemical properties will be facilitate expansion into new fields of science and technology. In terms of future directions for this field of research, I predict that multiphoton techniques will replace traditional methods that are widely used in science and medicine, and that organic chromophores will be designed in a manner that will establish their value as more demanding two-photon-based methods become the standard in the coming years.

6.Acknowledgements

I thank my supervisor Bengt Nordén, for giving me the opportunity to do the PhD in his group and for the enthusiasm and freedom to work he has given me.

I thank my co-supervisors, Bjorn Akerman and Marek Samoc, for providing excellent guidance and support whenever I needed it and my co-authors for fruitful cooperation in all the projects.

I am grateful to everyone at the Department of Physical Chemistry at Chalmers and the Institute of Physical and Theoretical Chemistry at WrUT for a pleasant atmosphere and for creating a good place to be and to work.

7.References

(1) Levene P. A.; Jacobs W. A. *J. Biol. Chem.* **1912**, *12*.
(2) Watson J. D.; Crick F. H. C. *Nature* **1953**, *171*, 737.
(3) M. Albota; D. Beljonne; J-L. Brédas; J. E. Ehrlich; J-Y. Fu; A. A. Heikal; S. E. Hess; T. Kogej; M. D. Levin; S. R. Marder; D. McCord-Maughon; J. W. Perry; H. Röckel; M. Rumi; G. Subramaniam; W. W. Webb; X-L. Wu; C. Xu *Science* **1998**, *281*, 1653.
(4) Norden B.; Rodger A.; Dafforn T. *Oxford Univ. Press* **2010**.
(5) C. M. Hassan; N. A. Peppas *Adv. Pol. Sci.* **2000**, *153*, 37.
(6) Chua C. K.; Leong K. F.; Tan K. H.; Wiria F. E.; Cheah C. M. *J. Mater. Sci.: Mater. Med* **2004**, *15*, 1113.
(7) Hyon S. H.; Cha W. I.; Ikada Y.; Kita M.; Ogura Y.; Honda Y. J. *Biomater. Sci., Polym. Ed.* **1994**, 397.
(8) Dai W. S.; Barbari T. A. *Biomater.* **2000**, *21*, 1363.
(9) Coluccio M. L.; Ciardelli G.; Bertoni F.; Silvestri D.; Cristallini C.; Giusti P.; Barbani N. *Macromol. Biosci* **2006**, 403.
(10) (a) Kimura T.; Nam K.; Mutsuo S.; Yoshiwaza H.; Okada M.; Furuzono T.; Fuijsato T.; Kishida A. *Mol. Ther.* **2006**, *13*, 75(b) Kimura T.; Okuno A.; Miyazaki K.; Furuzono T.; Ohya, Y.; Ouchi T.; Mutsuo S.; Yoshizawa H.; Kitamura Y.; Fujisato T.; Kishida A *Mat. Scien. Engin. C* **2004**, *24*, 797.
(11) Hanczyc P.; Akerman B.; Norden B. *Langmuir* **2012**, *28*, 6662−6669.
(12) Svozil D.; Kalina J.; Omelka M.; Schneider B. *Nuc. Ac. Res.* **2008**, *36*, 3690.
(13) Bloomfield V. A.; Crothers D. M.; Tinoco I. *University Science Books: Sausalito* **2000**.
(14) (a) Norden B.; Seth S. *Biopol.* **1979**, *18*, 2323(b) Shin M. K.; Kim S. H.; Jung S.; Kim S.I.; Kim S. J.; Kim B. J.; So I. *App. Phys. Lett.* **2008**, *93*, 171903(c) Papancea A.; Valente A J. M.; Patachia S.; Miguel M. G.; Lindman B. *Langmuir* **2008**, *24*, 273(d) Aoi K.; Takasu A.; Okada M. *Pol.* **2000**, *41*, 2847.
(15) Cui D.; Pan B.; Zhang H.; Gao F.; Wu R.; Wang J.; He R.; Asahi T. *Anal. Chem.* **2008**, *80*, 7996.
(16) (a) Hammond S.M.; Wood M.J.A. *Tren. in Genet.* **2011**, *27*, 196(b) Malik R.; Roy I. *Exp. Op. on Drug Discov.* **2011**, *6*, 507.
(17) Boussif O.; LezoualC'H F.; Zanta M.A.; Mergny M.D.; Scherman D.; Demeneix B.; Behr J.-P. *Proc. Natl. Acad. Sci.* **1995**, *92*, 7297.
(18) Sung S.-J.; Min S.H.; Cho K.Y.; Lee S.; Min Y.-J.; Yeom Y.I.; Park J.-K. *Biol. Pharm. Bullet.* **2003**, *26*, 492.
(19) Norden B.; Seth S. *Biopol.* **1979**, *18*, 2323.
(20) Hanczyc P.; Norden B.; Akerman B. *J. Phys. Chem. B* **2011**, *115*, 12192.
(21) (a) Seeman N. *Annu. Rev. Biochem.* **2010**, *79*, 65(b) Tumpane J.; Kumar R.; Lundberg E. P.; Sandin P.; Gale N.; Nandhakumar I. S.; Albinsson B.; Lincoln P.; Wilhelmsson L. M.; Brown T.; Norden B. *Nanolett.* **2007**, *7*, 3832(c) Andersen E; Dong M; Nielsen M. M; Jahn K; Subramani R; Mamdouh W; Golas M; Sander B; Stark H; Oliveira C. L. P; Pedersen J. S; Birkedal V; Besenbacher F; Gothelf K. V; Kjems J. *Nat. Lett.* **2009**, *459*, 73(d) Gambinossi F.; Banchelli M.; Durand A.; Berti Debora.; Brown T.; Caminati G.; Baglioni P. *J. Phys. Chem. B* **2010**, *114*, 7338.
(22) Holliday R. *Genet. Res.* **1964**, *5*, 282.
(23) Chen J. H.; Seeman N. C. *Nature* **1991**, *350*, 631.
(24) (a) Rothemund P. W. K. *Nat.* **2006**, *440*, 297(b) Shih M. W.; Quispe J. D.; Joyce G. F. *Nat. Lett.* **2004**, *427*, 618(c) Voigt N. V.; Tørring T.; Rotaru A.; Jacobsen M. F.; Ravnsbæk J. B.; R., S.;

Mamdouh W.; Kjems J.; Mokhir A.; Besenbacher F.; Gothelf K. V. *Nat. Nanotech.* **2010**, *5*, 200.
(25) Park S. Y.; Lytton-Jean A. K. R.; Lee B.; Weigand S.; G., S. C.; Mirkin Ch. A. *Nat.* **2008**, *451*, 553.
(26) Giljohann D. A.; Seferos D. S.; Daniel W. L.; Massich M, D.; Patel P. C.; Mirkin Ch. A. *Angew. Chem. Int. Ed.* **2010**, *49*, 3280.
(27) Keren K.; Berman B.; Buchstab E.; Sivan U.; Braun E. *Science* **2003**, *302*, 1380.
(28) Ghosh P.; Han G.; De M.; Kim Ch. K.; Rotello V. M. *Adv. Drug. Deliv. Rev.* **2008**, *60*, 1307.
(29) (a) Huschka R.; Zuloaga J.; Knight M. W.; Brown L. V.; Nordlander P.; Halas N. J. *J. Am. Chem. Soc.* **2011**, *133*, 12247(b) Chhabra R.; Sharma J.; Wang H.; Zou S.; Lin S.; Yan H.; Lindsay S.; Liu Y. *Nantech.* **2009**, *20*, 485201.
(30) Yun C. S.; Javier A.; Jennings T.; Fisher M.; Hira S.; Peterson S.; Hopkins B.; Reich N. O.; Strouse G. F. *J. Am. Chem. Soc.* **2005**, *127*, 3115.
(31) Zanchet D.; Micheel Ch. M.; Parak W. J.; Gerion D.; Alivisatos P. *Nano Lett.* **2000**, *1*, 32.
(32) (a) Claridge S.; Liang H W.; Basu S. R.; Fréchet J. M. J.; Alivisatos A. P. *Nanolett.* **2008**, *8*, 1202(b) Borovok N.; Gillon E.; Kotlyar A. *Biocon. Chem.* **2012**, *23*, 916−922.
(33) Bosaeus N.; El-Sagheer A. H.; Brown, T.; Smith S. B.; Åkerman B.; Bustamante C.; Norden B. *Proc. Natl. Acad. Sci.* **2012**, *109*, 15179.
(34) (a) Mirkin C. A.; Letsinger R. L.; Mucic R. C.; Storhoff J. J. *Nat.* **1996**, *382*, 607 (b) Fu A.; Micheel Ch. M.; Cha J.; Chang H.; Yang H.; Alivisatos A. P. *J. Am. Chem. Soc.* **2004**, 10832.
(35) Lerman L. S. *J. Mol. Biol.* **1961**, *3*, 18.
(36) Larsson A.; Carlsson C.; Jonsson M.; Albinsson B. *J. Am. Chem. Soc.* **1994**, *116*, 8459.
(37) Glazar A. N.; Peck K.; Mathies R. A. *Proc. Natl. Acad. Sci.* **1990**, *87*, 3851.
(38) Dervan P.B.; Becker M.M. *J. Am. Chem. Soc.* **1978**, *100*, 1968.
(39) Petty J.; Bordelon J. A.; Robertson M. E. *J. Phys. Chem. B* **2000**, *104*, 7221.
(40) Eriksson M.; Karlsson H. J.; Westman G.; Akerman B. *Nuc. Ac. Res.* **2003**, *31*, 6235.
(41) Carlsson C.; Larsson A.; Jonsson M.; Albinsson B.; Norden B. *J. Phys. Chem.* **1994**, *98*, 10313.
(42) Benson S. C.; Singh P.; Glazar A. N. *Nuc. Ac. Res.* **1993**, *21*, 5723.
(43) Gurrieri S.; Wells K. S.; Johnson I. D.; Bustamante C. *Anal. Biochem.* **1997**, *249*, 44.
(44) Quake S. R.; Babcock H.; Chu S. *Nature* **1997**, *388*, 151.
(45) J. van Mameren; P. Gross; G. Farge; P. Hooijman; M. Modesti; M. Falkenberg; G. J. L. Wuite; E. J. G. Peterman *Proc. Natl. Acad. Sci.* **2009**, *106*, 18231.
(46) Vos J. G.; Kelly J. M. *Dal. Trans.* **2006**, 4869.
(47) (a) Bivar T. *App. Spect. Rev.* **2012**, *47*, 272(b) Jaehnchen J.; Purwanto M.; Weisz K. *Biopol.* **2005**, *79*, 335(c) Barton J.; Olmon E.; Sontz P. *Coord. Chem. Rev* **2011**, *255*, 619(d) Bazhulinaa N.; Nikitina A.; Rodina S.; Surovayaa A.; Kravatskya Y.; Pismenskya V.; Archipovaa V; Martin R.; Gurskya G. *J. Biomol. Struc. and Dynam.* **2009**, *26*, 701(e) Norden B.; Rodger A.; Dafforn T. *Oxf. Uni. Pr.* **2010**.
(48) (a) Metcalfe C.; Thomas J. *Chem. Soc. Rev.* **2003**, *32*, 215(b) Kam-Wing Lo K.; Wing-Tat Choi A.; Ho-Tin Law W. *Dalt. Trans.* **2012**, *41*, 6021(c) Crespy D.; Landfester K.; Schubert U.; Schiller A. *Chem. Comm.* **2010**, *46*, 6651(d) Bruijnincx P.; Sadler P. *Curr. Op. in Chem. Biol.* **2008**, *12*, 197.
(49) (a) Barton J.; Danishefsky A.; Goldberg J. *J. Am. Chem. Soc.* **1984**, *106*, 20172(b) Mei H.; Barton J. *PNAS* **1988**, *85*, 1339.
(50) (a) Hiort C.; Lincoln P.; Norden B. *J. Am. Chem. Soc.* **1993**, *115*, 3448(b) Olofsson J.; Wilhelmsson M.; Lincoln P. *J. Am. Chem. Soc.* **2004**, *126*, 15458(c) Friedman A.; Chambron J.; Sauvage J.; Turro N.; Barton J. *J. Am. Chem. Soc.* **1990**, *112*, 960(d) Olson E.; Hu D.; Hormann A.; Jonkman A.; Arkin M.; Stemp E.; Barton J.; Barbara P. *J. Am. Chem. Soc.* **1997**, *119*, 11458(e) Jenkins Y.; Friedman A.; Turro N.; Barton J. *Biochem.* **1992**, *31*, 10809.
(51) (a) Hiort, C.; Lincoln, P.; Nordén, B. *J. am. Chem. Soc.* **1993**, *115*, 3448(b) Barton, J. K.; Danishefsky, A.; Goldberg, J. *J. am. Chem. Soc.* **1984**, *106*, 1941.

(52) (a) Wilhelmsson M.; Westerlund F.; Lincoln P.; Norden B. *J. Am. Chem. Soc.* **2002**, *124*, 12092(b) Lincoln P.; Norden B. *Chem. Comm.* **1996**, *18*, 2145(c) Wilhelmsson M.; Esbjorner E.; Westerlund F.; Norden B.; Lincoln P. *J. Phys. Chem. B* **2003**, *107*, 11784.
(53) Olofsson J.; Wilhelmsson L. M.; Lincoln P. *J. Am. Chem. Soc.* **2004**, *126*, 15458.
(54) (a) Novakova O.; Vrana H.; Rodger A.; Sadler P.; Brabec V. *Biochem.* **2003**, *42*, 11544(b) Wheate N.; Brodie C.; Collins J.; Kemp S.; Aldrich-Wright J. *Mi. Rev. Med. Chem.* **2007**, *6*, 627(c) Zhang J.; Zhang F.; Li H.; Liu C.; Xia J.; Ma L.; Chu W.; Zhang Z.; Chen C.; Li S.; Wang S. *Curr. Med. Chem.* **2012**, *19*, 2957.
(55) Bloembergen N. *World Scien.* **1965**.
(56) Lakowicz J. **2006**, *3rd edition*, 607.
(57) (a) He, G. S.; Markowicz, P.; Lin, T. C.; Prasad, P. N. *Nature* **2002**, *415*, 767(b) Bhawalkar, J. D.; He, G. S.; Prasad, P. N. *Rep. Prog. Phys.* **1996**, *59*, 1041(c) Wang Y.; Xie X.; Goodson III. T. *Nano Lett.* **2005**, *5*, 2379.
(58) (a) Pliss A.; Kuzmin A.N.; Kachynski A.V.; Prasad P.N. *Biophys. J.* **2010**, *99*, 3483(b) Mempel T.R.; Henrickson S.E.; Von Andrian U.H. *Nature* **2004**, *427*, 154(c) Bansal, D.; Miyake, K.; Vogel, S. S.; Groh, S.; Chen, C.-C.; Williamson, R.; McNei, P. L.; Campbell, K. P. *Nature* **2003**, *423*, 168(d) Masters B.R. *J. Biophot.* **2009**, *2*, 127.
(59) So P.T.C.; Dong C.Y.; Masters B.R.; Berland K.M *Ann. Rev. Biomed. Eng.* **2000**, *2*, 399.
(60) Wecksler S. R.; Mikhailovsky A.; Korystov D.; Ford C. P. *J. am. Chem. Soc.* **2006**, *128*, 3831.
(61) (a) Steil H.; Teuchner K.; Paul A.; Freyer W.; Leupold D *J. Photochem. Photobiol.* **1994**, *80*, 289(b) Fisher, W. G.; Partridge, W. P.; Dees, J. C.; Wachter, E. A. *J. Photochem. Photobiol.* **1997**, *66(2)*.
(62) (a) Campagnola, P. J.; Loew, L. M. *Nat. Biotech.* **2003**, *21*, 1356(b) Yuste R. *Nat. Meth.* **2005**, *2*, 902.
(63) Denk, W.; Strickler, J. H.; Webb, W. W. *Science* **1990**, *248*, 73.
(64) Zipfel, W. R.; Williams, R. M.; Webb, W. W. *Nat Biotechnol* **2003**, *21*, 1368.
(65) Xu, C.; Webb, W. W. *J Opt Soc Am B* **1996**, *13*, 481.
(66) Sheik-Bahae, M.; Said, A. A.; Wei, T. H.; Hagan, D. J.; Van Stryland, E. W. *IEEE Journal of Quantum Electronics* **1990**, *26*, 760.
(67) Olmsted, J.; Kearns, D. R. *Biochemistry-Us* **1977**, *16*, 3647.
(68) (a) Pawlicki, M.; Collins, H. A.; Denning, R. G.; Anderson, H. L. *Angew Chem Int Edit* **2009**, *48*, 3244(b) Bestvater, F.; Spiess, E.; Stobrawa, G.; Hacker, M.; Feurer, T.; Porwol, T.; Berchner-Pfannschmidt, U.; Wotzlaw, C.; Acker, H. *J Microsc-Oxford* **2002**, *208*, 108.
(69) (a) Girardot, C.; Lemercier, G.; Mulatier, J.-C.; Chauvin, J.; Baldeck, P. L.; Andraud, C. *Dalton Trans.* **2007**, 3421(b) Girardot, C.; Lemercier, G.; Mulatier, J.-C.; Andraud, C.; Chauvin, J.; Baldeck, P. L. *Tetrahedron Lett.* **2008**, *49*, 1753.
(70) (a) Jiang C-W.; Chao H.; Li R-H.; Li H.; Ji L-N. *Polyhedron* **2001**, *20*, 2187(b) Chao, H.; Yuan, Y.-X.; Ji, L.-N. *Trans. Met. Chem.* **2004**, *29*, 774.
(71) Feuvrie, C.; Maury, O.; Le Bozec, H.; Ledoux, I.; Morrall, J. P.; Dalton, G. T.; Samoc, M.; Humphrey, M. G. *J. Phys. Chem. A* **2007**, *111*, 8980.
(72) Coe, B. J.; Samoc, M.; Samoc, A.; Zhu, L.; Yi, Y.; Shuai, Z. *J. Phys. Chem. A* **2007**, *111*, 472.
(73) Hanczyc P.; Norden B.; Samoc M. *Dalt. Trans.* **2012**, *41*, 3123.
(74) D. J. Selkoe *Nature* **2003**, *426*, 900.
(75) (a) J. C. Rochet; P. T. Lansbury Jr *Cur. Op. in Struct. Biol.* **2000**, *10*, 60(b) S. B. Prusiner *PNAS* **1998**, *95*, 13363(c) F. Chiti; C. M. Dobson *Annu. Rev. Biochem.* **2006**, *75*, 333(d) R. M. Murphy *Annu. Rev. Biochem.* **2002**, *4*, 155.
(76) (a) J. L. Jimenez; E. J. Nettleton; M. Bouchard; C. V. Robison; C. M. Dobson *PNAS* **2002**, *99*, 9196(b) Cohen A.; Shirahama T.; Skinner M. *Academic London* **1982**, *3*, 165.
(77) J. F. Smith; T. P. J. Knowles; C. M. Dobson; C. E. MacPhee; Welland, M. E. *PNAS* **2006**, *103*, 15806.

(78) Oliviera C.; Behrens M.; Pedersen J.; Erlacher K.; D., O. *J. Mol. Biol.* **2009**, 147.
(79) Fortin D. L.; Nemani V. M.; Voglmaier S. M.; Anthony, M. D.; Ryan T. A.; Edwards R. H. *J. Neurosci.* **2005**, *25*, 10913−10921.
(80) Luk K. C.; Hyde E. G.; Trojanowski J. Q.; Lee V. M. Y. *Biochem.* **2007**, *46*, 12522−12529.
(81) (a) LeVine H. *Protein Sci.* **1993**, *2*, 404(b) Maskevich A. A.; Sisiapura V. I.; Kuzmitsky V. A.; Kuznetsova I. M.; Povarova O. I.; Uversky V. N.; Turoverov, K. K. *J. Protome. Res.* **2007**, *6*, 1392.
(82) Viegas M. S.; Martins T. C.; Seco, F.; do Carmo A. *Eur. J. Histochem.* **2007**, *51*, 59−66.
(83) Norden B. *App. Spec. Rev.* **1978**, *14*, 157.
(84) Matsuoka Y.; Norden B. *Biopol.* **1982**, *21*, 2433.
(85) Westerlund F.; Nordell P.; Blechinger J.; Santos T. M.; Norden B. *J. Phys. Chem. B* **2008**, *112*, 6688.
(86) Andersson J.; Li M.; Lincoln P. **2010**, *16*, 11037
(87) Tumpane J.; Kumar R.; Lundberg E. P.; Sandin P.; Gale N.; Nandhakumar I. S.; Albinsson B.; Lincoln P.; Wilhelmsson L. M.; Brown T.; Nordén B. *Nano Lett.* **2007**, *7*, 3832.
(88) Tokmakoff A. **2009**, *chapter 11*, 1.
(89) Sheik-bahae M.; Said A.A.; Van Stryland E. W. *Opt. Lett.* **1989**, *14*, 955.
(90) Sheikh-bahae, M.; Said, A. A.; Wei, T.; Hagan, D. J.; Stryland, E. W. v. *IEEE J. Quantum Electr.* **1990**, *26*, 760.
(91) Samoc M.; Samoc A.; Luther-Davies B.; Humphrey M. G.; Wong M. S. *Opt. Mater.* **2003**, *21*, 485.
(92) Matsuoka Y.; Norden B. *Biopol.* **1983**, *22*, 1731.
(93) Matsuoka Y.; Norden B. *J. Phys. Chem.* **1982**, *86*, 1378.
(94) (a) Tao N. J.; Lindsay S. M.; Rupprecht A. *Biopol.* **1989**, *28*, 1019(b) Franklin R. E.; Gosling R. G. *Acta Cryst.* **1953**, *6*, 673.
(95) Matsuoka Y.; Norden B. *Biopol.* **1983**, *22*, 1731.
(96) Lindsay S. M.; Lee S. A.; Powell J. W.; Weidlich T.; Demarco C.; Lewen G. D.; Tao N. J.; Rupprecht A. *Biopol.* **1988**, *27*, 1015.
(97) (a) Falk M.; Hartman K. A.; Lord R. C. *J. Am. Chem. Soc.* **1962**, *84*, 3843(b) Falk M.; Hartman K. A.; Lord R. C. *J. Am. Chem. Soc.* **1962**, *85*, 387.
(98) Pilet J.; Brahms J. *Biopol.* **1973**, *12*, 387.
(99) Norden B.; Rodger A.; Dafforn T. *Oxf. Univ. Pr.* **2010**.
(100) Z. Li; R. Jin; C. A. Mirkin; R. L. Letsinger *Nuc. Ac. Res.* **2002**, *30*, 1558.
(101) Vladescu I.D.; McCauley M.J.; Nunez M.E.; Rouzina I.; Williams M.C. *Nat. Met.* **2007**, *4*, 517.
(102) Norden B.; Kubista M.; Kurucsev T. *Quart. Rev. of Biophys.* **1992**, *25*, 51.
(103) P. Nordell; F. Westerlund; L. M. Wilhelmsson; B. Norden; P. Lincoln *Angew. Chem. Int. Ed.* **2007**, *46*, 2203
(104) Lyng R.; Rodger A.; Norden B. *Biopol.* **1991**, *31*, 1709.
(105) Westerlund F.; Nordell P.; Blechinger J.; Santos T.; Norden B.; Lincoln P. *J. Phys. Chem. B* **2008**, *112*, 6688.
(106) Nordell P.; Westerlund F.; Wilhelmsson M.; Norden N.; Lincoln P. *Angew. Chem. Int. Ed.* **2007**, *46*, 2203
(107) (a) Cook N. P.; Torres V.; Jain D.; Martí A. A. *J. Am. Chem. Soc.* **2011**, *133*, 11121(b) Cook N. P.; Kilpatrick K.; Segatori L.; Martí A. A. *J. Am. Chem. Soc.* **2012**, *134*, 20776.
(108) Rau I.; Szukalski A.; Sznitko L.; Miniewicz A.; Bartkiewicz S.; Kajzar F.; Sahraoui B.; Mysliwiec J. *App. Phys. Lett.* **2012**, *101*, 171113.
(109) (a) Mysliwiec J.; Sznitko L.; Sobolewska A.; Bartkiewicz S.; Miniewicz A. *App. Phys. Lett.* **2010**, *96*, 141106(b) Kawabe Y.; Wang L.; Horinouchi S.; Ogata N. *Adv.Mat.* **2000**, *12*, 1281.
(110) K. Smit; K. Ghiggino *Dyes and Pigments* **1987**, *8*, 83.
(111) K. Smit; K. Ghiggino *J. Pol. Sci. B: Pol. Phys* **1991**, *29*, 1397.

(112) E. S. Voropai; M. P. Samtsov; K. N. Kaplevskii; A. A. Maskevich; V. I. Stepuro; O. I. Povarova; I. M. Kuznetsova; K. K.Turoverov; A. L. Fink; V. N. Uverskii *J. Appl. Spectrosc.* **2003**, *70*, 868.
(113) Meshalkin Y. *Quan. Elec.* **1996**, *26*, 536.
(114) Samoc M.; Samoc A.; Grote J. G. *Chem. Phys. Lett.* **2006**, *431*, 132.
(115) Rativa D.; Da Silva D. J. S.; Del Nero J.; Gomes A. S. L.; De Araujo R. E. *J. Opt. Soc. Am. B* **2010**, *27*, 2665.
(116) (a) Roberts R. L.; Schwich T.; Corkery T. C.; Cifuentes M. P.; Green K. A.; Farmer J. D.; Low P. J.; Marder T. B.; Samoc M.; Humphrey M. G. *Adv. Mat.* **2009**, *21*, 2318(b) McDonagh A. M.; Humphrey M. G.; Samoc M.; Luther-Davies B. *Organomet.* **1999**, *18*, 5195(c) Chung S. J.; Kim K. S.; Lin T. C.; He G. S.; Swiatkiewicz J.; Prasad P. N. *J. Phys. Chem. B* **1999**, *103*, 10741.
(117) Drobizhev M.; Stepanenko Y.; Rebane A.; Wilson C. J.; Screen T. E. O.; Anderson H. L. *J. Am. Chem. Soc.* **2006**, *128*, 12432.
(118) Williams R. M.; Zipfel W. R.; Webb, W. W. *Biophys. J.* **2005**, *88*, 1377.
(119) Markowicz P. P.; Samoc M.; Cerne J.; Prasad P. N.; Pucci A.; Ruggerid G. *Opt. Exp.* **2004**, *12*, 5209.